DYE SENSITISATION OF PHOTO-CONDUCTION

IN SILICON DIOXIDE

BY

ROBERT J HOLWILL

A Thesis submitted for the degree of Doctor of Philosophy
at the University of Edinburgh

In

May 1981

EDINBURGEN EX BIBL UNIV.

This thesis has been composed by myself and is the result of my own work except where otherwise indicated.

Robert J. Holwill

ACKNOWLEDGEMENTS

I am indebted to Dr A.E. Owen and Professor J. Mavor for their supervision during the course of this work. In, addition I should like to thank Dr B.W. Flynn for his advice.

This work was carried out under the Science Research Council CASE award scheme in co-operation with ICI Limited, Corporate Laboratory, Runcorn and I am grateful to Dr E.W. Williams and Dr M.V. Twigg for their help during my visits to that institution.

ABSTRACT

The dye-sensitisation of the photo-conduction in SiO_2 has been investigated. Dye-sensitisation of the photographic process and of the photo-conductivity of various solids has been widely reported and this literature is reviewed. The relevant literature on conduction in insulators is also reviewed.

Preliminary investigations of the DC and optical properties of SiO_2 and metal-free phthalocyanine were undertaken, the results of which are consistent with previously published data.

The test sample used was a metal-dye-SiO_2-metal sandwich structure (MDIM). Under illumination, the sample current increased sharply and subsequently decayed to a value greater than the dark current. This photo-induced dye-sensitised current was characterised as a function of polarity, applied field, temperature and wavelength of illumination. Possible mechanisms are discussed qualitatively including the established theories of dye-sensitisation. The most likely mechanism is an injection of electrons from the dye to the insulator conduction band, possibly by some trap-assisted route.

The discharge of a MDIM capacitor structure was observed to occur at a higher rate under illumination. Preliminary experiments are described and discussed in terms of a simple dual-capacitor model.

The application of these phenomena in MOS devices is assessed and a simple forecast of device performance is presented.

CONTENTS.

CHAPTER ONE : INTRODUCTION

The purpose of the experiments presented in this thesis was to characterise the so-called dye-sensitised photo-current in silicon dioxide films and to elucidate the possible mechanisms of this phenomenon. The motivation developed from a British patent by Owen and Mavor[1] which described a novel light-sensitive transistor. The proposed transistor structure is shown in Figure 1.1. Contemporary MOS processing would be used for the fabrication but with the novel inclusion, over the gate electrode, of an organic dye layer which, under the influence of light, would control the operation of the transistor.

A short paper had been published by Nelson[2] in which he reported that a photo-current was induced in Pyrex glass by visible light, due to the action of an adsorbed organic dye film. It was noted that the wavelength of illumination was much longer than that required for intrinsic photo-effects in the glass itself. A similar dye-sensitised photo-current was hoped to be the mechanism by which the dye-sensitised transistor would be controlled; the spectral response to be tailored to a particular device application by choice of dye.

The phenomenon of dye-sensitisation has been the subject of investigation and some controversy for many years. The effect was originally recognised in photographic processes as the means by which

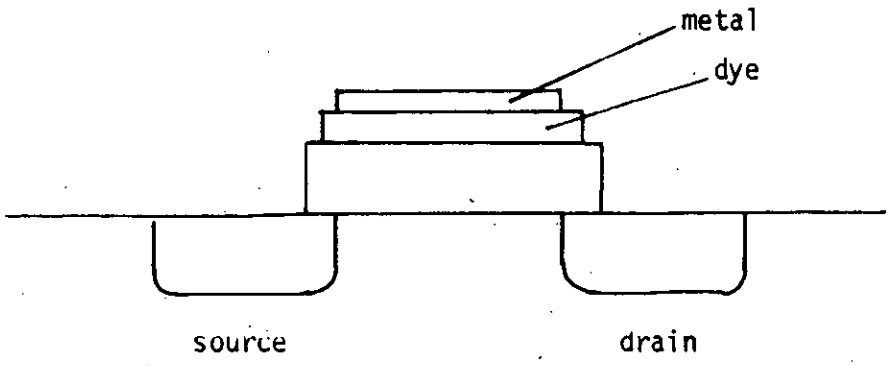

(a)

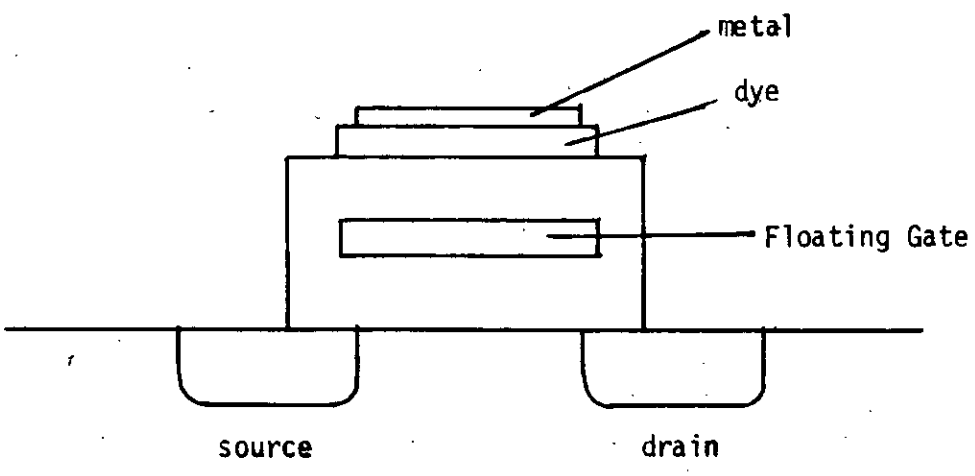

(b)

Figure 1.1: Proposed dye sensitised transistor structures.

the silver halide latent image formation is sensitised by dyes to photon energies less than that required by the intrinsic latent image formation. Much work was directed towards an understanding of the dye-sensitisation mechanism and two main theories evolved, charge injection and energy transfer. Photo-effects in semiconductors were also found to respond to dye-sensitisation and, in general, discussion in the literature revolved around the same theories. With the exceptions of the paper by Nelson and work published by Flynn, [3] little has appeared in the literature concerned with the sensitisation of photo-effects in silicon dioxide. The objectives of the present work were threefold,

i to characterise and quantify the dye-sensitised photo-conduction in silicon dioxide,

ii to discuss possible mechanisms for this phenomenon, and,

iii to assess the feasibility and suitability of incorporating the phenomenon into MOS devices.

The dye-sensitisation effect brings together two classes of materials, organic dyes and insulators. It is necessary therefore to review the electrical, physical and optical properties of organic dyes and this is presented in Chapter 2. A short appendix deals with the chemistry of the particular dye used in the experimental work presented in this thesis. Previous work on dye-sensitisation effects and the proposed mechanisms is also reviewed in Chapter 2.

The electrical properties of insulators, in particular those of SiO_2, are of crucial importance to an understanding of the photo-induced current. A brief survey is given in Chapter 3.

The experimental procedures and sample preparation are described in Chapter 4. Experimental results from the investigation of the electrical and optical properties of dye, SiO_2 and dye/SiO_2 systems are presented and discussed with reference, where appropriate, to previously published data in Chapter 5. Chapter 6 considers the implications of the findings to MOS fabrication techniques and devices. A simple quantitative forecast is made of device performance and some recommendations for future work are given. Finally, the main conclusions are summarised in Chapter 7.

CHAPTER ONE : REFERENCES

1. Owen, A.E. & Mavor, J. Improved Semiconductor Device Brit. Pat. No 24081/72.

2. Nelson, R.C. J. Opt. Soc. Am. 50, E1029 (1960).

3. Flynn, B.W., Mavor, J. & Owen, A.E. Solid State and Electron Devices 2, 94 (1978).

2. THE OPTICAL AND ELECTRICAL PROPERTIES OF ORGANIC DYES AND THE DYE-SENSITISATION OF ELECTRICAL EFFECTS IN SOLIDS

Historically, the dye-sensitisation of the electrochemical reactions basic to the silver halide photographic process, were first observed by Moser and Rigollot[1] over 100 years ago. Since that time, the development of the photographic process has been accompanied by related work reporting the sensitisation of photoelectrical effects in inorganic materials and although there has been considerable speculation about the mechanism of dye-sensitisation the problem remains unresolved. In this Chapter the physical properties of organic dyes are first reviewed. Particular attention is given to photo-conductivity as this is especially important in dye-sensitisation. The discussion will be illustrated by reference to various dyes but the emphasis will be on the phthalocyanines which have been used in most of the sensitisation experiments which are described later (Chapter 5).

2.1 STRUCTURE AND ABSORPTION SPECTRA OF DYES

The molecular structures of some dyes, including metal-free hydrogen phthalocyanine are shown in Figure 2.1 (H_2Pc will be used to represent metal-free phthalocyanine). The hydrogen

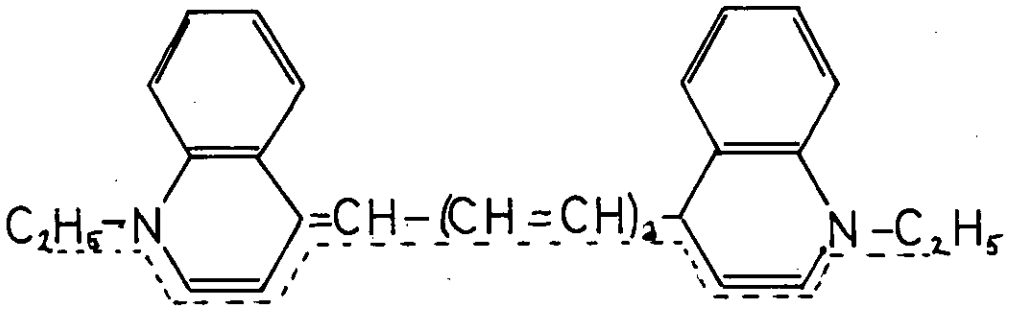

(a) cyanine

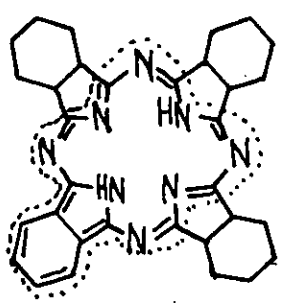

(b) phthalocyanine

FIGURE 2.1: Dye Molecules

in H_2Pc can easily be substituted by various metals and certain metal phthalocyanines are very well-known; e.g. CuPc is the bright azure dye used extensively nowadays for colouring fabrics etc. Brief details of the chemistry and preparation of H_2Pc are given in Appendix 1.

i Free Electron Model for Molecular Orbitals

A common feature of many dye molecules is a conjugated π electron system i.e. a chain of alternating single and double bonds (shown as a dotted line in figure 2.1) and a free electron model has been developed to explain the light absorption by isolated molecules (e.g. gas phase) of this kind. The π electrons are regarded as free within the constraint of the conjugated chain and light absorption takes place by excitation of the π electrons i.e. $\pi \rightarrow \pi^*$ excitations. For a linear molecule e.g. Figure 2.1(a), the potential energy of a delocalized π electron is nearly constant within the chain; strong coulombic forces exist at the chain ends, preventing the π electron escaping from the molecule, and the situation is approximated by a single electron trapped in a potential "box". If the length of the molecule is L, the energy eigenvalues for a single electron are given by[2]

$$E_n = \frac{L^2}{8mh^2} n^2 (n = 1, 2 \ldots.) \qquad 2.1$$

For an isolated molecule with N π electrons in the chain, the first absorption band i.e. the band of longest wavelength, appears at wavelength λ where

$$\lambda = \frac{8mcN^2L^2}{(N+1)h} \qquad 2.2$$

For a cyclic system such as phthalocyanine

$$\lambda = \frac{8mcN^2L^2}{4(N+1)h} \qquad 2.3$$

This simple model has been applied to various molecules, with appropriate perturbations arising from structural effects (e.g. the influence of end groups) by Bayliss[3] and Kuhn[4] and others. The data for cyanine dyes shown in Table 1 (after Simpson [5]) demonstrate the remarkable agreement with observed absorption bands.

On transition from the gas phase to a solid molecular crystal, the general features of the absorption spectrum are preserved. There is a shift to higher energies and some "splitting" of the absorption bands but the fact that the general features remain unchanged suggest that there are only weak interaction between molecules. The interaction is strong enough however for a scheme of energy bands to exist in the solid. Narrow bands ($\sim 10^{-2}$eV) exist in many organic dyes and, as will be shown, they may have a dominant effect on the transport of electronic carriers. It is possible to consider the conduction in molecular crystals using Bloch's

Position of Absorption Bands in Spectra of Cyanine Dyes		
u (π electrons)	λ calc. (n.m.)	λobserved (μm)
6	309	309
8	409	409
10	509	511

Table 1:

theory developed for covalently bonded crystalline materials.

Frenkel [6] developed a theory in which he regarded a crystal as analogous to a molecule. On absorption of light, the electronic excitation is not confined to a single molecule but spreads throughout the crystal as an "excitation wave". The importance of this concept is that the excitation is mobile and can, for example, cause ionization of trapped charge at another site. The term "exciton" has been used to describe this excitation and can be thought of as a quasi particle, mobile throughout the crystal. Corresponding to singlet and triplet states of a molecule there are singlet and triplet excitations in a crystal.

2.2 THE ORIGIN OF CHARGE CARRIERS

Charge carriers can be generated by several processes and the distinction of intrinsic and extrinsic generation is useful. For dyes with an energy difference of less than 2eV between the ground state and the first excited singlet state, it is possible to assume an intrinsic generation process i.e. charge carriers are formed by the thermal or optical transfer of an electron from the ground state to the excited state. This can be derived from the agreement between,

(i) the thermal activation energy ΔE and the optical excitation energy

(ii) the photoconduction and absorption spectra, and

(iii) the thermal activation energy ΔE and the optical activation energy derived from the long wave limit of photoconductivity.

For CuPc, ΔE = 1.7eV and ΔE_{opt} = 1.63 eV and/or
pinacyanole ΔE = 1.8eV and ΔE_{opt} = 1.77eV.

In the case of compounds with energy gaps greater than 2eV between the ground state and the excited state, charge carriers can be generated by excitation of defects (e.g. absorbed gases) or by injection from electrodes. Illumination with light of high intensity can result in trapped charge being released due to excitation ionisation. Harrison[7] has reported that the photoconduction in phthalocyanines is due to both singlet and triplet excitation interaction with trapping centres, possibly absorbed oxygen. Such extrinsic conduction is thought to be the mechanism by which the ambient atmosphere can enhance or reduce the photo-conduction in dyes.

2.3 TRANSPORT OF CHARGE CARRIERS

In general, electronic transport in molecular solids may occur by one or more of several processes, i.e. tunnelling (direct and phonon-assisted), thermally activated hopping and

transport in a "band" (valence or conduction). These processes are discussed briefly in the following paragraphs (and more fully in the following Chapter). Much of the literature on this subject is concerned with materials such as anthracene but the basic ideas could also be relevant to organic dyes such as the phthalocyanines.

i Tunnelling

The tunnelling mechanism postulates that an excited electron (e.g. in a singlet state) can tunnel through the potential barrier to reach an unoccupied electronic state in a neighbouring molecule.

The frequency for direct tunnelling to take place is 10^{11}- 10^{14} s^{-1} which is greater than that for the electron returning to the ground state, 10^{8} - 10^{9} s^{-1}. Such a mechanism would appear to be in agreement with the observed anisotropy of the conductivity of some crystals[8] but the strong temperature dependence of the conductivity of, for example, anthracene[9] does not support a direct tunnelling mechanism.

ii Hopping

In solids with broad intermolecular barriers (>10Å) that cannot be crossed by tunnelling, electrons can migrate by a "hopping" mechanism from one molecule to the next. Such carrier transport, which is characterized by a low mobility

($<0.1\ cm^2/vs$) which increased with temperature is thought to occur in some organic polymers.[10] However, low mobility increasing with temperature can also be observed in the case of band conduction due to multiple trapping. Such cases can be distinguished by their different frequency dependence of conductivity. In the case of band conduction, σ decreases with increasing frequency; with the hopping mechanism, σ increases with increasing frequency.

iii Band Model

As already mentioned, the intermolecular interactions are consistent with the formation of a system of energy bands. This is especially true as the intermolecular distances decrease (<10Å). A number of theoretical and experimental results confirm the existence of a band structure in many organic solids e.g. quantum mechanical calculations give bandwidths of the order of kT, mobilities of 10^{-5} to $10^{-3}\ m^2/vs$ and mean free paths corresponding to the various lattice constants. Other work confirms that for many organic semiconductors, carrier mobilities are in the range 10^{-5} to $10^{-2} m^2/vs$.

A valence and conduction band separated by a forbidden energy gap can generally be defined, analogous to inorganic semiconductors.

2.4 DARK CONDUCTIVITY

Most dyes have conductivities in the range 10^{-8} to 10^{-12}

Ω^{-1} m^{-1} as a consequence of the relatively broad forbidden gap between valence and conduction bands. For intrinsic dye semiconductors

$$\sigma = \sigma_o \exp(-\Delta E/2kT) \qquad 2.4$$

where ΔE is the forbidden energy gap.

For extrinsic conduction ΔE, may be replaced by ΔE_A and ΔE_D, the appropriate activation energies for acceptors and donors. With broad forbidden gaps, carrier injection from the electrodes may contribute to the dark current and experimentally therefore it is possible to find activation energies smaller than the forbidden gap. If ohmic contacts, are made the density of injected carriers may exceed the concentration of carriers produced by intrinsic or extrinsic excitation, and a transition from ohmic to space-charge-limited currents then occurs. The nature of the contact has great influence on the observed properties of dye samples.

2.5 PHOTOCONDUCTIVITY

The steady state photoelectric current, I_{phot}, can be expressed formally by the equation,

$$I_{phot} = e\eta I_A V \mu \tau \mathcal{E}/L \qquad 2.5$$

where e is the electronic charge, η the primary quantum efficiency,

I_A the quanta absorbed per unit volume, V the volume of the sample, μ the mobility, τ the free carrier lifetime, $\mathcal{E}$ the field strength and L the distance between the electrodes. As μ and τ are often small in organic materials, the photocurrents are only observable at small electrode spacing. The generation rate, g, is given by

$$g = \eta I_A \qquad 2.6$$

and depends on the field. Only high fields can separate generated carriers before recombination takes place. With the steady density of photogenerated electrons

$$\Delta n = g\,\tau \qquad 2.7$$

and the transit time

$$T = L/\mu\mathcal{E} \qquad 2.8$$

Equation 2.5 can be written

$$I_{phot} = e\Delta n\, V/T \qquad 2.9$$

For a photoconductor with mobile holes and electrons, the photoconductivity is given by

$$\sigma_{phot} = e(\Delta n\mu_n + \Delta p\mu p) \qquad 2.10$$

The photoconductive gain, G, defined as the number of charge carriers passing through the sample per absorbed photon can be derived from equation 2.5

$$G = \frac{I_{phot/e}}{I_A V} = \eta\mu\tau\mathscr{E}/L \qquad 2.11$$

and if $\eta = 1$

$$G = \frac{\tau}{T} \qquad 2.12$$

Since the parameters controlling the mean carrier lifetime depend considerably on structural effects and on chemical purity, G can vary within wide limits (up to a factor of 10^{10}) in different samples of the same compound. Great care is thus necessary when comparing published data.

With blocking contacts G has a maximum value of 1. The current-voltage curve becomes saturated at high voltages if all photogenerated carriers reach the electrodes. With ohmic contacts, G may exceed unity because the primarily excited carriers, after extraction from the sample by the electric field, can be replenished by the injecting contact. Space charges generally cause the photocurrents to saturate at high fields, so that maximum gain is obtained. In low resistivity photoconductors, without traps or with deep traps which increase the transition voltage from ohmic to space-charge-limited currents, gains greater than 1 can be observed e.g. 2.3 in merocyanine dyes.[11]

2.6 PHOTOVOLTAIC EFFECTS

Photocurrents and photovoltages may be observed without the application of auxiliary voltages. For example, the formation of space charge layers at contacts or at the surface of a dye may lead to the generation of photovoltages. This type of photo-emf results from the separation of electron-hole pairs under the influence of the electric field in the contact or surface space charge layer.

For the situation where a blocking contact exists, as in Figure 2.2, a simple expression for the photovoltage can be derived. The diffusion voltage V_D and the barrier width W are given by

$$W = \left(\frac{2\epsilon\epsilon_o V_D}{eN_D}\right)^{\frac{1}{2}} \qquad 2.13$$

where N_D is the number of donors per unit volume. The electric field at the interface is

$$\mathcal{E}_o = -\,{}^{2V_D}/_{W}$$

The photovoltage can be expressed as

$$\mathcal{E}_{phot} = \left(\frac{kT}{e}\right) \ln\left[1 + \frac{I_l}{I_o \exp\left(-\Delta E/kT\right)}\right] \qquad 2.14$$

where I_l is the induced current under illumination and $I_o \exp(-{}^{\Delta E}/kT)$ the dark current. For small I_l

$$\mathcal{E}_{phot} = \left(\frac{kT}{e}\right)\left(\frac{I_l}{I_o}\right) \exp\left[\frac{\Delta E}{kT}\right] \qquad 2.15$$

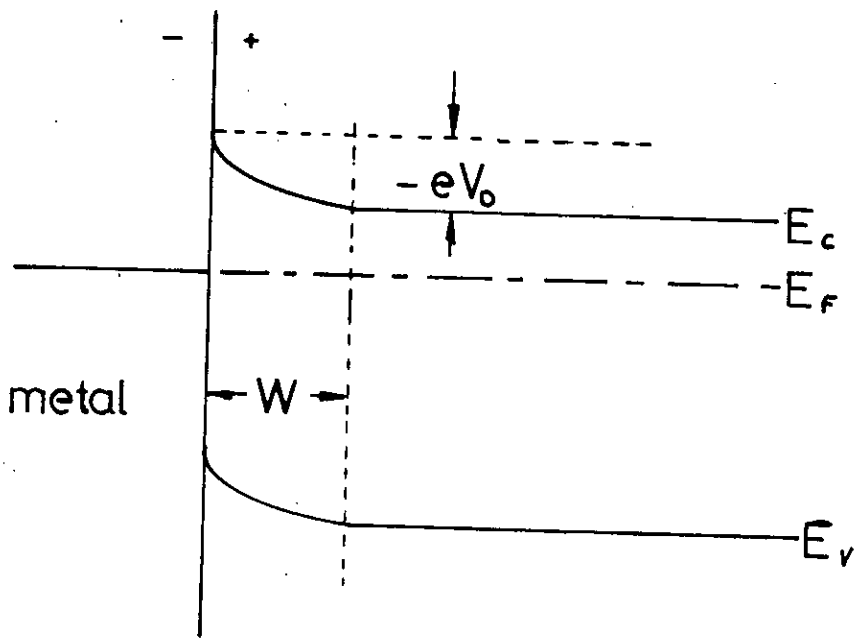

Figure 2.2: Blocking Contact

At equilibrium, the diffusion current (= eDdn/dx) and field current (= $en\mu_n\mathcal{E}$) cancel i.e.

$$j = ne\mu_n\mathcal{E} + eD\,dn/dx = 0 \qquad 2.16$$

Photovoltages of the order of 1-15mV have been observed [11] metal-aromatic junctions, whilst tetracene films sandwiched between Au and Al electrodes gave open circuit voltages of up to 0.6V. [12]

Light can affect contact potentials involving organic semiconductors because excitation of electrons into the conduction band raises the fermi level by ΔC where

$$\Delta C = kT \ln \left(\frac{n_C}{n_D}\right) \qquad 2.17$$

where n_L and n_D are the densities of free electrons in light and dark respectively. Nelson has reported a change in contact potential between H_2Pc and CdS of 120mV under illumination, when the substrate was biased positively. [13]

2.7 CLASSIFICATION OF DYES

It should be noted that illuminated dyes can be classified into n and p-type photoconductors. This classification correlates in many cases with the structure of the dyes.

i Triphenylmethane derivatives and rhodamines are characterised by n-type photoconductivity.

ii Merocyanines, phthalocyanines and pyrazines exhibit p-type photoconductivity. However structural changes and ambient effects can change the classification of a particular dye. Reported data on electrical parameters is very variable - sample purity and preparation have a crucial influence.

2.8 SPECTRAL SENSITISATION

In the process of spectral sensitisation the photon energy absorbed by a dye in contact with a solid substrate is transferred to the solid causing it to show photochemical or photoelectrical effects. The substrate can be either a semiconductor or an insulator.

The sensitised effects, brought about by absorbed dyes, are induced by quanta of energy less than those required to cause an intrinsic photoeffect in the substrate. This transfer of photoeffects to longer wavelengths is characteristic of dye sensitisation. The oldest, and most significant example of dye sensitisation, is used in the photographic process. The formation of an intrinsic latent image in (1) silver bromide is represented by

$$Br^- \rightarrow Br + e^-$$

$$Ag^+ + e^- \rightarrow Ag \leftarrow \text{latent image}$$

This process is sensitive to light only in the near-UV or at correspondingly higher energies. If the silver halide grains are coated with certain organic dyes, notably cyanines, however image formation can occur at all wavelengths in the visible region, and indeed into the near infra-red. A large number of dyes are known to have this effect. Conversely some dyes can also shift the response further into the UV (and are classed as desensitisers) but the mechanism of desensitisation is outside the scope of this review. An understanding of photographic sensitisation has been the driving force of much of the past work on spectra-sensitisation.

Reports have been published of a large number of photo-electrical effects which have been successfully sensitised by dyes. Such effects include the photovoltaic Becquerel effect, the Dember effect in intermittent light, changes in photocontact potentials. Also, more importantly, sensitisation has been observed in the photoconductivity of surface and sandwich cells, and in the photodischarge rate of the xerographic process. Sensitisation has been demonstrated in the following materials: Ge[14], Se[15], halides (including Ag halides[16]), CdS[17], oxides (ZnO[18], PbO[16], SiO_2[19]). A large number of dyes, have been shown to be effective for sensitisation including anionic dyes (easin, fluorescein, erythrosin) and cationic dyes (malachite green, fuschia, rhodamines, pinacyanole) and neutral dyes (phthalocyanine, merocyanine, chlorophyll).

An illustration from the work of Albrecht & Meier[20] of the photoconductivity of a CdS surface gap cell with and without sensitisation with nerocyanine dye is shown in Figure 2.3. The peak of photoconductivity is seen to shift from 5100Å without sensitisation to 6050Å in the presence of merocyanine. The sensitised photoeffect is also seen to be of comparable magnitude to the intrinsic effect.

Photographic desensitisers can also sensitise photoeffect in solids and this points to a difference in the mechanism of sensitisation of photoconductive effects on the one hand and photographic sensitisation on the other (possibly due to the requirement that in the photographic process, electrons have to be generated for replenishment of the dye molecule).

With such an array of examples it is difficult to draw universal conclusions but some general observations can be made.

1. The dye must be strongly adsorbed at the surface of the solid.[21] It has been suggested that this points towards a charge transfer from dye to substrate, however, on reflection this seems difficult to justify as the efficiency of any mechanism would surely be increased by good contact between dye and substrate. It is thought that if the photon energy absorbed by the dye molecule is transferred to the substrate, to release trapped charge carriers, the sensitisation could still take

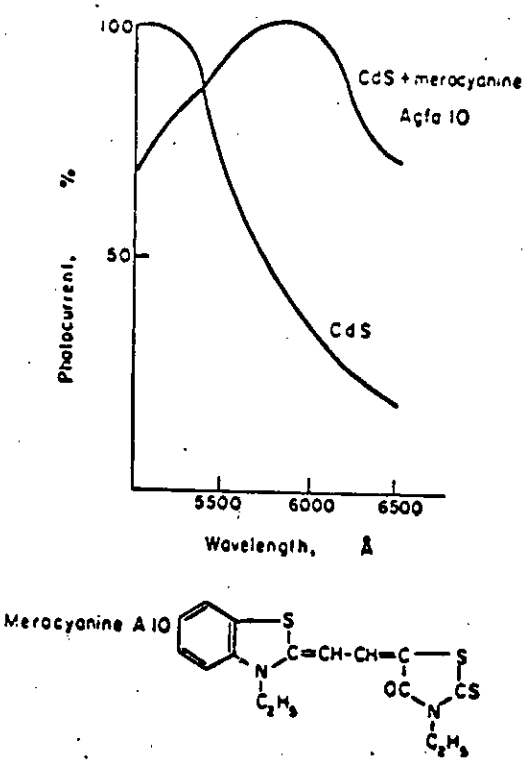

Fig. 1. Photoresponse spectra of sensitized CdS (layer thickness of dyestuff ≈ 1 μm).

Figure 2.3: (after Albrecht and Meier reference 20)

place with a small but finite distance between dye and the substrate. Planar molecules have been found to be more efficient in sensitisation.

2. The dye molecules in the sensitising layer can sensitise several times on average. Measurement of photocurrents in sensitised semiconductors (sandwich cell arrangements) show stability over long periods of illumination. In ZnO, about 250 electrons can be formed for each dye molecule i.e. no destruction of the dye molecule takes place.[22] The sensitised photocurrent in CdS is seen to saturate in 10^{-2}s and remain stable under constant illumination. These observations suggest that the sensitisation effect is electronic rather than chemical.

3. Sensitisation is not limited to regions in close proximity to the dye-solid interface. Increasing dye thickness (up to 6000Å in the case of Se [15]) gives more efficient sensitisation in some cases. Similarly, efficient sensitisation has been reported by Nelson in CdS coated with 1μm thick dye layers.[23]

4. The sign of the photostimulated charge carriers in the solid is, in general, the same as in the intrinsic photoeffect. This result was obtained by Teremin, Putzeiko and Akimov[24] during a series of experiments on the Dember effect and changes in contact potentials.

They found that in layers of ZnO, which is an n-type semiconductor, the photoinduced charge carriers are negative both in the intrinsic and sensitised effects. In AgI and TiI, which are both p-type semiconductors, the carriers are positive for both the sensitised and normal photoeffects. However, there are some exception to this rule and it has been demonstrated that a sensitised photocurrent in AgI is possible in which the charge carriers are electrons.[25] A similar dependence on sensitising dye has been reported for Se, where hole currents have been measured when sensitised with methylene blue and phenosafranine, but electron currents when sensitised with crystal violet and pinacyanole. It would seem that in n-type material the charge carriers are always negative but, there exists the possibility changing the sign of carriers in p-type material. Note should be taken, however, of the wide variance in data reported for apparently the same material. Much must presumably be due to the variation in sample preparation techniques.

5. The sensitised photoeffect may reach 80% to 100% of the intrinsic photoeffect i.e. the quantum efficiency of the sensitisation may approach unity.[26]

6. The spectral response of sensitisation effects show either a maximum at the wavelength of maximum absorption

of the monomolecularly 'isolated' absorbed dye or, in the case of crystal violet and pinacyanole the broadened spectral maxima due to the dye being in an agregated form.[27] Thus it is to be expected that the sensitisation should be closely related to the photoconductivity.

2.9 MECHANISMS FOR THE DYE-SENSITISATION EFFECT

Two theories of dye-sensitisation of photographic effects have been postulated. The older is the electron transfer theory first proposed by Mott and Gurney[28] and developed later by Meier[29], Nelson[30] and other workers.[31] This theory postulates that an absorbed photon creates an excited state in a dye molecule and the excited electron is transferred through the interface into the substrate. In the case of the sensitisation of photoeffects in a substrate, the electron is transferred into the conduction band of the substrate. This model has been updated to allow for hole injection. Importantly, the charge carrier contributing to conduction originates in the dye. To allow regeneration of the dye molecule to permit repeated sensitisation, it was suggested that the dye can be replenished by an electron from donor levels in the substrate. The early models of electron transfer can be summarised therefore as the generation of a free electron in the excited level of the dye which can travel through the closely packed layer of dye molecules to be transferred to the substrate and the subsequent replenishment of the dye molecule by an electron from a donor

state in the substrate, in the case of photographic sensitisation or from the metal contact for the case of sensitisation of photoeffects. An alternative theory has been proposed in which the energy absorbed by the dye is transferred, by some resonant coupling mechanism, to release a charge carrier from a trap in the substrate and the carrier could then contribute to conduction. In the energy transfer mechanism the carrier originates from within the substrate not from the dye.[26] The dye molecule, having released its absorbed energy, without emission of radiation returns to the ground state and is again ready to contribue to sensitisation.

The fundamental difference between the mechanisms is seen to be the origin of the charge carrier contributing to latent image formation or to conduction. The two mechanisms are illustrated in Figure 2.4.

The relative position of the energy levels in dye and substrate is of crucial importance and it is appropriate to consider this topic before a detailed discussion of the experimental evidence proposed for each sensitisation mechanism.

2.10 DYE AND SEMICONDUCTOR ENERGY LEVELS

The band model will be taken to apply to both the organic dye and the substrate which may be an insulator or a semiconductor and a scheme of energy levels is shown in Figure 2.5. All energies are measured in relation to the vacuum level at infinity, and are

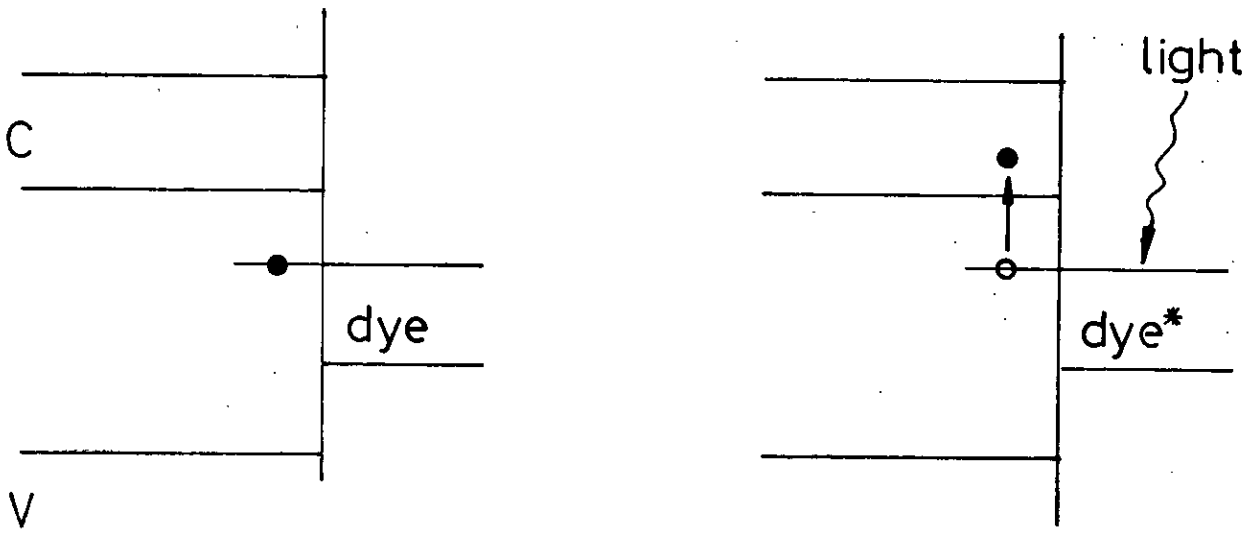

a) resonant mechanism

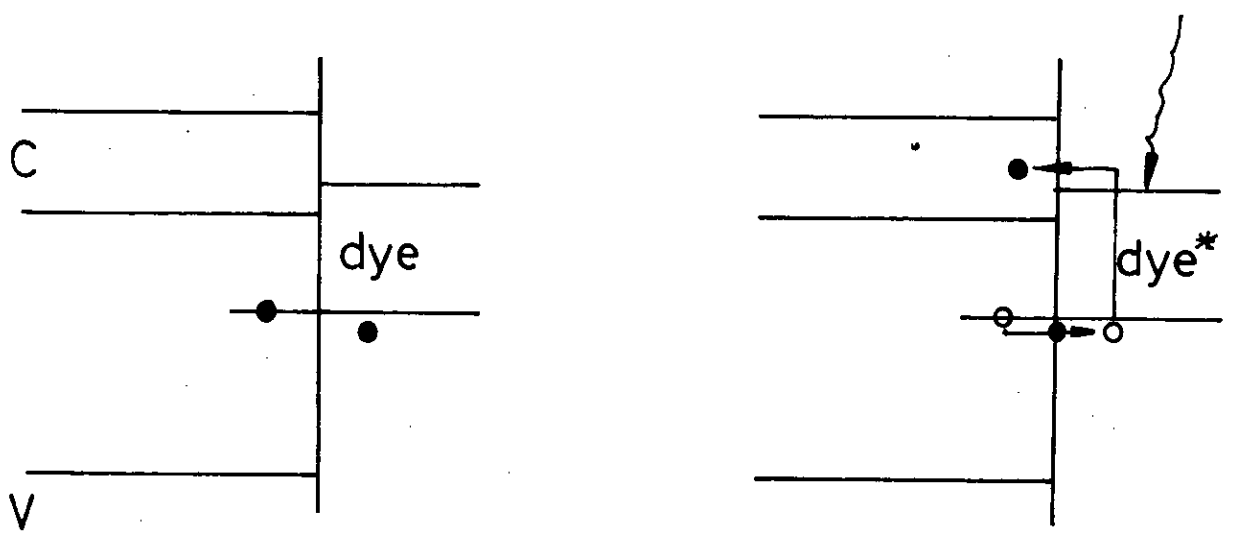

b) charge transfer mechanism

Figure 2.4: Sensitisation Mechanism

given in electron volts. No space charge effects are considered, but they could easily be accomodated by introducing a macropotential as a reference level; any space charge would appear as an offset between the macropotential and the vacuum level. It is important to note that any shifting of the macropotential will displace all other levels in an analogous manner.

The Fermi level, E_F, lies between the valence and conduction bands, nearer to the conduction band for n-type material and nearer the valence band for p-type.

The Fermi level lies at an energy ψ, the thermoelectric work function in vacuo below the zero level. The work function is defined as the energy required to raise an electron from the Fermi level to the top of any potential barrier existing at the surface. It can be calculated from measurements of the contact potential of the semiconductor and a metal. This potential is the difference between the work functions of semiconductor and metal.

The work functions of various dyes have been measured by Nelson [32] using the electron beam retardation method. Atmospheric and space charge effects can influence the work function, and thus the Fermi level of many materials, including dyes, is not known with great precision. The relative energies of the Fermi levels of two materials is of great importance in determining the nature of the contact between the materials.

The photo-electric work function, Φ, can be obtained from the long wavelength limit of the external photo-electric effect. This is equivalent to the ionisation potential of a solid or the energy of the valence band of the dye. Values for dyes have been obtained by Vilesov, Nelson and others.[33] [34] [35]

The optical energy gap, E, between valence and conduction bands can be obtained from measurements of the optical absorption edge. In some circumstances a band gap can also be calculated from measurements of the dark conductivity as a function of temperature and from the threshold energy of photoconductivity. Generally, however, there is no equivalence between band gaps obtained by different methods. The energy of the bottom of the conduction band relative to the vacuum level is defined as the electron affinity, χ, it is the negative work done in bringing an electron from outside into the conductive state. From measurement of the work function ψ Nelson[32] deduced the values of electron affinity for some dyes in which the Fermi level is near the conduction band. Terenin & Akimov[26] calculated values of the electron affinity from the difference between the photo-electric work function and the energy gap, thus

$$\chi = \Phi - E \qquad 2.18$$

Electrochemical methods can be used to gain further information (ies). Table 2 shows data collected from the literature for the energy levels of some typical dyes and semiconductors.

Solid	Type	ψ e.v.	Φ e.v.	χ e.v.	E. e.v.	Contact Potential m.v.
AgBr	p	5.33	6.0	3.5 3.5	2.5	Pd. -380 W -290
TlI	p	5.4	5.6	3.0	2.5	Pd. -450
CdS	n			3.5		
ZnO	n	4.84	7.3 6.3	4.3	3.0	Pd. +110
Rhodamine B	n	4.45 4.6	5.2 5.1	3.2	2.0	Pd. +500
Eryth-rosin	p	4.64	5.5 5.5	3.3 3.4	2.2 2.0	Pd. +310
Malachite green	n	4.86 4.6	... 5.2 5.2	... 3.2	2.0 1.6	Pd. +90
Pina-cyanol	(n)	4.55 3.1	4.9 7.28 4.6	3.1 5.1 3.0	1.8 1.6	Pd. +400 Cds. +320
Mero-cyanine	p	5.3	5.8 7.35 5.6	3.5 4.8 3.3	2.3 2.3	
Crystal violet	n	3.32 4.5	5.1 5.0	3.0	1.7	Cds. +180
Phthalo-cyanine	p		6.0	4.3	1.7	
Pheno-safranine		5.0	5.4	3.3	2.1	
Methy-lene blue Dye	p	5.2	5.4	3.6 3.4	1.8	

Table 2:

It should be noted that the electron affinity of many dyes is approximately 3.5eV. Schiebe[36] has postulated that the first excited electronic state of many organic molecules is situated 3.4eV below the vacuum level. This rule has been obtained from a study of the absorption bands of dyes in solution. The fact that the measured values of electron affinity in solid dye films are similar to the universal value of Schiebe confirms the identity of the position of the excited level of a single dye molecule with the conduction band of aggregated dye molecules. The shift of the energy level of dyes when absorbed on semiconductors is small, typically 0.1 to 0.2eV.

It is possible from data such as that collected in Table 2 to construct band diagrams which show the relative positions of the semiconductor (dye energy levels). Figure 2.6 shows such diagrams for AgBr/dye and ZnO/dye combinations.

The conduction band (or excited singlet level) of aggregated dye molecules is above the conduction band of some semiconductors, according to the data of Nelson and Schiebe.[34 36]

It must be bourne in mind, however, that according to measurements by Terenin & Akimov[26] of the photoionisation potential of dye molecules in the gas phase, the excited singlet level lies below the semiconductor conduction bands. It is unfortunate therefore that no firm conclusions can be drawn from existing knowledge of dye energy levels - the data for many dyes is conflicting.

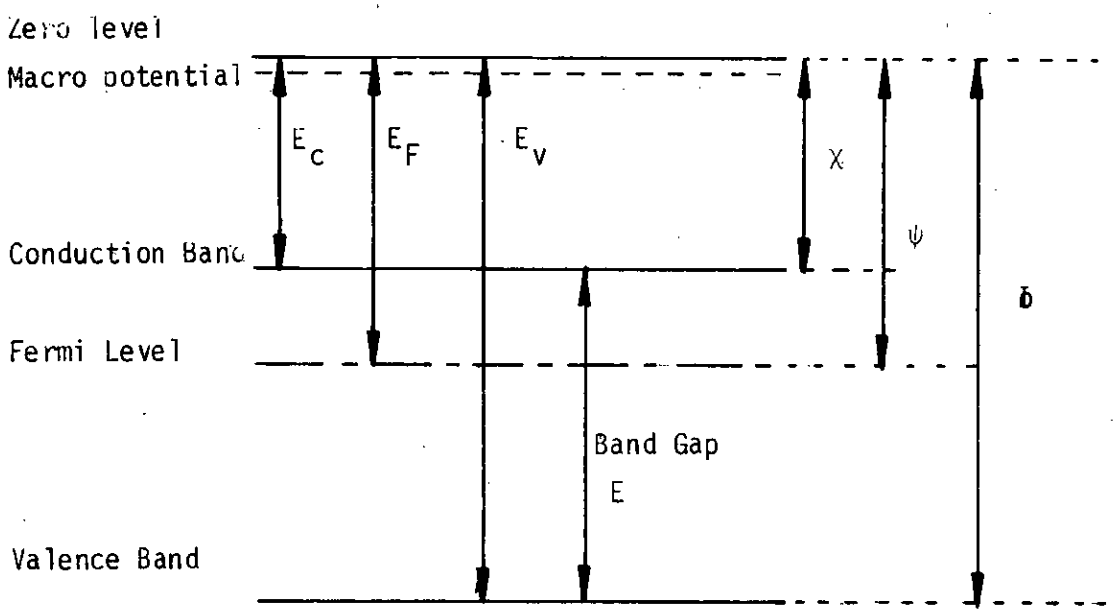

χ Electron Affinity

ψ Thermoelectric Work Function

ϕ Photoelectric Work Function

Figure 2.5: Energy Levels

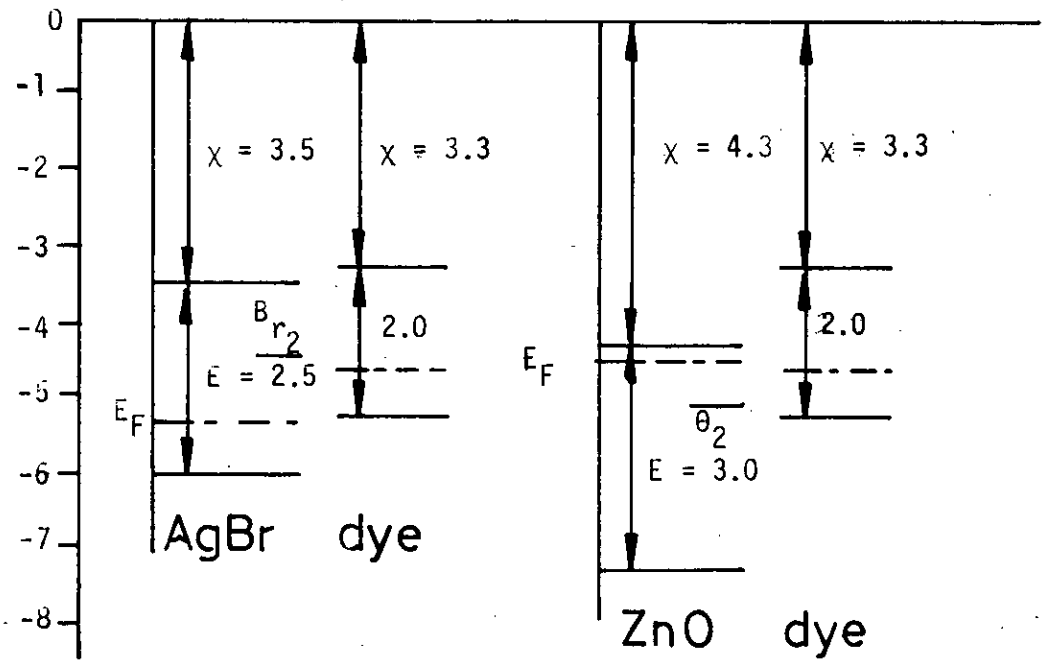

Figure 2.6:

2.11 RESONANT ENERGY TRANSFER MECHANISM

The energy transfer mechanism has been developed by Terenin, Akimov and Kuhn[37 38]The photon energy absorbed by the dye is transferred to intermediate and surface states which release their trapped carriers to the conduction band of the substrate. As can be seen from Figure2A, the energy requirement is that the excited dye level should be close to a trap-level which lies below the conduction band of the semiconducting (or insulating) substrate. Evidence exists to show that this energy scheme is possible, particularly from the calculation of Coulson[37] and Akimov which suggest that the excited level, of the dye is too low to permit electron transfer to the conduction band of the substrate. There is no doubt that suitable trapped charge exists in many semiconductors, and especially in insulating materials in which it is known that conduction is often extrinsic. These traps can arise from surface effects, grain boudaries, defects and from absorbed impurities e.g. electronegative gases such as oxygen and bromine which produce an enhancement of the sensitised photo-conductivity in silver halides.

Evidence in favour of the energy transfer mechanism is provided by the experiments of Kuhn [39] which prove that energy can be transferred from one system to another over distances of 50 - 100 Å. In these experiments a layer of dye excited fluorescence in a second dye layer even though the layers were seperated by a film of an insulating fatty acid salt.

Kuhn also observed latent image formation in a system where the sensitising dye was seperated from the AgBr surface by arachidate monolayers. Thus, there is experimental evidence in favour of an energy transfer mechanism. The energy transfer would be limited to a distance of 50 - 150 Å and it is difficult therefore to explain why strong absorption of the dye is necessary and why the sensitisation efficiency increases with increasing dye thickness. It seems unlikely that exciton propogation could explain this behaviour. It must also be recognised that electrons can travel through insulating films of several molecular layers, either by tunneling or by Schottky and Poole-Frenkel emission. Some doubt must remain regarding the interpretation of the experiments of Kuhn.

2.12 CHARGE TRANSFER MECHANISM

The electron transfer mechanism involves the excited dye molecule transferring an excited electron to the substrate. Various experimental observations support this theory e.g. the necessity for good absorption, sensitisation with thick dye layers and the regeneration of photo-ionised dyes.

Electron transfer implies that the lowest vacant level of the dye is above the conduction band of the semiconductor (or, for hole transfer that the highest occupied energy level of the dye is below the valence band of the semiconductor). Schiebe's rule would in general support this scheme (as a

consequence the groundstate lies at about 5eV). Thus there is evidence, both theoretical and experimental, for the energy levels of dyes and semiconductors which support the electron transfer hypothesis. Some results are given in Table 3.

2.13 MECHANISM OF INJECTION

a. Direct Injection[40]

Photoexcited dye molecules inject electrons into the conduction band or holes into the valence band. In addition to the photon energy, an energy ΔE must be supplied for the electron to travel through the potential barrier between dye and semiconductor. The quantum yield, γ will be

$$\gamma = \frac{f.t.\tau}{1 + f.t.\tau} \exp(-\Delta E/kT) \qquad 2.19$$

where t is the transparency of the barrier, τ, the lifetime of the excited state ($\sim 10^{-9}$s) and 'f' the frequency of the electron in the potential well ($\sim 10^{15}$ s^{-1}). This equation predicts a high efficiency, approaching unity, for barriers of 5Å width.

b. Combined Dark and Photo Processes

Grossweiner and co-workers[41] have postulated a Schottky barrier model for ZnO/dye systems. A Schottky barrier is formed

Observation	In Favour of	
	Charge transfer	Energy Transfer
1. Absorption condition	+	
2. Regeneration of the dye		
(a) Photoconductivity	+	+
(b) Photoionisation	+	
3. Sensitisation by thick layers	+	
4. Hole and electron injection		
(a) Normal effect ($\ominus \rightarrow n; \oplus \rightarrow p$)	+	+
(b) Dependence of λ_{max} (dye)	+	
5. Quenching of dye fluorescence	+	+

Table 3: Experimental Facts on Photosensitisation

in the dark by transfer of electrons from the ZnO to the dye with the electrons retained in trapping levels near the interface. Under illumination the trapped electrons are transferred back. The dye has to provide electron trapping levels close to the ground level of the dye molecules. That the ZnO resistance increases on addition of the dye and that the surface potential changes during light flashes is taken as support for this mechanism. Evidence exists for a Schottky barrier being formed at the interface.

Meier[42] has extended this model by postulating that in the dark, an electrostatic field builds up by an electron exchange between dye and substrate as a consequence of the overall tendency to make the electrochemical potential of electrons equal on both sides of the boundary. Under illumination, there is a seperation of optically formed electron-hole pairs under the internal field. The relative positions of the Fermi levels and of valence and conduction bands before contact of dye and semiconductor are decisive for the electron transfer. Electron transfer may be observed during illumination when the Fermi level of the dye is below the Fermi level of the semiconductor. That is, photosensitisation of an n-type solid can be obtained with either a p-type or an n-type dye characterised by a Fermi level which lies below that of the substrate (photo conductor).

Regensberger and Petruzella[43] reported the sensitisation of the Zerographic effect in selenium by H_2P_c. The effect is strong-

ly field-dependent and was interpreted in terms of a Schottky-type emission across a barrier between sensitiser and substrate. The injection efficiency, G, is given by

$$G = \exp\ (\beta\mathcal{E}^2/2kT) - (Wo/kT) \qquad 2.20$$

where β is the Schottky coefficient, $\mathcal{E}$ the applied field and Wo the activation energy. The data yielded a value for the electron barrier less than 0.1eV.

In conclusion, it would appear that the weight of opinion is in favour of the electron transfer hypothesis. However the variation in published data must be remembered in any analysis and apparently conflicting observation could often be due to "local" variations in sample preparation technique.

CHAPTER TWO : REFERENCES

1. Moser, J. & Rigollot, H., Compt. rend. acad. sci. Paris 116, 873.

2. See for example "Pigments: An introduction to their Physics and Chemistry", ed. D. Patterson, EPL.

3. Bayliss, N., J. Chem. Phys., 16 (1948) 287.

4. Kuhn, H., J. Chem. Phys., 16 (1948) 840.

5. Simpson, W.T., J. Chem. Phys., 16 (1948) 1124.

6. Frenkel, J., Phys. Rev., 37 (1931) 17.

7. Harrison, S.E., J. Chem. Phys., 50 (1969) 4739.

8. Hansel, H., Ann. Physik. 24 (1970) 147.

9. Kepler, R.G., Phys. Rev., 119, (1960) 1226.

10. See "Organic semiconductors and Biopolymers", Hazzard, New York: Plenum Press (1970).

11. Inokuchi, H., Maruyama, Y. & Akamatu, H., "Electrical conductivity in organic solids", pp 69, New York - London, John Wiley (1961).

12. Ghosh, A.K. & Feng, T., J. Appl. Phys. 44, (1973) 2781.

13. Nelson, R.C., J. Chem. Phys. 29, (1958) 388.

14. Terenin, A. & Putzeiko, E., Angew. Chem. 70, (1958) 508.

15. Ing, S.W. & Chiang, Y.S., J. Chem. Phys. 46 (1967) 478.

16. Akimov, I., Phot. Sci. Eng. 3, (1959) 197.

17. Nelson, R.C., J. Opt. Soc. Am. 46, (1956) 13.

18. Meier, H., "Spectral Sensitisation". Focal Press, New York - London (1968).

19. Nelson, R.C., J. Opt. Soc. Am. 50, (1960) 1029.

20. Meier, H., J. Phys. Chem. 69 (1965) 719.

21. Bourdon, J., J. Phys. Chem. 69, (1965) 705.

22. Matejec, R., Z. Elektrochem. 65, (1961) 183.

23. Nelson, R.C., J. Opt. Soc. Am. 51, (1961) 1182.

24. Terenin, A., Putzeiko, E. & Akimov, I., Discussions of Faraday Soc. 27, (1953) 83.

25. Terenin, A. & Putzeiko, E., "Proceedings of the International Colloquim Liege 1959", Pergamon Press, Oxford, 1962, pp 532-543.

26. Terenin, A. & Akimov, I.A., Z. Physik, Chem. 217, (1961) 307.

27. Scheibe, G., Z. Elektrochem. 52, (1948) 283.

28. Gurney, R.W. & Mott, N.F., Proc. Roy. Soc. (London) A164 (1938) 151.

29. Noddack, W. & Meier, H., Z. Elektrochem. 63 (1959) 971.

30. Nelson, R.C., J. Opt. Soc. Am. 48, (1958) 948.

31. Scheibe, G. & Dorr, F., "Proceedings of the International Colloquim Liege 1959", Pergamon Press, Oxford, 1962 pp. 515-531.

32. Nelson, R.C., J. Opt. Sci. Am. 46 (1956) 1016.

33. Vilesov, F.I., Dokl. Akad. Nauk SSSR, 132, (1960) 632.

34. Nelson, R.C., J. Opt. Soc. Am. 51 (1961) 1186.

35. Taft, E.A., Phillips, H.R. & Apker, L., Phys. Rev. 110, (1958) 876.

36. Scheibe, G., Bruck, D. & Dorr, F., Chem. Ber., 85, (1952), 867.

37. Terenin, A. & Akimov, I., J. Phys. Chem. 69, (1965), 730.

38. Bucher, H., Kuhn, H., Mann, B., Mobius, D., von Szentpaly, L. & Tillman, P., Phot. Sci. Engng. 11, (1967) 233.

39. Kuhn, H., "Dye Sensitisation - Symposium Bressanone", ed. Berg W.F. Focal Press, London and New York (1970) pp. 199.

40. Nelson, R.C. & Selsby, R.G., Phot. Sci. Engng. 14 (1970) 342.

41. Dudkowski, S.J., Kepka, A.G.& Grossweiner, L.I., J. Phys. Chem. Solids 28, (1967) 485.

42. Meier, H., J. Phys. Chem. 69 (1965) 719.

43. Regensburger, P.J. & Petruzella, N.L., J. Non-crys. Sol. 6, (1971) 13.

3. CONDUCTION IN INSULATORS

Thin insulating films have assumed great technological importance especially in integrated circuit production. In particular films of silicon dioxide are crucial to the operation of MOS IGFET devices. Currently, film thicknesses down to 1000 Å are used but future developments in VLSI may well see the routine use of dielectric films less than 100 Å thick. It is appropriate to consider the possible conduction processes in thin insulators and the techniques for their production. Experimental techniques commonly use metal-insulator-metal or metal-insulator-semiconductor test structures.

3.1 FILM PREPARATION

For D.C. measurements in particular, films of thickness less than 1μm are required. The thin film sample allows high electric fields to be generated which force currents to flow at levels which are easily measured. Insulators such as SiO_2, Si_3N_4, PVK and Al_2O_3 have all been investigated as thin films. SiO_2 and Si_3N_4 play important roles in contemporary MOS processing and consequently great effort has been expended in refining their preparation techniques.

The most common techniques for the preparation of thin films are thermal oxidation, vacuum evaporation and sputtering, chemical vapour deposition and anodisation. With all methods of preparation, great care has to be taken to prevent the inclusion of unwanted

impurities. Thermal oxidation is used for the production of SiO_2 and Al_2O_3. For example oxygen or wet oxygen can be passed over silicon heated to 900 - 1000°C and a coherent film of SiO_2 will be grown on the surface. The deposition rate decreases with time in a hyperbolic fashion due to the requirement of the oxidising species to diffuse through the existing oxide to the substrate for subsequent reaction. The oxidising atmosphere must be carefully controlled in terms of composition, temperature and pressure if reproducible results are to be obtained. Contamination, particularly by ionic species can occur from the oxidising atmosphere. The kinetics of the silicon oxidation are discussed in reference 1.

Vacuum deposition techniques allow insulator materials to be deposited on any substrate material, independent of substrate composition or crystallographic nature. By these methods, for example, films can be deposited over metal electrodes. During vacuum evaporation the source material is heated directly either by an electrical filament or by a focussed electron beam. For compound materials, some non-stoichiometry of the evaporated film can be encountered due to the components having different evaporation rates. This same reason results in the composition of the source changing with evaporation and thus analytical checks on film composition are desirable. Sputtering can either be radio-frequency powered or, less usually, D.C. powered. Compounds can be sputtered without as great a risk of composition change or loss of stoichiometry. During vacuum evaporation, contamination can arise due to residual gases in the vacuum chamber; at least

10^{-5} torr should be used. In sputtering, the plasma support gas can lead to contamination. Both techniques suffer from evaporation of the source crucible which can be incorporated in the deposited film. Substrate temperature control is possible and to some extent allows film structure to be controlled. Under the same deposition conditions, the deposition rate is constant. These techniques have been used to prepare films of SiO_2, PVK, teflon, CdS and many other materials.

Chemical vapour deposition (CVD) requires the passing of a mixture of reactive gases over heated substrates. The products from the reaction which takes place at the hot surfaces, are deposited as a coherent film.[2,3] For example, SiO_2 can be produced by passing silane gas and oxygen over heated substrates; the reaction.

$SiH_4 + 2O_2 \xrightarrow{450^oC} SiO_2 + 2H_2O$ occurs. Silicon nitride, can be produced from the reaction of dichlorosilane, SiH_2Cl_2 with ammonia at 800^oC. These processes are used in semiconductor processing and are characterised by a high deposition rate and by the ability to intentionally dope the deposited film e.g. phosphorus can be incorporated in SiO_2 by adding phosphine to the gas mix. These processes are used at atmospheric or reduced pressure (~300 millitorr). The deposition rate is constant.

The film structure is amorphous or polycrystalline, depending strongly on factors such as deposition rate and substrate temperature. Poor adhesion of the films to the substrate and the subsequent application of contacts to the film are both problems which are frequently encountered. It will be appreciated that

all these processes are controlled by many parameters and careful control is needed if films of reproducible quality are to be obtained. Indeed it should be borne in mind that many materials produced are unique to their particular laboratory and this must account for some of the variation in results reported on apparently the same material.

3.2 BAND STRUCTURE OF INSULATORS

Band structure, developed for materials with a periodic lattice e.g. metals and crystalline semiconductors, can be applied with modification to amorphous and polycrystalline materials. From studies of the band structure of semiconductors on the transition from a crystalline phase to liquid phase, it is seen that the concept of band structure is still valid although the long-range order of the semiconductor is lost. A broadening of the bands takes place and a tail in the density of states, containing localised states or traps, stretching into the energy gap is found to be present.[4,5] The short range order i.e. nearest neighbour interaction is found to dominate in the production of an energy band system. That an energy gap exists in amorphous materials is demonstrated by the fact that glass is transparent to visible light. However, having noted the presence of the localised states, the band structure of amorphous materials will be represented with a well defined energy gap, the smearing of the band edges will, to a first approximation, be ignored.

Conduction is, in general, extrinsic; the activation energy for electronic conduction is usually less than half the optical band gap. For SiO , the optical band gap is 9eV, whereas the activation energy for conduction is less than 1eV. The current density is often much higher than would be expected. The source of this extrinsic conductivity is thought to be the inherent defect nature of amorphous materials. Defects arise from many sources, e.g. non-stochiometry of the film can result in donor centres in the film. Contamination from, for example, the crucible material can also contribute. The role of impurity atoms in amorphous materials is less clear than in crystalline semiconductors. Electrical activity of the impurities is less in amorphous materials possibly due to the structure being more able to accommodate the impurity through dangling bonds and vacancies. Trap centres arise due to the lack of periodicity, grain boundaries and internal stresses within the film. These traps contribute to the extrinsic conduction.

3.2.1 Traps in Insulators

Traps and the kinetics of trapping and detrapping will be reviewed in this section with particular reference to SiO_2, the insulator used in the present work. Firstly the trapping phenomenon will be discussed.

i Trapping

Trapping sites can be either coulombic attractive, neutral or

coulombic repulsive will capture cross-sections in the ranges 10^{-16} - 10^{-18} m^2, 10^{-18} - 10^{-22} m^2 and 10^{-22}- 10^{-25} m^2 respectively. Energy is given off during capture usually by phonon emission (non-radiative capture) although photon emission has been reported.[6]

a. Coulombic attractive capture

When a thermal carrier moves within the capture radius r_c of a coulombic attractive centre (approx 100 Å at room temperature) it can be captured by losing energy in steps, emitting a single phonon with each step. The carrier has a finite probability of absorbing phonons and being re-emitted to the conduction band. Consequently, the capture cross section increases as temperature decreases, as the probability of re-emission is reduced. The cross section also depends on the -3/2 power of electric field.[7]

b. Neutral centre capture

The majority of trapping centres in SiO_2 fall into this class. These traps are neutral initially and are usually deep. The capture cross sections exhibit weaker temperature and field dependences than that of coulombic attractive centres.[8]

c. Coulombic repulsive capture

Little is known about these traps but they are thought to

exist near interfaces e.g. Na^+ sites near the Si - SiO_2 interface. Cross section is an increasing function of temperature and field.[6]

ii Detrapping [9]

Once an electron is captured by a trapping site, it can be discharged by phonons, photons, field emission (tunneling) or by impact ionisation. First order rate equations can be used to describe detrapping e.g.

$$\frac{dN_t}{dt} = k_c (N - N_t) - k_p N_t - k_t N_t \qquad 3.1$$

where $k_c = n_c \, Vth \, \sigma_c$

$k_p = F_p \, \sigma_p$

$k_t = N_c \, Vth \, \sigma_c \exp(-E_t/kT)$

N_t is the trapped charge density, N the total trap density, N_c the conduction band electron density, Vth the thermal velocity, σ_c the captive cross section, F_p the local photon flux, σ_p is the photo-ionisation cross section, N_c the effective density of states in the conduction band and E_t is the trap energy depth from the conduction band edge. The evolution of trapped charge Q(t) is given by

$$Q(t) = Q(0) \exp(-t/\tau_p) \qquad 3.2$$

where τ_p is the photo-ionisation time constant, and there is little significant retrapping (a reasonable assumption in SiO_2).

iii Traps in SiO_2

a. Sodium related traps

There is in thermally grown SiO_2 a coulombic attractive centre at 2.4eV below the conduction band. The trap is spatially distributed in a uniform manner in the SiO_2 layer and densities between 10^{18} m^{-3} to 10^{21} m^{-3} have been measured. Considerable detrapping takes place on heating to 160°C. [10]

b. Water related traps

These neutral sites are believed to be related to H_2O incorporation into the SiO_2 during growth. The traps are not uniformly distributed throughout the oxide but occur in greater numbers near the interface. The traps will discharge thermally at temperatures of 200°C or above with an activation energy of 0.35eV.[11]

c. Other traps

Many traps, incorporated into SiO_2 films by ion implantation have been studied but of particular importance to semiconductor device performance are P and As related traps. Hole traps are thought to exist near the Si-SiO_2 interface but their investigation is difficult due to the difficulty in causing detrapping.[9]

UNIV. EDINBURGH EX BIBL

3.3 CONTACTS TO INSULATORS

The conductivity of an electrode-insulator-electrode system is not necessarily determined solely by the bulk properties of the insulator but also by the electrode-insulator interfaces. Conduction can be either bulk-limited, in which the insulator properties dominate, or electrode limited in which the electrode-insulator interaction dominates. Measurements on such systems, must be interpreted in view of the contact existing.

Contact between an electrode and an insulator gives rise to a potential barrier in the insulator. The height of this barrier and the shape of the insulator conduction band base are governed by two conditions:

i The vacuum and Fermi levels of the insulator and electrode are continuous across the interface.

and

ii Beyond the interface, the energy difference between the insulator vacuum and Fermi levels will equal ψ_i the work function of the insulator. If the barrier height is $\emptyset$, the metal work function ψ_m and the insulator electron affinity χ, condition (i) can be written

$$\emptyset = \psi_m - \chi \qquad 3.3$$

Three possibilities exist for contacts: $\psi_m < \psi_i$, $\psi_m = \psi_i$ and $\psi_m > \psi_i$. Different properties can be expected for each case.

a) Ohmic Contact

An ohmic contact arises when $\psi_m < \psi_i$ and the resulting energy band system is shown in Figure 3.1a. To achieve equilibrium, electrons are injected from the metal into the insulator conduction band giving rise to a space charge region, the accumulation region.

(During this discussion of contacts and conduction processes, electron flow will be considered, hole currents can be treated similarly but it should be borne in mind that in most insulators, the electron mobility is much greater than the hole mobility e.g. in SiO_2, the electron mobility is 10^{-2} $m^2V^1s^{-1}$ whereas the hole mobility is 10^{-8} $m^2V^{-1}s^{-1}$).

The accumulation region acts as a reservoir of charge and can supply electrons as required. The conduction is limited by processes in the bulk of the insulator and not by the rate of supply of electrons by the electrode and is called bulk limited. The width of the accumulation region, λ, to where the conduction band edge is flat is given by.

$$\lambda = \frac{\pi}{2} \left(\frac{2kT\, K\, \epsilon_0}{e^2 Nt}\right)^{\frac{1}{2}} \exp\left(\frac{\psi_i - \chi - Et}{2kT}\right) \qquad 3.4$$

where Nt is the density of shallow traps at energy Et below the conduction band. For $\psi_i - \chi - Et = 0.4eV$ and $Nt = 10^{26}m^{-3}$ then $\lambda = 2\mu m$. For thin samples i.e. thickness, $L \simeq 2\lambda$, the energy bands across the width of the insulator are curved. An electric field exists throughout the sample and the space charge swamps the intrinsic charge i.e. the conduction is extrinsic.

b) Neutral Contact

When $\psi_m = \psi_i$, no transfer of charge between metal and insulator takes place and hence no band bending is present. At low current levels, the contact can supply all the charge required by bulk processes and the contact is ohmic. However, when the current exceeds the limit imposed by the thermionic emission over the barrier, the contact is no longer ohmic. The neutral contact is illustrated in Figure 3.1b.

c) Blocking Contact

When $\psi_m > \psi_i$, electrons flow from insulator into the metal, a region of positive charge called the depletion region exists in the insulator and the contact is termed blocking. This contact is also referred to as a Schottky barrier. A negative charge, equal to the charge contained in the depletion region exists on the metal electrode. A local electric field exists in the insulator which causes the conduction band to bend downwards,

until, in the bulk of the insulator, it lies ψ_i below the vacuum level as illustrated in Figure 3.1(c). The free electron density in the depletion region is lower than in the bulk and the conduction of electrons through the system will be limited by the rate at which electrons can flow over the Schottky barrier, i.e. the conduction is electrode limited.

Any voltage bias applied to the system, will, once equilibrium has been established, be absorbed across the depletion region as the conductivity in this region is lower than in the bulk. The width of the depletion region, λ, is given by

$$\lambda = \left(\frac{2(\psi_m - \psi_i)K\epsilon_0}{Nde^2}\right)^{\frac{1}{2}} \qquad 3.5$$

where Nd is the donor density in the bulk. On application of a negative bias, V to the metal

$$\lambda = \left(\frac{2(\psi_m - \psi_i + eV)K\epsilon_0}{Nde^2}\right)^{\frac{1}{2}} \qquad 3.6$$

i.e. the depletion region stretches further into the bulk. For $Nd = 10^{25}\ m^{-3}$, $V = 0$ then $\lambda = 10^{-8}$m..

The investigation of the conductivity of insulator films can be seen to depend crucially on the type of contact formed: often a blocking contact forms, the conductivity is electrode limited and very little information can be gathered about bulk conduction processes. Sample thickness must be taken into account as shown in the discussion of ohmic contacts.

Surface states, when present can change the barrier height. These states exist at the insulator surface and can be due to the loss of periodicity (Tamm States), and to the chemical nature of the surface e.g. non-stoichiometry, absorbed gases and ionic impurities. Their presence depends to a great extent on the preparation of the film but some procedures can reduce their concentration. For example, the surface state density at the Si - SiO_2 interface (after thermal oxidation) can be reduced by annealling at high temperatures in an inert atmosphere. The electronic properties can be dominated by these states. Due to the strong dependence on the past history of the surface, it is difficult to draw strong conclusions from the experimental investigations of surface states reported in the literature. The following discussion of conduction mechanisms will ignore surface states.

For a further discussion of contact properties see references 12 and 13.

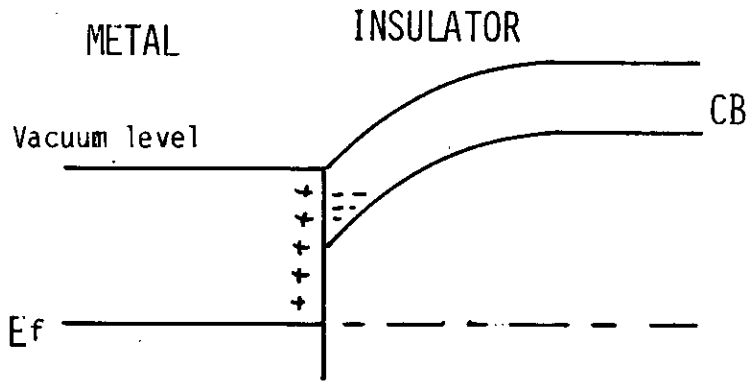

a) ohmic contact

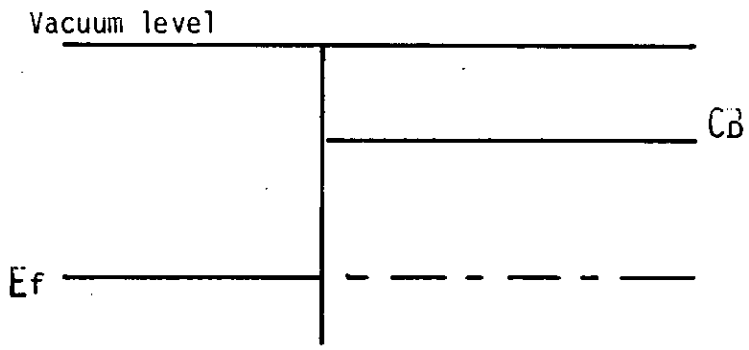

b) neutral contact

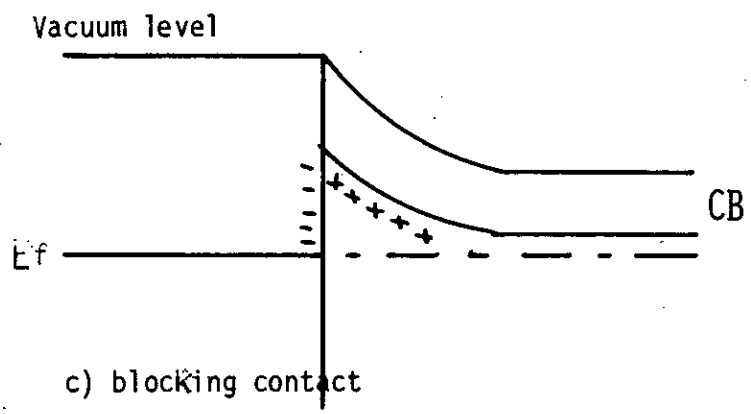

c) blocking contact

Figure 3.1: Contact energy levels.

3.4 CONDUCTION MECHANISMS

Two classes of conduction are possible in insulators, ionic conduction and electronic conduction.

a Ionic Conduction [14]

Ionic conduction depends principally on the rate of drift of ions through the insulator due to an applied field. The defects drift due to the movement of ions over a potential barrier from one defect site to another. Ionic currents are characterised by the presence of polarisation effects in a constant field. If ionic currents are dominant then the resistivity of the film at constant applied field, will increase with time. A possible explanation is that the ions migrate to one electrode and, as they are not discharged, a build up of space charge takes place. Most of the applied voltage is dropped across the space charge region causing the field in the insulator to be non-uniform. The resistivity could be expected to rise under these conditions. Alternatively the dielectric relaxation theory suggests that the increase in resistivity is due to a time-dependent reorientation of the dipoles existing in the material. Other characteristics of ionic conductivity are material transport to one electrode and long ion transit times. Material transport can be observed by biasing the film to a high current and noting chemical changes at the electrode.

Much work has been published regarding ions in SiO_2 usd for MOS device applications. The most common ions present are

thought to be Na^+ and a hydrogen species H_3O^+. Both ions are highly mobile at temperatures above 100^oC. The mobility is highly temperature activated, with activation energy for Na^+ of 1.48eV but decreasing with increasing sodium concentration.[15] Ions will be mobile at any temperature in high fields ($\sim 10^7 V m^{-1}$). There is evidence that Na^+ can be trapped and prevented from drifting. A layer of phosphorus doped glass is used for this purpose in MOS technology. Ions can cause instabilities in devices and shortening of device lifetime, and thus great care is taken to prevent ionic contamination.

Nauta and Hillen[16] have used the thermally stimulated ionic current method to investigate mobile ions in SiO_2. The ionic drift current is monitored during heating of the film. Peaks in current corresponding to the release of ions from traps are seen.

b. Electronic Conduction[17]

i Space Charge Limited Currents (SCL)

Only single carrier currents will be discussed. Initially a trap free insulator and an insulator with a single shallow trap level will be considered.

When an ohmic contact exists on an insulator and when the insulator thickness is less than twice the accumulation layer width, the current is space charge limited. For a trap-free insulator, the current-voltage relationship is given by an equation

developed by Mott and Gurney[18]

$$I = \frac{9\mu K\varepsilon_o}{8S^3} V^2 \qquad 3.7$$

where V is the applied bias and S the sample thickness. Although the parabolic dependence on V has been observed in practice, the current predicted by 3.7 is much higher than measured. Also, a temperature independence is implied which is contrary to observation. This simple theory must be extended towards a more realistic model, that of an insulator with traps.

When an insulator contains traps, much of the injected space charge is trapped and the free carrier density is much lower than for the trap free case. Also, since the occupancy of traps is temperature dependent, the SCL is predicted to be temperature sensitive. To extend the theory, consider an insulator containing Nt traps at an energy Et below the conduction band. Then as stated by Rose[19], the ratio of free to trapped charge, θ, is

$$\theta = \frac{N_c}{N_t} \exp\left(\frac{Et}{kT}\right) \qquad 3.8$$

and equation 3.7 is modified thus

$$J = \frac{9\mu K\varepsilon_o\theta}{8S^3} V^2 \qquad 3.9$$

θ is small and temperature dependent. Some observation is adequately described by equation 3.9.

At low voltages, the injected free carrier density is smaller than the volume generated free carrier density and ohmic conductivity will be observed. The voltage for transition to SCL conductivity is given by [17]

$$Vx = \frac{en_0 S}{\theta K \varepsilon} \qquad 3.10$$

where n_0 is the bulk free carrier density. At high voltages, the traps become filled and the insulator is effectively trap free. A large increase in current is observed and the conductivity is described by equation 3.7. The voltage, above which trap-free conductivity is seen is given by

$$V_T = \frac{e N_t S^2}{2K\epsilon_0} \qquad 3.11$$

Thus the conductivity is expected to show a transitions from ohmic to trap-limited SCL to trap-free SCL. From the structure of the J-V characteristic, information should be deduced about the trapping levels in the insulator. The current bulk is limited.

Early work by Flynn [20] suggested that the dye-sensitised photo-injected current into SiO_2 was described by a trap-free SCL.

Exponential Trap Distribution.

In amorphous materials, a distibution of trap levels is expected rather than a discrete level of traps. Rose [19] has considered the case of space charge limited conduction in the presence of an exponential distribution of traps i.e.

$$N_t = A \exp\left(-E_t/kT_c\right) \qquad 3.12$$

where E_t is the energy measured from the bottom of the conduction band and T_c is a characteristic temperature greater than that at which the current is measured. Then

$$J \propto V^{(T_c/T+1)} \qquad 3.13$$

which means that since $T_c > T$, the current increases more rapidly with applied field than in the case of the trap-free or discrete trap level.

ii Tunnelling [12]

If an insulator film is thin (less than 40 Å thick) direct tunnelling of carriers from one electrode to the other can take place. This conduction is characterised by a very slight quadratic dependence on temperature. In this work, insulator films were always greater than 1000 Å thick and it is unlikely that direct tunnelling would be exhibited. With the advent of VLSI, a gate oxide thickness will be reduced to around 100 Å or less and it is possible that tunnelling will become more important. However, Fowler-Nordheim tunnelling is a possible conduction mechanism and should be considered.[21]

When blocking contacts exist on an insulator, the contact potential barrier depends on the applied bias. If a high bias is applied, the barrier is narrowed and becomes triangular in shape. Carriers can tunnel through the barrier from the metal Fermi level into the conduction band of the insulator. At high fields, the barrier width can be reduced to below 50 Å. The isothermal Fowler-Nordheim current is described by

$$J = \frac{3.38 \times 10^{10} F^2}{\Phi} \exp\left(-\frac{0.69\,\Phi^{3/2}}{F}\right) \qquad 3.14$$

Lenzlinger and Snow[21] studied tunnelling in Si - SiO_2-Al structures. The oxide was of thickness 600 - 5000 Å and at applied fields of 5×10^8 V $<m^{-1}$, $\ln J/F^2$ was found to be proportional to F^{-1}, as predicted by equation 3.10. The Fowler-Nordheim currents are electrode limited.

iii Schottky Emission

As well as the possibility of tunnelling through the potential barrier at a blocking contact, carriers can also be emitted over the barrier into the conduction band of the insulator a process known as Schottky emission. It is analogous to thermionic emission except that the applied field lowers the potential barrier height through the interaction of the electrode image-force with the field at the metal-insulator interface and is given by [12]

$$\Delta\phi_S = \left(\frac{e^3}{4\pi\epsilon_0 K}\right)^{\frac{1}{2}} F^{\frac{1}{2}}$$

$$= \beta_S F^{\frac{1}{2}} \qquad 3.15$$

This current, like tunnelling currents, is electrode limited and the conductivity is given by

$$\sigma = \sigma_0 \exp \left(\frac{e^3}{4\pi\epsilon_0 K}\right)^{\frac{1}{2}} F^{\frac{1}{2}}/kT \qquad 3.16$$

Schottky emission gives rise to currents which are of similar magnitude to tunnelling currents and thus experimental evidence for Schottky emission is not entirely convincing. However, Pollack [22] has reported currents conforming to 3.12 in Al_2O_3. The strong temperature dependence of Schottky currents allows the seperation from tunnelling currents. Above 200K the current is strongly temperature dependent - Schottky emission; but below 200K is essentially temperature independent - tunneling current.

iv Poole-Frenkel Effect

The Poole-Frenkel effect is the bulk analogue of the Schottky effect, applied to the thermal excitation of electrons from traps into the conduction band. When a field is applied to the insulator the coulombic potential barrier bounding the trap is lowered by an amount[2 3]

$$\Delta\Phi_{PF} = \left(\frac{e^3}{\pi\varepsilon_o k}\right)^{\frac{1}{2}} F^{\frac{1}{2}} = \beta_{PF} F^{\frac{1}{2}} \qquad 3.17$$

This reduction in potential means that the probability of an electron being thermally excited out of the trap into the conduction band is increased. The current is given by

$$J = J_o \exp\left(\frac{\beta_{PF} F^{\frac{1}{2}}}{kT}\right) \qquad 3.18$$

Poole-Frenkel conductivity will be observed only when the conduction process is bulk-limited. Although the functional dependence of conductivity is the same for both Schottky and Poole-Frenkel mechanism, a plot of $\ln\sigma$ versus $F^{\frac{1}{2}}/kT$ should allow the mechanism to be differentiated. For Poole-Frenkel conduction, the slope of the plot will be

$$\beta_{PF} = \left(\frac{e^3}{\pi\varepsilon_o K}\right)^{\frac{1}{2}} \qquad 3.19$$

and for Schottky,

$$\beta_S = \tfrac{1}{2}\left(\frac{e^3}{\pi\varepsilon_o K}\right)^{\frac{1}{2}} \qquad 3.19a$$

However confusion has arisen in the literature from the interpretation of results which were thought to represent bulk limited conduction. For example, in films of SiO_2, the coefficient of $F^{\frac{1}{2}}$ is compatible with the Schottky effect rather than Poole-Frenkel effect.[23] A value of 12 for the high frequency dielectric constant of SiO, calculated from the measured β_{PF} is clearly wrong. Assuming Schottky emission, a value of 3 is returned. This anomalous Poole-Frenkel effect was resolved by Simmons,[23] who, in an analysis which considered a system containing Nd deep traps and Nt neutral shallow traps, suggests

$$J = J_o \exp\left(\frac{\beta_{PF} F^{\frac{1}{2}}}{2kT}\right) \qquad 3.20$$

Thus it is seen that conduction in insulators which follows the Schottky law is not necessarily electrode limited.

v Impurity Conduction

If an insulator contains an array of impurity states, say donor states, and if some of these states are vacant, then an electron trapped at one impurity site can move to a neighbouring vacant site. The transfer between sites is accomplished by the emission or absorption of a phonon. The charge transfer will be random in the absence of an electric field and no net current will flow. However, an applied field will cause a donor state energy gradient and the net electron flow will be to lower energy - a current will flow.

Two mechanisms of transfer are possible,

a. tunnelling through the potential barrier between sites

and

b. hopping over the potential barrier between sites.

Tunnelling theory predicts that the conductivity ρ, at temperature T will be given by [14]

$$\log \rho(T) = f(N) + (\varepsilon_1/kT) \qquad 3.21$$

f(N) is a function of the majority carrier density N. The value of ε_1 the activation energy is dependent on the compensation in the insulator. Experimental evidence has been reasonably in agreement with the tunnelling theory at low temperatures. In an effort to explain the activation energy at high temperatures, the hopping theory has been developed. If impurities are distance a apart, the activation energy ε_2 is given by

$$\varepsilon_2 = \varepsilon_a - \left(\frac{3e^2}{ka}\right) \qquad 3.22$$

where k is the dielectric constant and ε_a is the ionisation energy of an isolated impurity. It can further be shown that the activation energy is proportional to $\frac{1}{N3}$ where N is the concentration of impurities. A similar expression to 3.21 for the resistivity

is obtained by the hopping theory. Impurity conduction is a bulk limited process; the limiting effect is the carrier-phoron interaction.

Some of the conduction mechanisms outlined in the preceding sections are summarised in Figure 3.2. It will be appreciated that the dominant conduction process in an insulator film will depend on the shape and height of the potential barriers at the contacts and on the trapping levels present in the bulk of the insulator. It is not always clear whether conduction is electrode or bulk limited. Simmons and other workers[24, 25] have considered the transition from bulk to electrode limited conduction due to the dielectric relaxation effects.

Traps in insulators can have extremely long lifetimes. Doherty[26] has reported transient dielectric relaxation currents in SiO_2, produced by applying a voltage step to a thin sample, which last for several weeks. The depth of the trapping level determines the relaxation time e.g. if the trap depth is 0.5 eV below the conduction band and the density is $10^{20}cm^{-3}$, the relaxation current will decay to half its value in 10^{-5} seconds. However, if the trap is 1.5 eV deep, the time is 10^{12} seconds. The thermal emission from traps is the mechanism by which a depletion region is established in an insulator, and it can be seen that on application of a bias voltage, some time may elapse before the depletion region has formed. In Figure 3.3a an insulator with blocking contacts is seen with no bias applied. After applying a bias, but before the depletion region has formed, the energy bands are

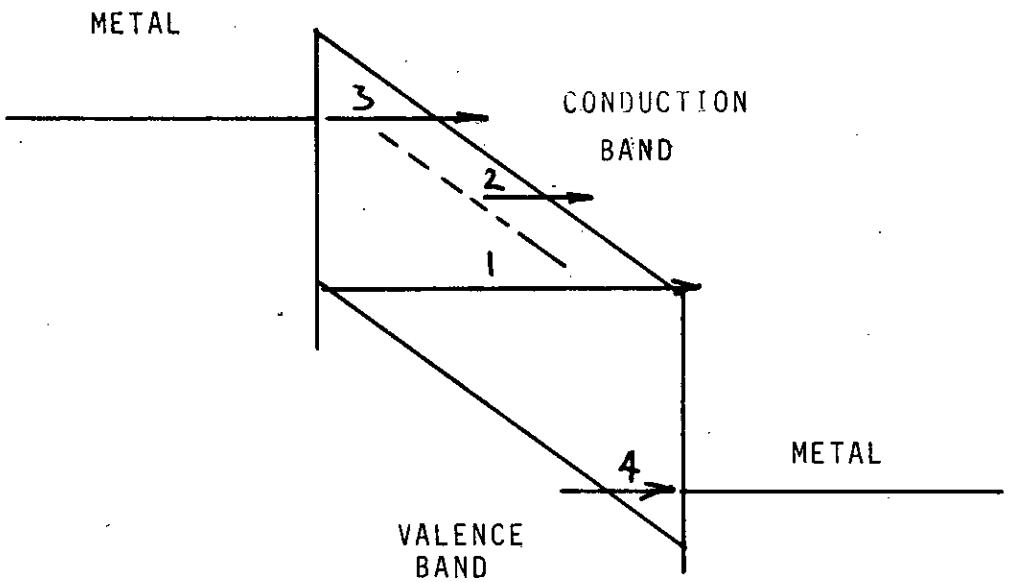

1) Zener breakdown

2) Field ionization of traps

3) Electron tunneling

4) as 3

Figure 3.2: Conduction mechanisms

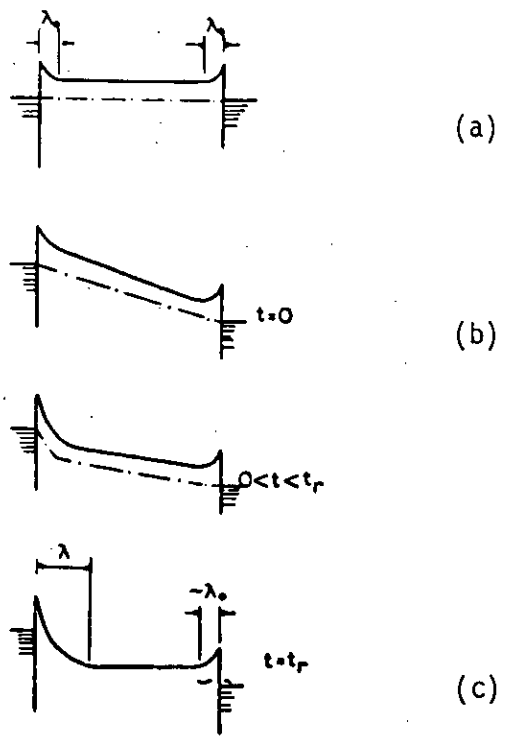

Figure 3.3: Insulator energy bands during dielectric relaxation experiment.

distorted as in Figure 3.3b. This is a non-equilibrium situation. After some time, equilibrium is achieved as in Figure 3.3c. Most of the applied bias appears across the reverse biased depletion region. It has been postulated[24] that the non-steady state currents measured during the formation of the depletion region are bulk limited. The steady state situation is electrode limited. The transition from bulk to electrode limited conduction can be demonstrated by measuring the current as a function of temperature. Typical results (after Simmons et al[27]) are shown in Figure 3.4. Log I is plotted against T for a Al- C eF_3-Al sample. These results are discussed in terms of trap kinetics as follows. When a biasing voltage is applied to the sample at low temperature, the time for traps to depopulate, and for the potential barrier at the contact to establish itself, is long compared with experimental times. Thus, in this particular case, the bias conditions are changed at low temperatures but, because the probability of the traps emptying is low, a non-equilibrium field distribution exists across the oxide. As the temperature is increased a point is reached at which the characteristic release time of carriers from traps becomes comparable with the experimental time. The field then adjusts itself to the steady state distribution and the contact barrier is established. Because the density of trapped carriers decreases with increasing temperature, the rate of increase of current also, decreases, so that at some temperature the current actually decreases with

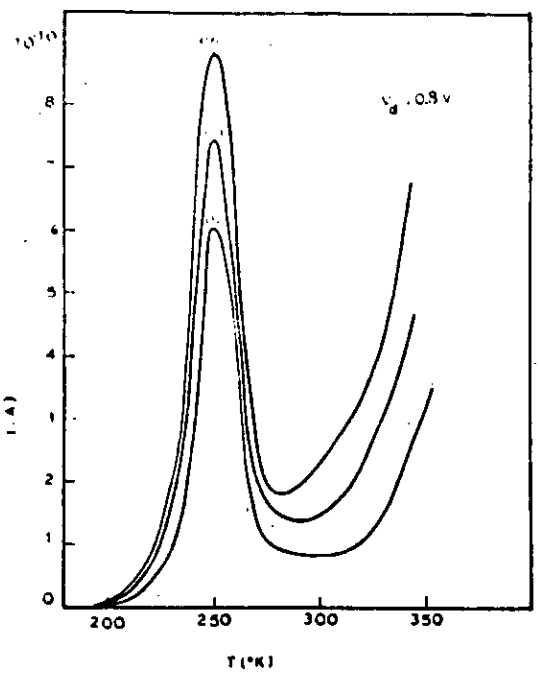

FIG. 12. Family of I–T characteristics for case 6.

Figure 3.4: log I vs. T for Al - CeF_3 - Al sample (after Simmons et al ref.27).

further increase in temperature i.e. there is a maximum in current versus temperature. At temperatures below that of the current peak, the conduction is bulk limited, above the peak the conduction is electrode limited. From the temperature of the current maximum, Gupta et al [25] predict trap depth and trap density. Similar results have been reported for SiO_2 films.

The significance of this work is in demonstrating the care which has to be exercised before conclusions can be drawn about the field distribution in an insulator. It seems highly probable that some of the published work on thin insulators has been mis-interpreted due to ignoring non-steady state dielectric relaxation currents. Indeed at room temperatures, an extremely long time would have to pass before traps have depopulated and the potential barrier has grown.

CHAPTER THREE : REFERENCES

1. Ho C.P. & Plummer, J.D., J. Electrochem Soc. 126, 1523 (1979)

2. Kern, W. & Fisher, A.W., RCA Rev. 31, 715 (1970)

3. Gdula, R.A., J. Electrochem. Soc. 123, 42 (1976)

4. Mott, N., Advanc. Phys. 16 49 (1967)

5. Harstein, A., Weinberg, Z.A., & DiMaria, D.J., "The Physics of SiO_2 and its Interfaces" p51,ed. S.T. Pantelides, Pergamon New York, 1978

6. Rose, A., "Concepts in Photoconductivity", Chapter 7, Interscience, New York, 1963

7. Dussel, G.A. & Bube, R.H., J. Appl. Phys. 37, 2797 (1966)

8. DiMaria, D.J., J. Appl. Phys. 47, 4073 (1976)

9. ref. 5, p 164

10. Williams,R., Phys. Rev. 140, A569 (1965)

11. Nicollian, E.H., Goetzberger, A., Berglund, C.N., Appl. Phys. Lett. 15, 174 (1969)

12. Simmons, J.G., J. Phys. D, 4, 613 (1971)

13. Bube, R.H., "Photoconductivity of Solids", chapter 5, Wiley New York, 1960

14. Lamb, D.R., "Electrical Conduction Mechanisms in Thin Insulating Films", chapter 3, Methuen, London.

15. Ridley, B.K., J. Appl. Phys. 46, 998 (1975)

16. Nauta, P.K., Hillen, M.W., J. Appl. Phys. 49, 2862 (1978)

17. Lampert, M.A. & Mark, P., "Current Injection in Solids", Academic Press, New York, 1970

18. Mott, N.F. & Gurney, R.W., "Electronic Processes in Ionic Crystals", OUP, New York, 1948

19. Rose, A., Phys. Rev. 97, 1538 (1955)

20. Flynn, B.W., Owen, A.E. & Mavor, J., J. Phys. C 10,4051 (1977)

21. Lenzlinger, M. & Snow, E.H., J. Appl. Phys. 40, 278 (1969)

22. Pollack, S.R., J. Appl. Phys. 35, 877 (1963)

23. Simmons, J.G., Phys. Rev. 155, 657 (1967)

24. Simmons, J.G., Phys. Rev. B 6,4084 (1972)

25. Gupta, H.M., van Overstraeten, R.J., J. Phys. C 7, 356¼ (1978)

26. Doherty, J.G. & Ryan, W.D., ESSDERC '77, University of Sussex

27. Simmons, J.G. & Nadkarni, G.S., Phys. Rev. B 6, 4815 (1972)

4. SAMPLE PREPARATION AND EXPERIMENTAL TECHNIQUES

4.1 SAMPLE PREPARATION

The dye metal-free hydrogen phthalocyanine, H_2Pc, was used for most measurements. It was chosen because it is a known photographic sensitiser, it has been reported to sensitise the Xerographic discharge of selenium[1], it is extremely resistant to chemical reaction and it sublimes, in vacuo, to form a coherent film with good adhesion to a glass substrate coated with gold.

The stability of the metal-free phthalocyanine arises from its porphyrin ring structure (see Chapter 2); other dyes e.g. pinacyanole, were used for initial experiments but it is almost certain that under vacuum evaporation, the molecular structure of these compounds change due to the inherently weak linear molecule. Hydrogen phthalocyanine was available from Imperial Chemical Industries as a blue crystalline powder with a purity guaranteed to be better than 99.99%. Various work has been published on the structure of sublimed H_2Pc films[2,3]. Sublimation on to substrates at room temperature results in films of the α polymorphic form. In this form, the plate-like molecules are arranged parallel to one another but in a less ordered structure than in the β polymorph.

For electrical measurements, extensive use was made of either metal-insulator-metal (MIM) or metal-dye-insulator-metal (MDIM) test samples in a sandwich-type structure. The test sample

was defined by the overlapping region of top and bottom strip electrodes, each 0.5 mm wide. The electrodes crossed at right angles with the insulator or insulator/dye combination sandwiched between them. The structure is shown schematically in Figure 4.1. Some use was made of surface gap cells (gap width 10μm to 100μm) for photoconductivity studies of the dyes. The metal electrode pattern was defined photolithographically.

The procedure for preparing the sandwich cells was as follows. The substrate material was Corning 7059 borosilicate glass, 25 mm x 25 mm and 1 mm thick. The substrates were cleaned by ultrasonic agitation for 20 minutes in a 10% solution of Decon 90 in de-ionised water. After rinsing in de-ionised water, the substrates were subjected to ultrasonic agitation in methanol (Analar grade). Blow drying with nitrogen completed the cleaning procedure.

The first deposition stage was to deposit and define the bottom electrodes. Gold was used most frequently for the electrodes but some work was carried out with aluminium electrodes. Masking during deposition was used to define the electrode pattern (a 10 electrode interdigitated pattern as shown in Figure 4.1). Out-of-contact shadow masks were used, through which the metal was evaporated onto the substrate. The masks were of copper foil, produced by photolithographic techniques from glass master plates. Gold was deposited by electron-beam evaporation at a pressure less than 2×10^{-5} torr. To promote adhesion of the electrodes to the glass substrate, an extremely thin film of

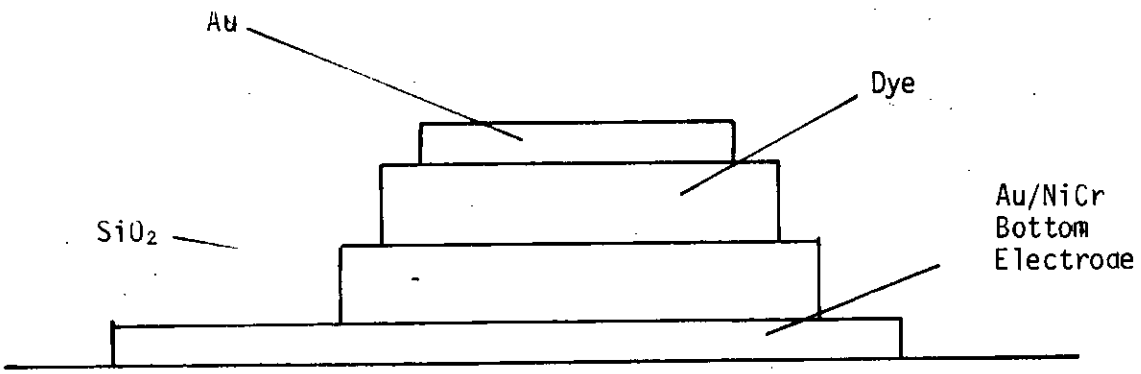

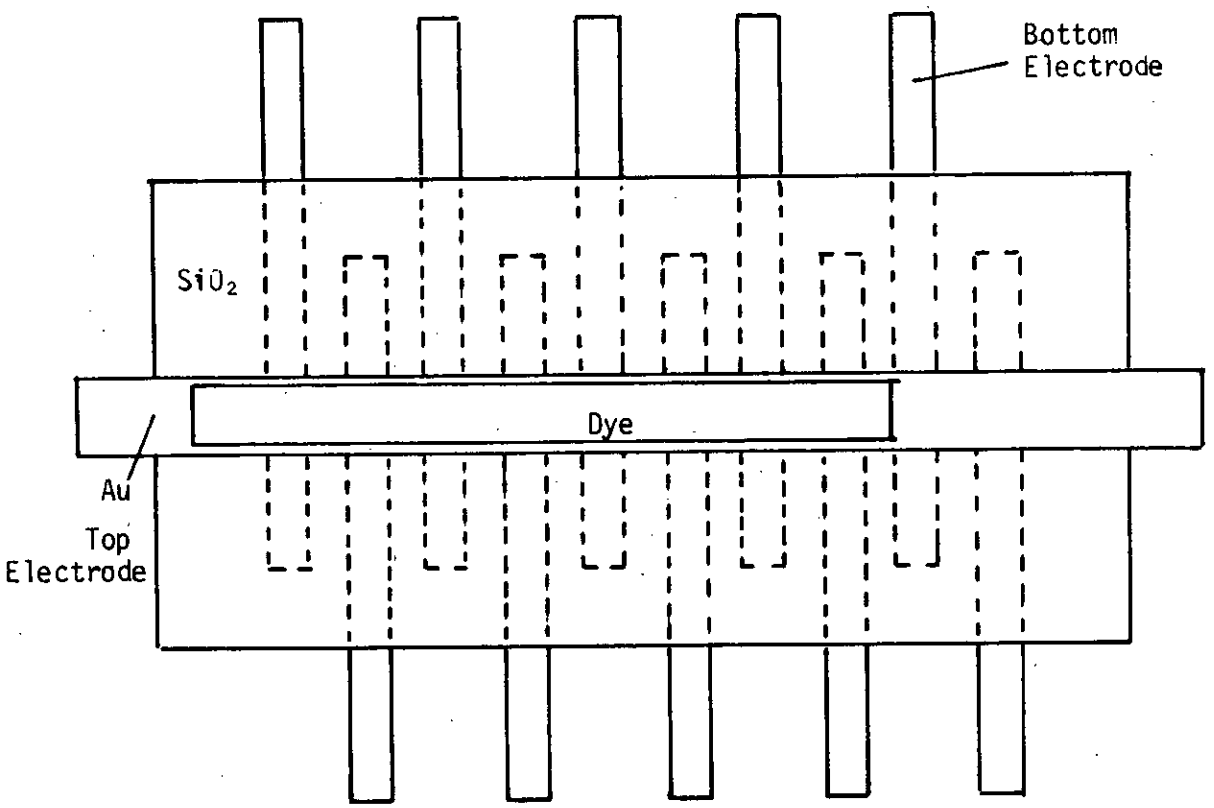

Figure 4.1: Test sample structure

nichrome was first deposited. The electron-beam gun has interchangeable hearths which allowed deposition of both metals in consecutive operations through the same masks, without breaking vacuum. Aluminium could be deposited directly onto the substrate, with good adhesion by vacuum evaporation from an electrically-heated tungsten filament source.

The insulator used was silicon dioxide, compatible with conventional MOS semiconductor processing. As can be seen from Figure 1.1, the proposed structure of a dye sensitised MOS transistor has the controlling oxide which is dye-sensitised lying over a floating gate. This gate could be either of metal or of polycrystalline silicon. Even if the latter material, it would not be possible to grow a sufficiently thick oxide by thermal oxidation. If metal, then obviously no thermal oxide could be grown. MOS processing currently uses chemical-vapour phase-decomposition techniques to deposit silicon dioxide (Silox process) to thicken the field isolation oxide and for overlay passivation layers, and it seems likely that this could be used in the dye sensitised transistor. Consequently most work was carried out using this type of oxide but, r.f. sputtered silicon dioxide was also investigated for comparative purposes.

The Silox process for the deposition of silicon dioxide took place in a quartz lined furnace, heated to 450^{o}C. (More conventional systems utilise a hot-plate on which the substrates lie or use reduced pressure in a furnace tube; neither was available). Dilute silane gas, SiH_4, (1% with nitrogen balance) was

mixed with oxygen and passed into the furnace tube. Nitrogen was used as carrier gas to extend the zone in which deposition took place. The system is shown in diagrammatic form in Figure 4.2. The reaction which takes place is

$$SiH_4 + 2O_2 \xrightarrow{450^oC} SiO_2 + 2H_2O$$

This reaction is exothermic and is known to produce films of silicon dioxide which can be very nearly stochiometric if an excess of oxygen is present in the gas phase. In fact a 50% excess of oxygen was used and deposition took place at atmospheric pressure. The water, produced as a reaction by-product, should have been exhausted, but infra-red spectroscopy showed evidence of incorporation of water in the film as OH groups; IR absorption bands characteristic of the Si-OH, bond were observed at 3650cm wavelength. After deposition, the substrates were left in the furnace with nitrogen flowing for one hour. The deposition was confined to the required area by placing the substrates on a flat quartz boat, and masking the unwanted areas with quartz plates. The insulator thickness could be calculated from estimates of colour fringing. It was possible, as a check, to measure the film thickness using a Taylor-Hobson Talysurf but this procedure was difficult as the film edge was not well defined and had a rounded profile. Approximately 0.5μm of SiO_2 was deposited in 20 minutes.

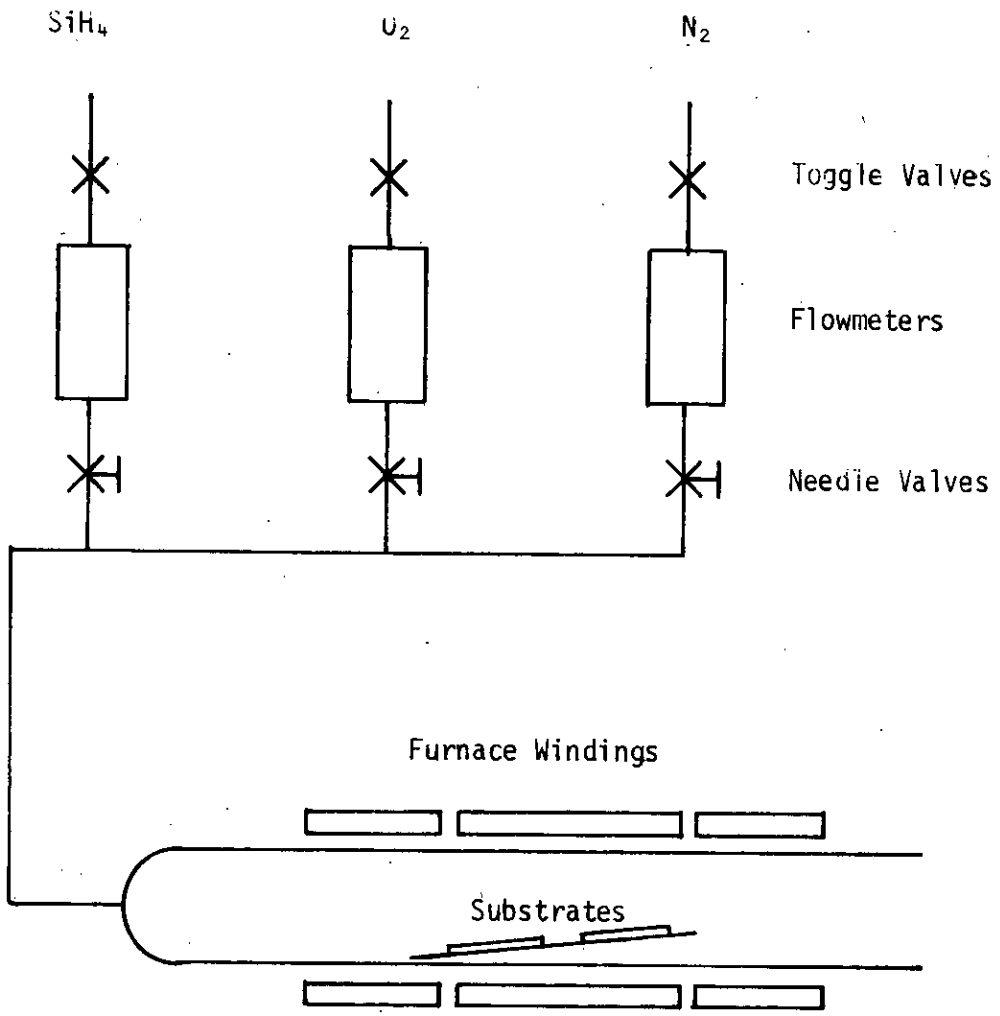

Figure 4.2: Silox process equipment

Sputtered silicon dioxide was prepared from a quartz target. Argon was used to support an r.f. plasma at 25 mtorr pressure. The frequency was 13.56 MHz. The masking was the same as for the Silox process but the deposition rate was much slower.

In MDIM samples, the dye was deposited by vacuum evaporation. Some works have deposited dyes by applying a solution of the dye in a volatile solvent. Once the solvent evaporates, the dye is left as a residue. This technique avoids the danger of destroying the molecular structure of the dye during thermal vacuum evaporation. Hydrogen phthalocyanine is soluble only in concentrated acid however and thus, this technique is obviously impracticable.

The powdered dye was placed in a small quartz crucible (8 mm diameter x 10 mm depth) which was heated by a tungsten filament coiled around it. For thickness measurements, an extra substrate with no electrodes or oxides, was included in each evaporation. The dye film thickness would be measured with the Talysurf, but it was found that the stylus scratched the soft film. Thus it was necessary to evaporate a metal over the dye to give a strong surface across which the stylus could slide. Alternatively, the dye film thickness could be calculated from a measurement of its optical absorption. Films up to 0.5μm were used. At that thickness the H_2Pc film was still semi-transparent.

Sample preparation was completed by the evaporation of a metal top electrode over the dye. This metal was deposited in the

same way as the bottom electrode except that no nichrome layer was required. To allow illumination of the dye, the top electrode was semi-transparent and only thick enough to be electrically continuous. MIM samples were prepared in a similar way except that the dye layer was omitted.

4.2 EXPERIMENTAL TECHNIQUES

i Optical Measurements

Spectrographic investigations of dye films in the visible spectrum were made with a Zeiss spectrophotometer. The dye was evaporated on to a glass slide which was mounted at the exit aperture of the spectrometer. Both tungsten and mercury lamps were available to cover the wavelength range 300 nm to 2.5μm. No attempt was made to normalise the results to compensate for the instrumental response. All spectrographic experiments used this instrument and thus the results can be compared directly. The absorption spectra of dyes could be measured and also the spectral dependence of the photoconductivity by placing a gap cell at the exit aperture.

For measurements in the infra-red, the dye was evaporated onto potassium bromide substrates which are transparent in the infra-red. A Perkin-Elmer Model 580 double-beam spectrometer at ICI Corporate Laboratory was used. For infra-red studies of Silox grown silicon dioxide, high resistivity silicon was used as a substrate; an

identical piece of silicon could be placed in the reference beam to cancel substrate effects.

ii Current Measurements

The variation of the current flowing through MIM and MDIM samples was measured as a function of time, applied field, and temperature, and the measurement circuit is shown in Figure 4.3a. Biasing voltages of either polarity were supplied from a Fluke 415B stabilised power supply. Current measurement was by a Keithley 640 vibrating capacitor electrometer. The electrometer had switchable shunt resistors (10^8, 10^{10}, $10^{12}\Omega$) and could be used in "fast" mode to increase the speed of response.

It was capable of measuring currents as low as 10^{-17} amp and so currents above 10^{-15} amp, which were normal in these experiments could be measured with accuracy. The sample was mounted rigidly to the input connector of the electrometer; microphonic noise was thus virtually eliminated. A quartz rod was inserted through the enclosure lid to enable illumination to be concentrated onto the test sample. The complete electrometer head assembly with sample was placed on an optical bench at the exit aperture of the Zeiss spectrometer to enable illumination at known wavelengths to be applied. White-light illumination was by a focussed microscope lamp or by a high intensity quartz-halogen projector bulb. The output of the electrometer was fed to a chart recorder (X-T) for recording temporal response.

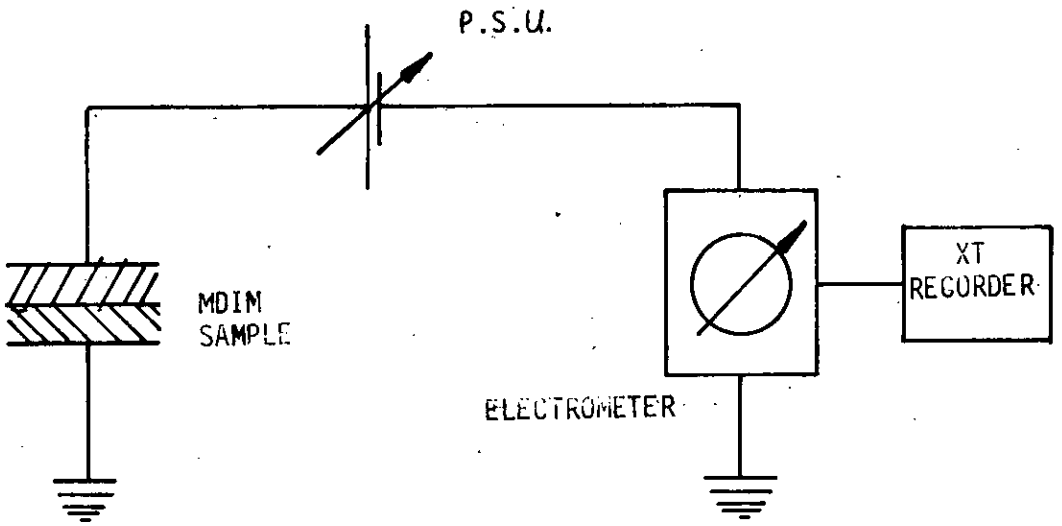

4.3a

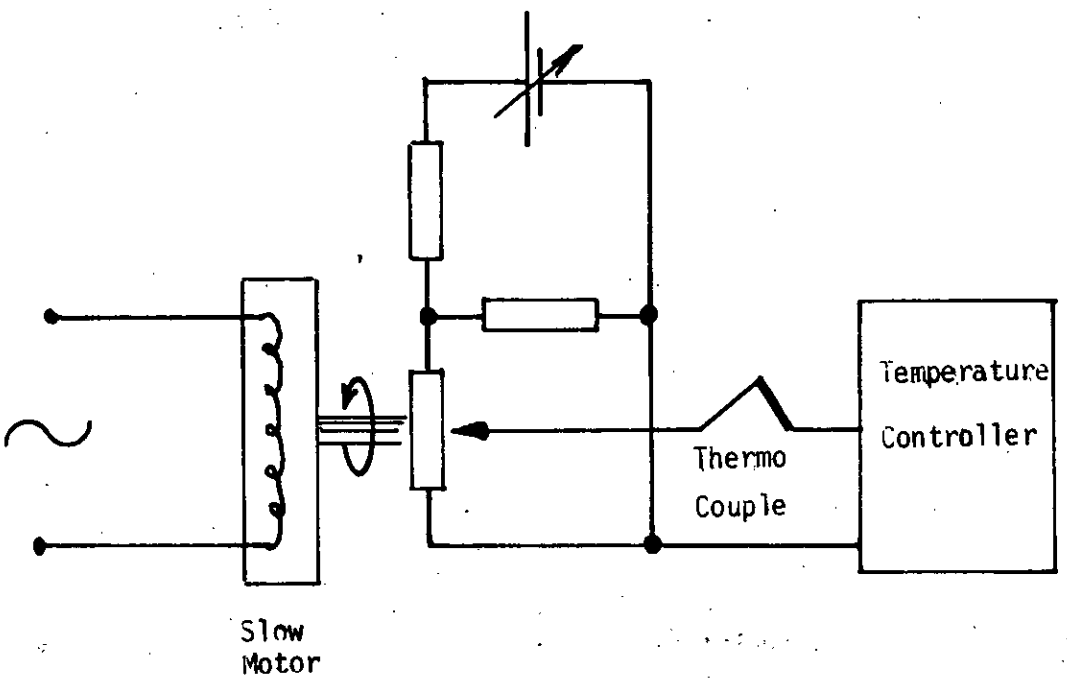

Figure 4.3: Test systems

Connection to the electrodes of the test sample was by fine copper wires, bonded by silver DAG. The dye-sensitised current was measured by placing a MDIM sample in the electrometer test enclosure, and a bias was applied. After the dark current has apparently stabilised, a shutter was opened to allow illumination of the sample and the resulting current flow recorded on the chart recorder. The magnitude and polarity of the bias-voltage was varied. The dark current was allowed to decay to a constant value after each change in bias, before illumination took place. The spectral dependence of the photo-induced current was measured, using a Zeiss spectrometer as light source. The dark current behaviour of MIM samples was also investigated with this apparatus.

An Oxford Instruments liquid nitrogen cryostat was used to study the temperature dependence of the dark and photo-sensitised currents in MDIM samples. The cryostat chamber in which the test sample was mounted, was pumped by an oil diffusion pump to prevent condensation of water onto the sample. Liquid nitrogen was drawn from a Dewar, through a vacuum jacketted transfer tube, to flow through a metal block which formed the sample mounting. A "heat-sink" compound was used between the sample and its mounting to ensure good thermal contact.

The nitrogen flow was controlled by a needle valve. A wire-wound resistor was also mounted on the sample block and electric current passed through to provide heating, which offset the cooling effect of the liquid nitrogen. By controlling the heating current, any

temperature in the range of 77K to 450K could be maintained. The temperature was monitored by a iron/gold thermocouple. A three-term temperature controller was used. A diagram of the cryostat is shown in Figure 4.4. Temperature control was $\pm 0.2^{o}$K over the range. The cryostat chamber was equipped with quartz windows which allowed the sample to be illuminated. The connecting cable between the cryostat and the Keithley 640 was kept as short as possible in an effort to reduce noise.

iii Thermally-Stimulated-Dielectric-Polarization Experiments

A series of experiments was conducted using the thermally-stimulated-dielectric-polarization technique to investigate the insulator trapping levels. The basis of these experiments is to submit the test sample to a linear temperature increase and to observe peaks in sample current as the field distribution reaches equilibrium. It was necessary to equip the cryostat controller with a controllable temperature ramping facility as follows.

The controller set-point was set at zero i.e. the controller changed the heater current to achieve equilibrium with zero input from the thermocouple. In series with the thermocouple, but with opposite polarity, was added another voltage. Equilibrium was reached when the thermocouple voltage equalled this control voltage. Thus, by making the control voltage increase, the temperature was increased to make the thermocouple output equal

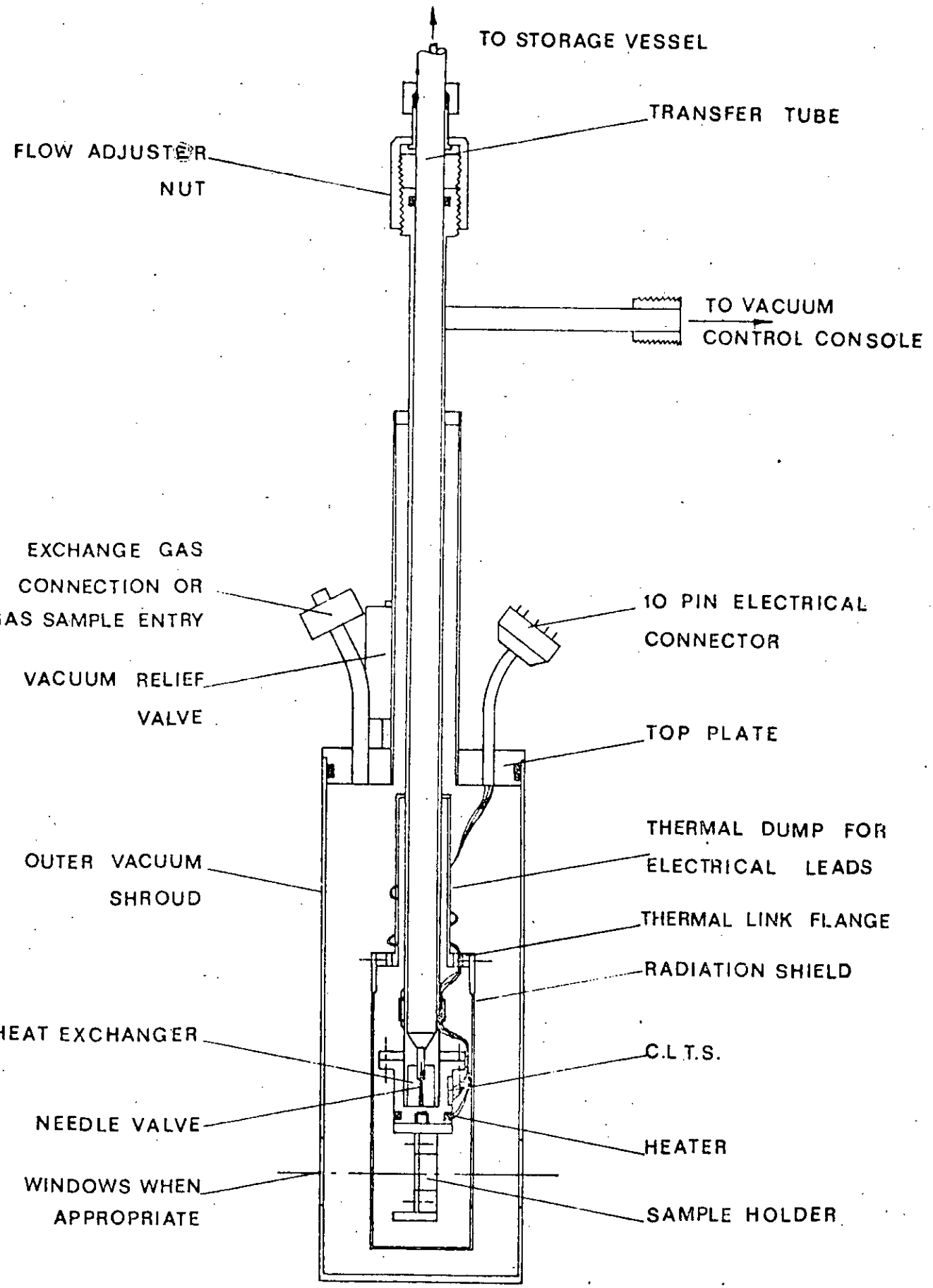

Figure 4.4: Schematic View of a Continuous Flow Cryostat

at all times to the control voltage. Over the range of temperature 150K to 450K, the thermocouple output is linear with temperature and thus for a linear control voltage increase, the temperature of the cryostat increased linearly. The temperature could be measured by a DVM connected to the thermocouple. As a test of this system, an independent thermocouple was mounted in the cryostat to monitor sample temperature. At ramping rates up to $4^{o}K\ min^{-1}$ the temperature was indeed found to increase at a constant rate.

The voltage ramp was obtained by taking a multi-turn potentiometer of high linearity and coupling its shaft to a slow (~1 revolution per hour) synchronous motor. By adjusting the voltage across the potentiometer, the voltage ramp rate (as appearing on the potentiometer wiper) could be set to any value e.g. 0.041 mv min^{-1} would result in a temperature increase of 2K per minute. The starting point could also be set by manually turning the potentiometer to the required output; a friction coupling was used between motor and potentiometer. Ramping downwards could be achieved by reversing the polarity of the supply. Figure 3b shows the circuitry for controlling the temperature ramping.

The procedure for the thermally-stimulated-dielectric-polarization experiment will be described. The sample was mounted in the cryostat and the chamber was evacuated. At room temperature (or above) an initial bias voltage was applied. This was usually zero volts but any value could be chosen. The sample was cooled rapidly to about 150K and allowed to stabilise. The bias was

changed to a new value and the heating started. The heating took place at a known constant rate, typically $2^{o}K\ min^{-1}$, and during this stage of the experiment, the current flowing through the sample was measured. Peaks in current were observed during heating. Once the temperature had reached 450K the experiment was concluded. The experimental procedure is summarised below.

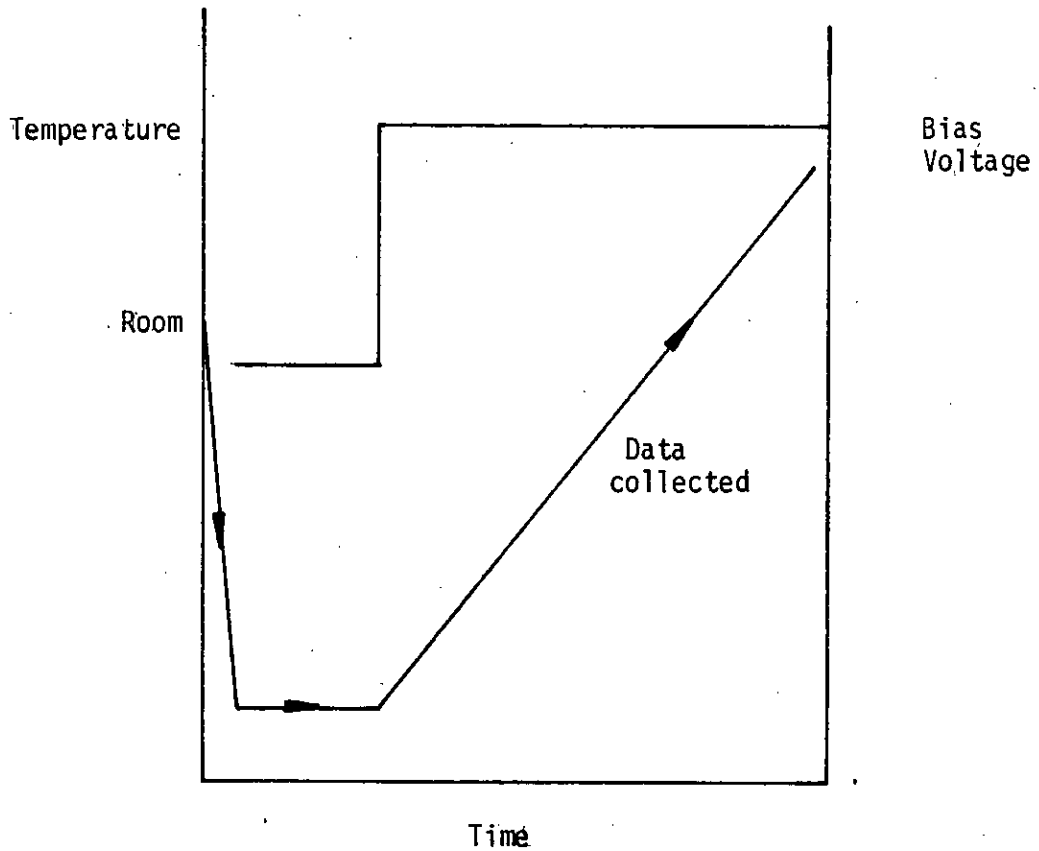

MIM samples were used and the dark-current measured, or MDIM samples in which case both dark- and photo-sensitised current was measured.

iv Photo Discharge Experiment

The electrometer was used as a high impedance, $10^{16}\Omega$, voltmeter. A MDIM sample was mounted in the electrometer sample enclosure, and a biasing voltage applied, as in Figure 4.5a. Typically 30V was used. The power supply was disconnected, as in Figure 4.5b, and the sample voltage was measured. The decay of voltage with time was recorded on the chart recorder with the sample in the dark, and under illumination (white light and monochromatic light). The decay rate, on illumination, was measured as a function of polarity of charge and of wavelength of illumination. Discharge through the electrometer was very slow due to the high impedance, and the capacitance of the electrometer input was much smaller than the MDIM sample which was usually ~100 pF.

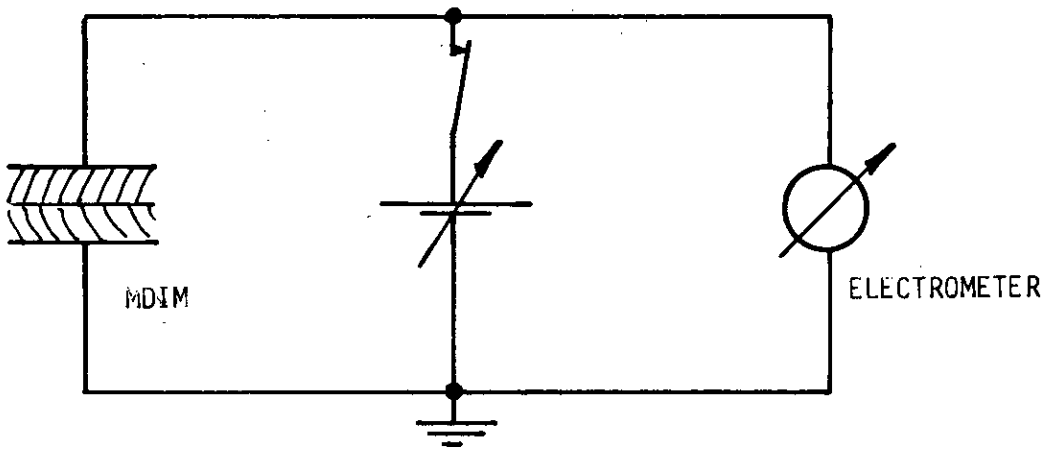

CHARGE

4.5a

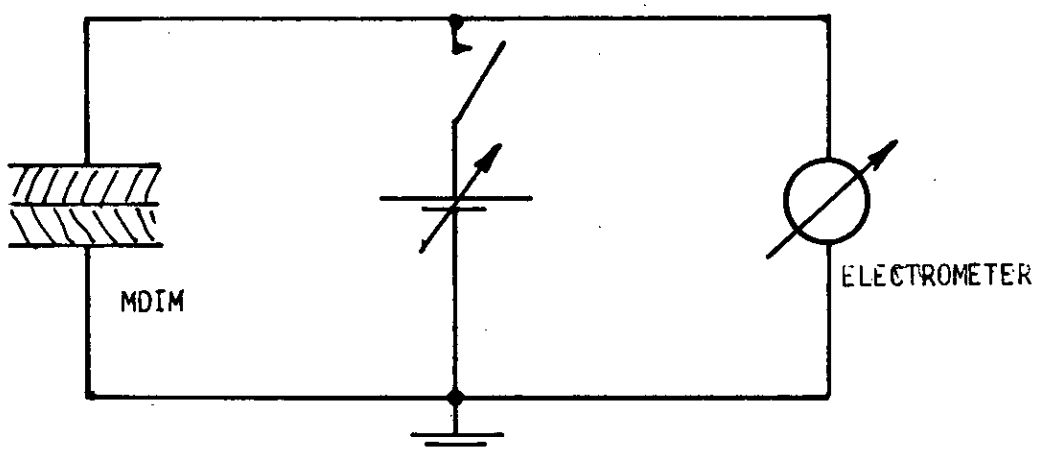

DISCHARGE

4.5b

Figure 4.5: Photo-discharge test circuit.

CHAPTER FOUR : REFERENCES

1. Regensburger, P.J. & Petruzella, N.L., J. Non-Crys. Sol. 6, 13 (1971).

2. Harrison, S.E. & Ludewig, K.H., J. Chem. Phys. 45, 343, (1966).

3. Sharp, J.H. & Miller R.L., J. Phys. Chem, 72, 3335, (1968).

CHAPTER FIVE : RESULTS AND DISCUSSION

The primary objective of the work described in this Thesis was to quantify, so far as possible, the so-called dye-sensitised photo-injection phenomena in silicon dioxide and to determine the most likely mechanism(s) of photo-injection. The relevant results and their interpretation are presented in this Chapter. A secondary purpose was to assess the feasibility of utilising the dye-sensitised charge injection process in optically-sensitised MOS devices and this aspect of the work is considered in Chapter 6.

As explained earlier, the basic experimental device, for studies of dye-sensitised charge injection is the metal-dye-silicon oxide-metal (MDIM) sandwich structure and the properties of this device will clearly depend upon the properties of its individual elements, particularly of the dye and the SiO_2. Although it is true that there is a substantial literature on the electronic and optical properties of SiO_2 films and on various dyes such as H_2P_C, it is also true to say that there are considerable variations in reported experimental data, which are probably attributable to different experimental conditions, purity and homogeneity of materials etc. It was decided therefore that a necessary preliminary would be a series of experiments to determine, separately, the electrical properties of the dye and SiO_2 films, prepared under the identical experimental conditions used to fabricate the more complex MDIM structures. Thus, the first two sections of this Chapter describe experiments on metal-dye-metal (MDM) and metal-SiO_2-metal (MIM) structures and wherever

possible the results are compared and contrasted with previously published data.

5.1 MDM STRUCTURES

5.1.1 Field Dependence of Conduction

The field dependence of the dark and photo-conduction of a Au-H_2P_c-Au gap cell at room temperature is shown in Figure 5.1. The electrode width was 3 mm, electrode spacing was 20μm. At the higher applied voltages, the field across the gap cell is roughly of the same magnitude as the field across the dye layer (thickness approx 0.5 m) in the MDIM structures described in section 5.4.The dark resistivity of the dye is 7.5 x 10^9Ωm. Values reported in the literature vary between 4 x 10^7Ωm[1] and to 10^{15} Ωm.[2] There are no obvious trends in the values quoted in the literature in terms of preparation conditions, sample structure of electrode material. In those cases where the polymorphic form is stated, however, the α form appears to be more conductive than the β form by 2 or 3 orders of magnitude. The sample preparation technique must be crucially important in the resulting film properties. Some data reported in the literature has to be treated with caution e.g. a resistivity of a H_2P_c of 1Ωm has been reported.[3]

5.1.2 Temperature Dependence of Conduction

The temperature dependence of the dark current and photo-current of a similar gap cell (of electrode spacing 80μm and electrode

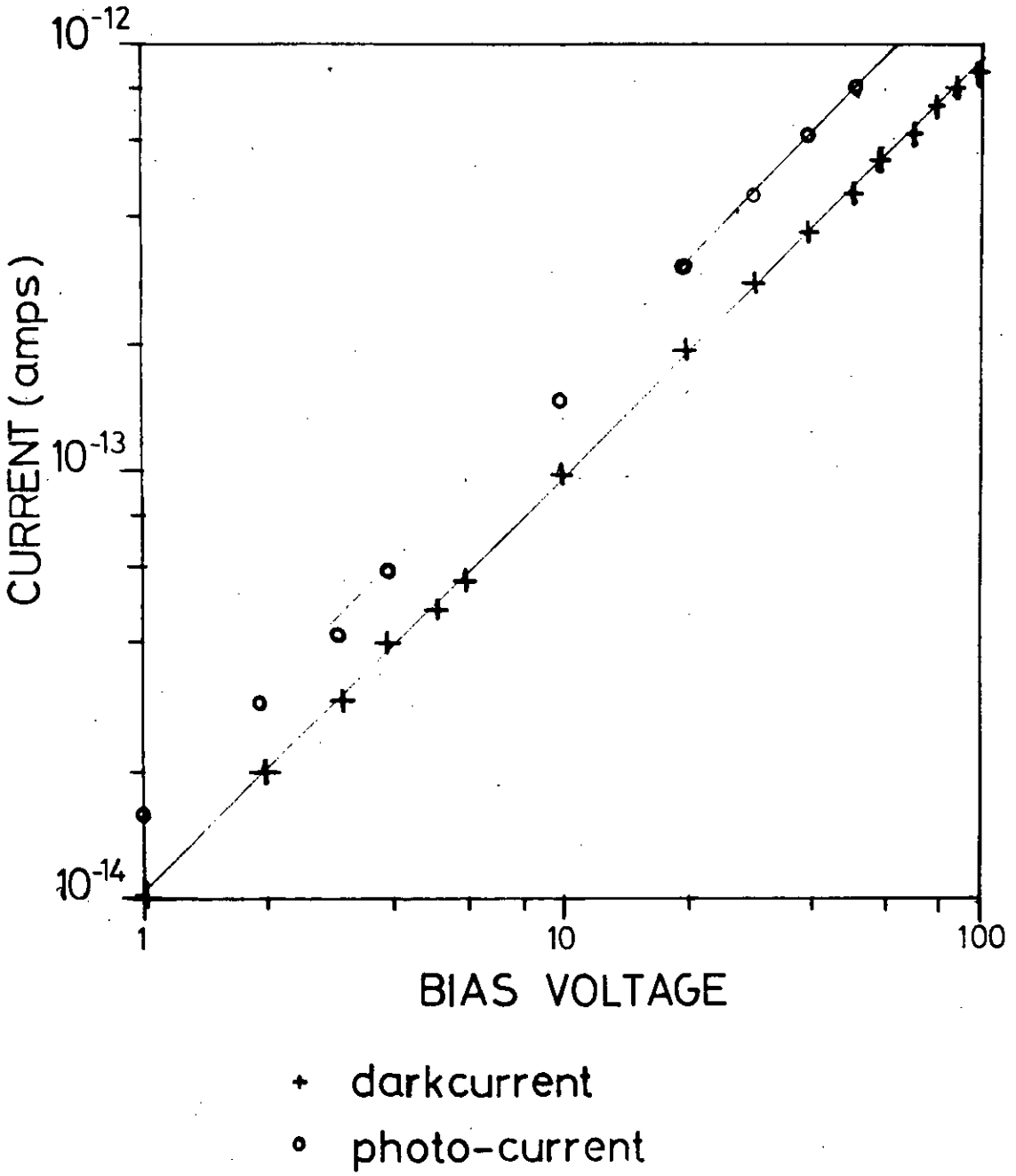

5.1

Field dependence of dark and photo-current in Au - H_2P_c - Au gap cell.

width 1 mm) with 40V applied is shown in Figure 5.2. The slope of the log (current) versus 1/T plot correspond to activation energies of 0.1eV and 0.38eV for the photo- and dark currents respectively. The deviation from the straight line is probably an artefact of the measurements at such low currents. The values of activation energy (for dark conduction) reported in the literature, vary in magnitude from 0.24eV[1] to 0.85eV.[4] The only conclusion derivable from these observations is that conduction is probably extrinsic as the singlet level for H_2P_C molecules in solution has been estimated from the optical absorption edge to be 1.7eV above the ground state.[5] The thermal activation energy for photo-conduction is reported to vary between 0.2[6] and 0.6eV.[7] The magnitude of the photo-current is variously reported to be 10 times to 10^4[8] times the dark conductivity compared with about 100 times the dark current (at room temperature) in the results of 5.2. Once again great variation is seen in the data reported in the literature. It is not possible to detect trends in this data, due to sample type or preparation, which would lend order.

5.1.3 Electrical Contact Properties

Gold was used most frequently as the electrode material and to establish the nature of the gold/H_2P_C contact, an experiment was conducted in which the resistance of Au/H_2P_C/Au gap cells of varying width measured. The results are shown in Figure 5.3. It can be seen that the cell resistance is proportional to the gap width that the plot extrapolates to the origin. The voltage applied to each cell was adjusted to make the field applied to 5×10^5 Vm^{-1} in each

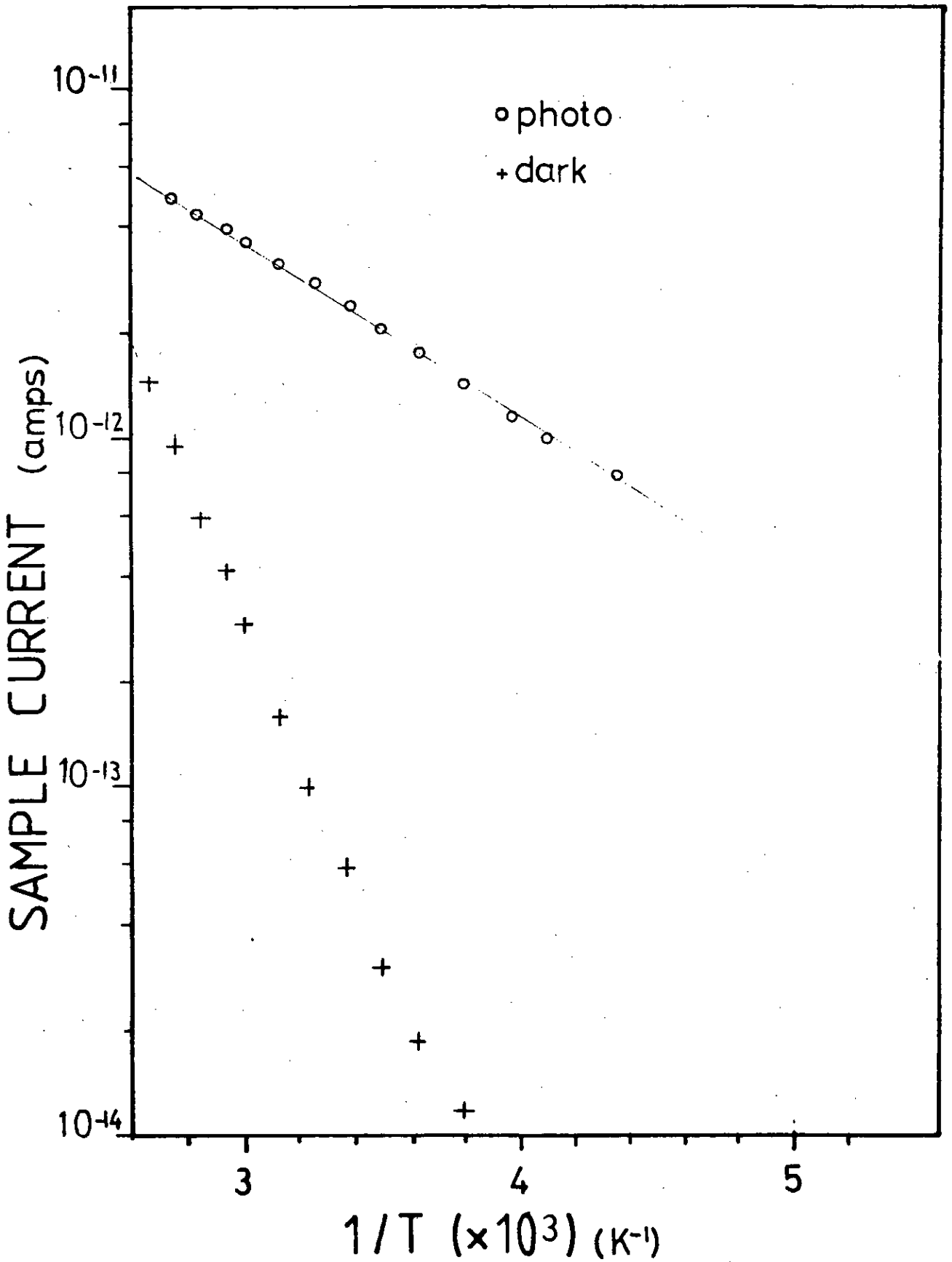

5.2

Temperature dependence of dark and photo-currents in Au-H_2P_c-Au gap cell.

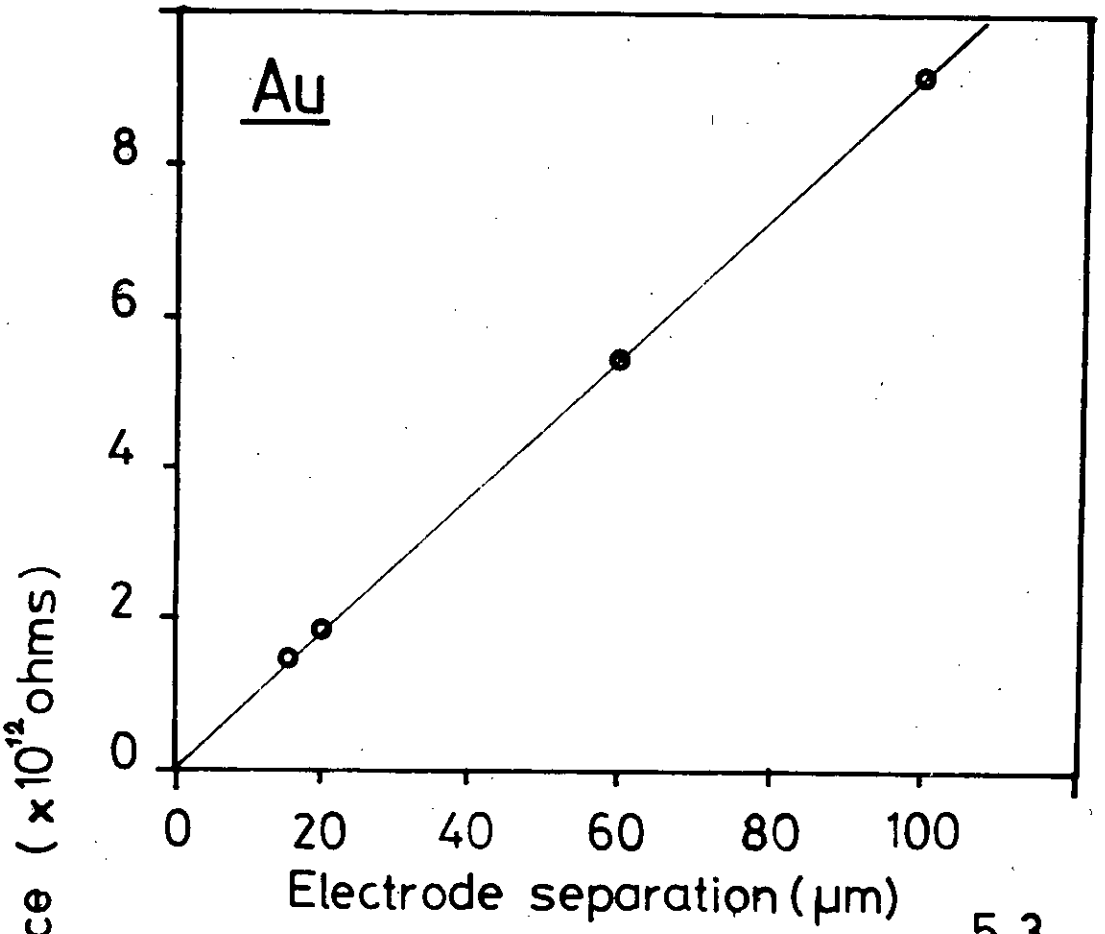

5.3

Gap resistance vs gap width.

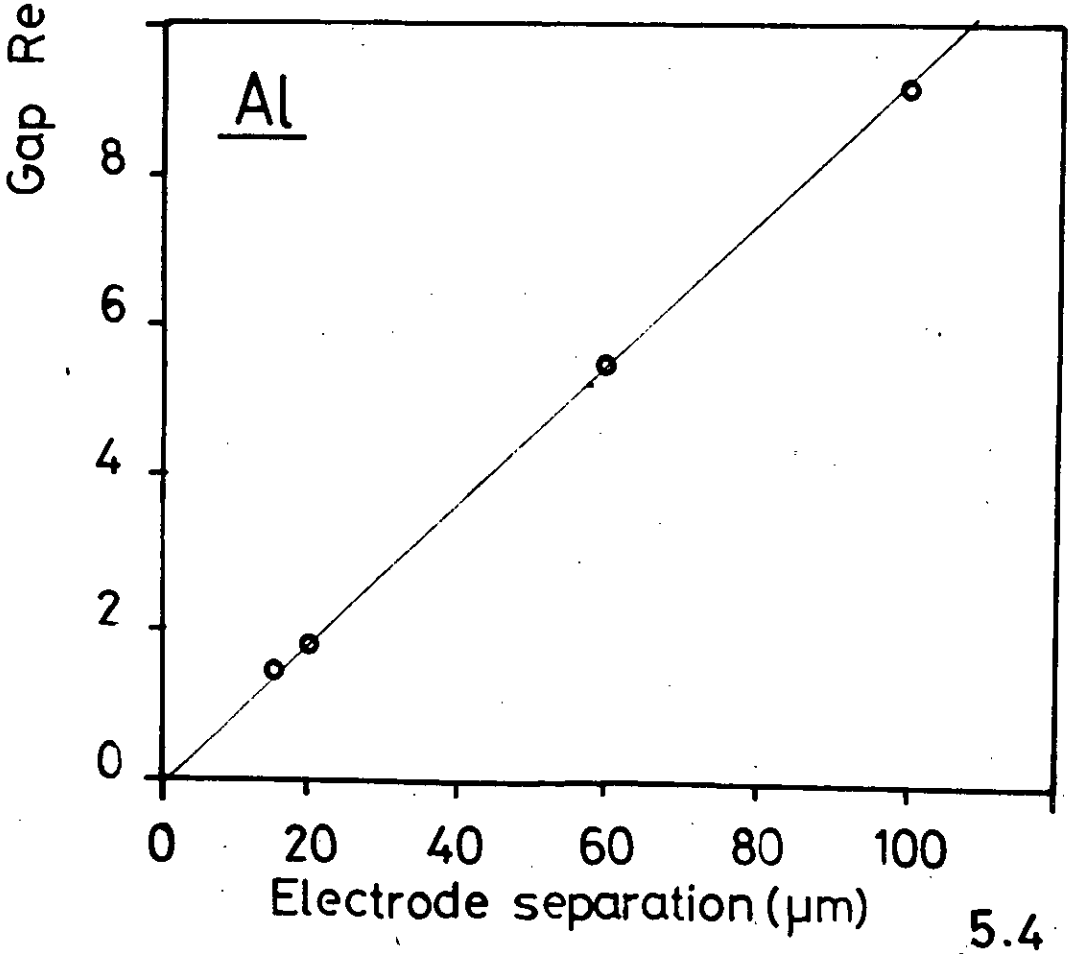

5.4

case and the results show the Au/H_2P_c contact is ohmic.

A similar experiment was conducted with Al electrodes with the result is shown in Figure 5.4. The Al/H_2P_c contact is also ohmic. Both experiments were conducted in the dark.

5.1.4 Spectral Dependence

The absorption spectrum of an evaporated H_2P_c film is shown as plot (a) in Figure 5.5. The film was evaporated onto a microscope slide and was of the typical thickness (approx 0.5μ) used in all other experiments. The spectral response plots in Figure 5.5 have not been normalised for the instrumental response of the spectrometer, but as the same spectrometer was used for all experiments, the plots can be directly compared.

The spectral response of the photo-current through a coplanar gap cell of evaporated H_2P_c with gold electrodes was measured and is shown in plot (b) of Figure 5.5. The gap was 20μ x 3 mm and, in common with all other gap cells used, was defined by photolithographic means. The plot shows a maximum at 750 nm wavelength and a smaller peak at 570 nm. This shift towards longer wavelengths (as compared with the absorption spectrum) has been attributed by Harrison[8] to triplet exciton interaction with trapping centres, possibly absorbed gases. Also shown in Figure 5.5 are the spectral responses of the photo-induced current and photo-discharge rate, both of which will be discussed later in this Chapter.

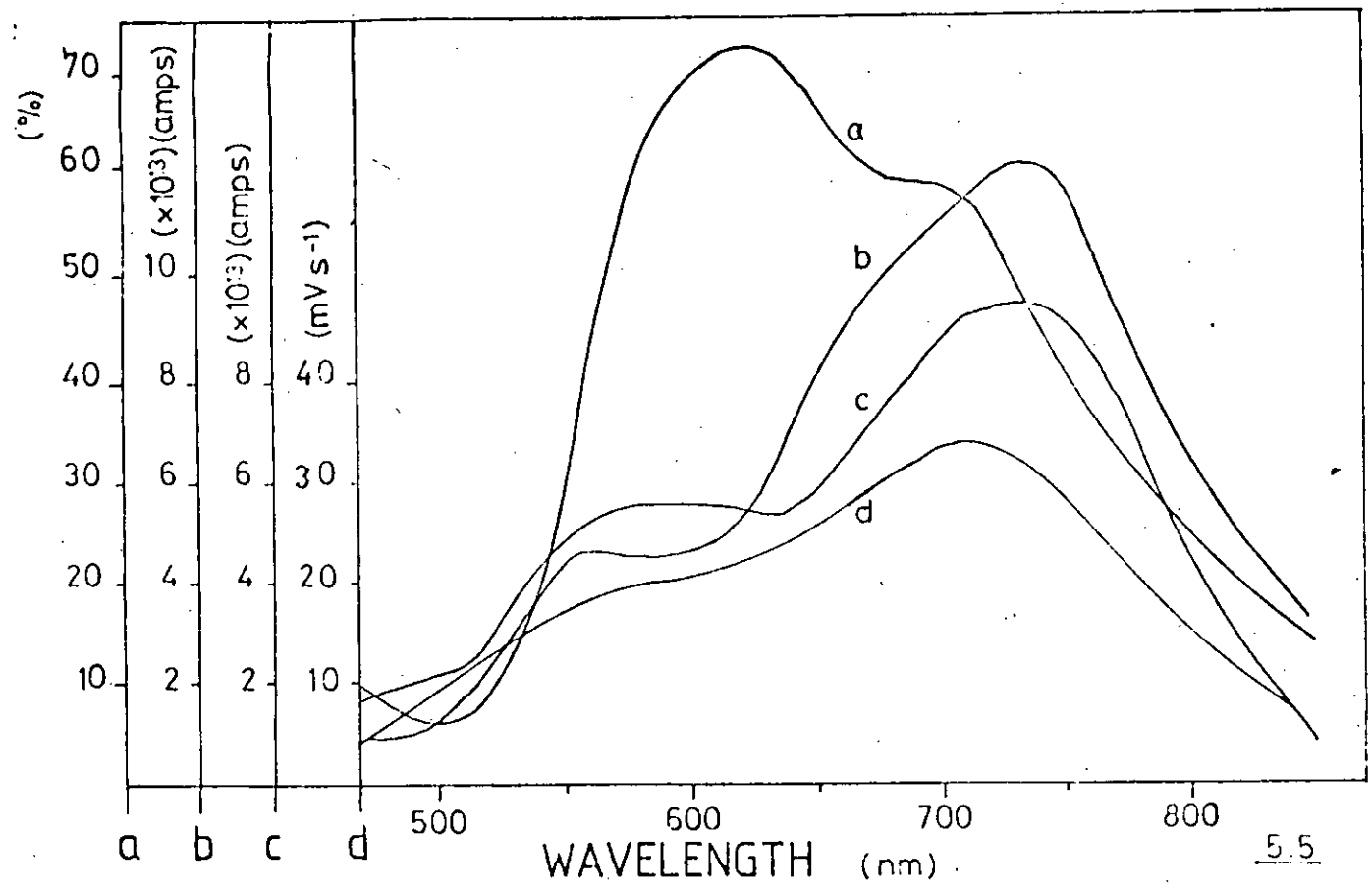

Spectral dependence of a) dye absorption, b) dye photo-conductivity, c) photo-induced current, d) photo-discharge rate.

5.2 MIM STRUCTURES

5.2.1 Field Dependence

As would be expected, MIM structures show no photo-conduction effects under illumination with wavelength longer than that of the UV.

The field dependence of the current through a Au-SiO_2-Au sandwich cell (SiO_2 thickness approx 0.5μm) is shown in Figure 5.6. The range of field was obtained by applying to the cell bias voltages of 0 to 50V. The straight line obtained by plotting log (current) against (applied field)$^{\frac{1}{2}}$ is indicative of Poole-Frenkel or Richardson-Schottky conduction. The gradient of the line gives for β the Poole-Frenkel coefficient, a value of $5.8 \times 10^{-24} JV^{-\frac{1}{2}}m^{\frac{1}{2}}$. From β, a value of the dielectric constant can be obtained and it is found to be consistent with that obtained from a direct measurement of capacitance. The value of the dielectric constant was measured to be 11.

Similar measurements also obtained at room temperature, are shown in figure 5.7. This figure also shows theoretical points calculated from the equation proposed by Gupta[9] for the current density, J, flowing by the trap-controlled and bulk-limited Poole-Frenkel effect in semiconductors, i.e.

$$J = q \mu N_c F_i \exp(-E_{cF}/kT)\exp(2\beta F^{\frac{1}{2}}/kT) \qquad 5.1$$

or, more simply,

$$J = AF \exp(BF^{\frac{1}{2}}) \qquad 5.2$$

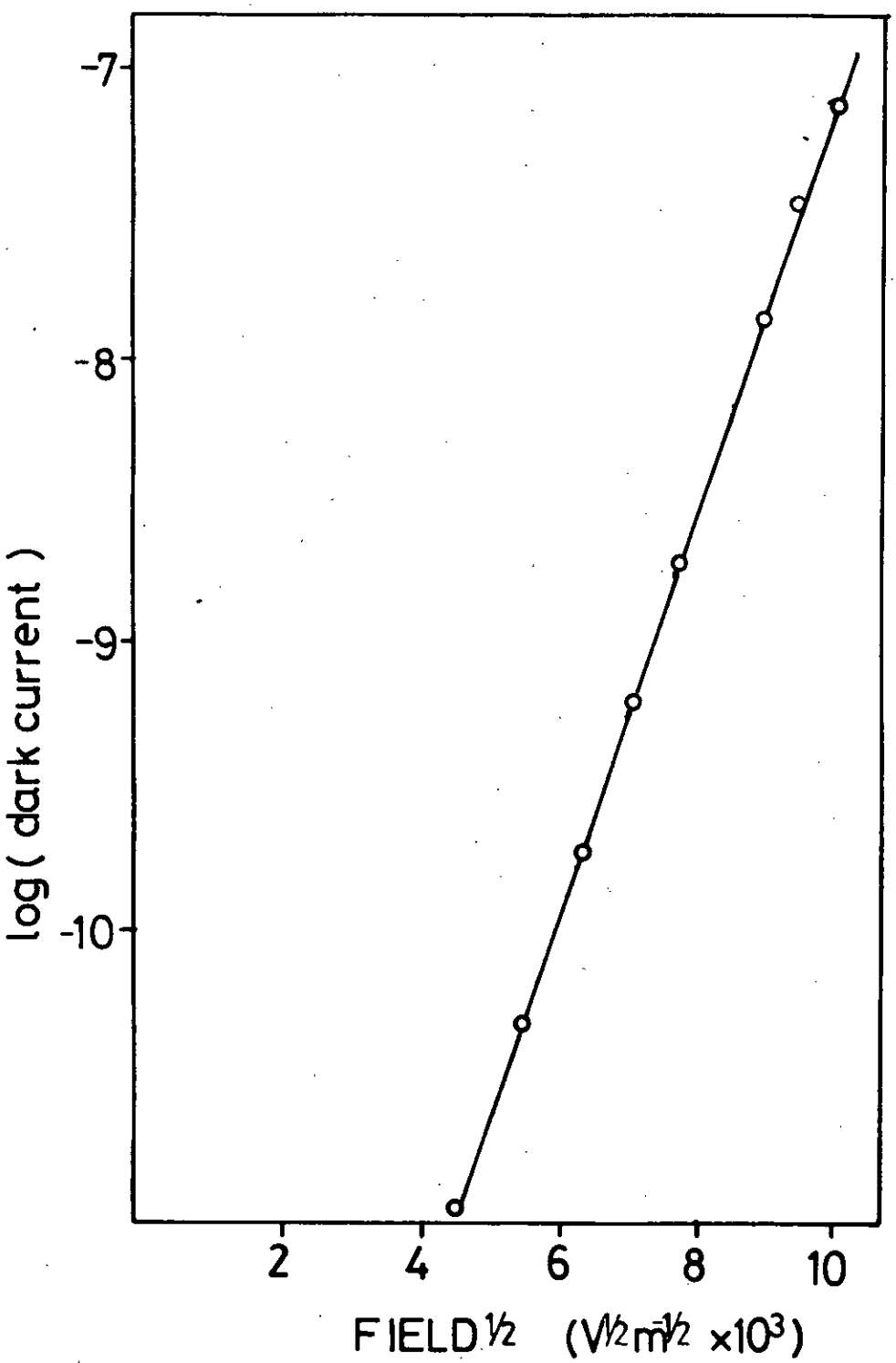

Field dependence of dark current in MIM cell. 5.6

In equation 5.2 F is the applied field, while A and B are constants (for a given temperature) which can be deduced by comparison with equation 5.1. The calculated points in Figure 5.7 were obtained from equation 5.2 by taking $A = 1.5 \times 10^{-13} (AV^{-1}m^{-2})$ and $B = 3.3 \times 10^{-4} (Vm^{-1})^{-\frac{1}{2}}$.

The mechanism of conduction in films of SiO_2 thickness greater than that consistent with direct tunneling has been discussed by several authors. Langlinger and Snow[10] concluded that at high fields Fowler-Nordheim tunneling from the electrode into the insulator conduction band is the dominating mechanism. Forgacs et al[11] found a Poole-Frenkel effect in layers thinner than 400Å but no measurable current for thicker films; Deal[12] et al also found a Poole-Frenkel effect. The apparent discrepancy between these results has been considered by Krause and Grünler[13] who suggest a hopping mechanism at low fields, a Poole-Frenkel effect at higher fields and Fowler-Nordheim tunneling at even higher fields. The transition between these mechanisms will depend on temperature and also on the distribution of energy states in the forbidden band. Different results may thus be due to different film preparation conditions. The results of Krause and Grunler suggest that for both thermally grown and pyrolytically deposited SiO_2, the transition from Poole-Frenkel to Fowler-Nordheim tunneling takes place at a field of approximately 2.5×10^8 Vm^{-1}. Poole-Frenkel conduction is also thought to be dominant if there is a large density of traps of medium depth.

The field regimes suggested would seem to be consistent with the observation of a Poole-Frenkel type of conduction in the present work.

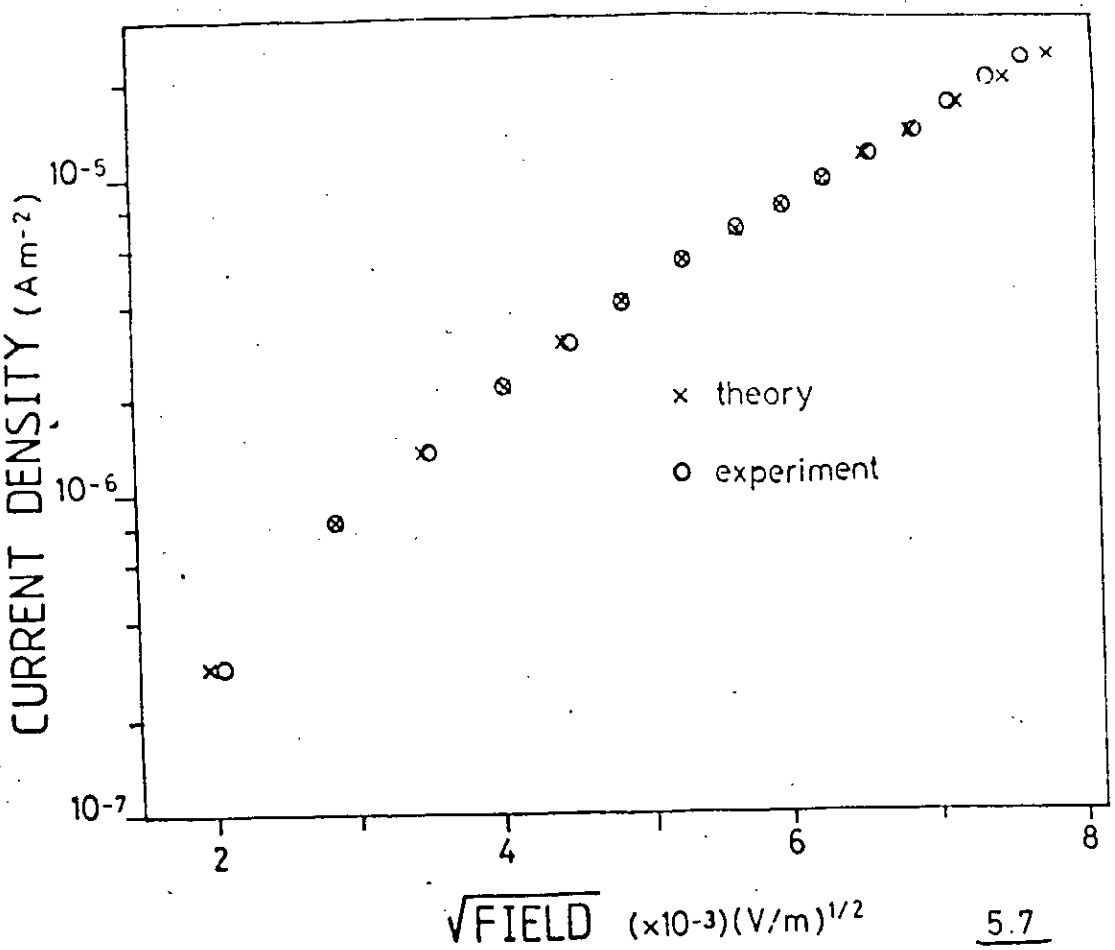

Experimental and calculated field dependence of current through MIM sample.

A further observation by Krause and Grunler was that results were not reproducible, there apparently being some "forming", effect which made the measured currents depend strongly on the previous electrical history of the sample.

5.2.2 Temperature Dependence

The temperature dependence of the current in MDIM sample was studied by the thermally stimulated dielectric polarization technique described in Chapter 4. The results are presented in Figures 5.8, 5.9, 5.10, 5.11 and 5.12 which correspond to slightly different schedules of temperature cycling and biasing and the conditions used are summarised as follows.

Figure 5.8	Sample cooled with 0V bias heated with 40V applied at 2K min^{-1} Plotted logarithmically vs 1/T.
Figure 5.9	as Figure 5.8
Figure 5.10	Data as Figure 5.8 Plotted linearly vs 1/T
Figure 5.11	Sample cooled with 0V bias heated with 10V applied at 2K min^{-1} cooled with 10V applied Plotted logarithmically vs 1/T
Figure 5.12	Cooled with 0V applied Heated with 40V applied Cooled with 40V applied Heated with 20V applied Plotted linearly as 1/T.

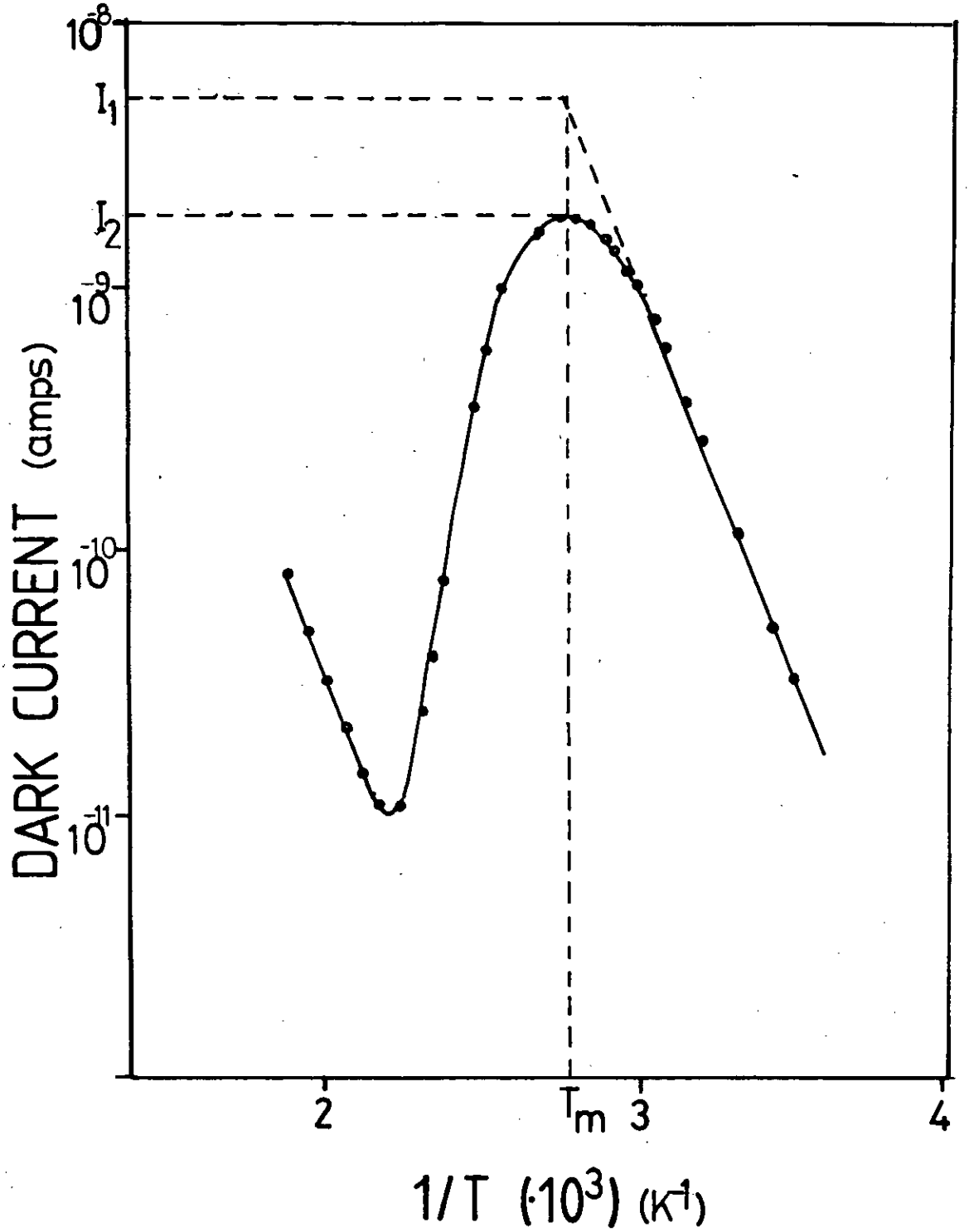

Temperature dependence of dark current through MIM cell.

5.8

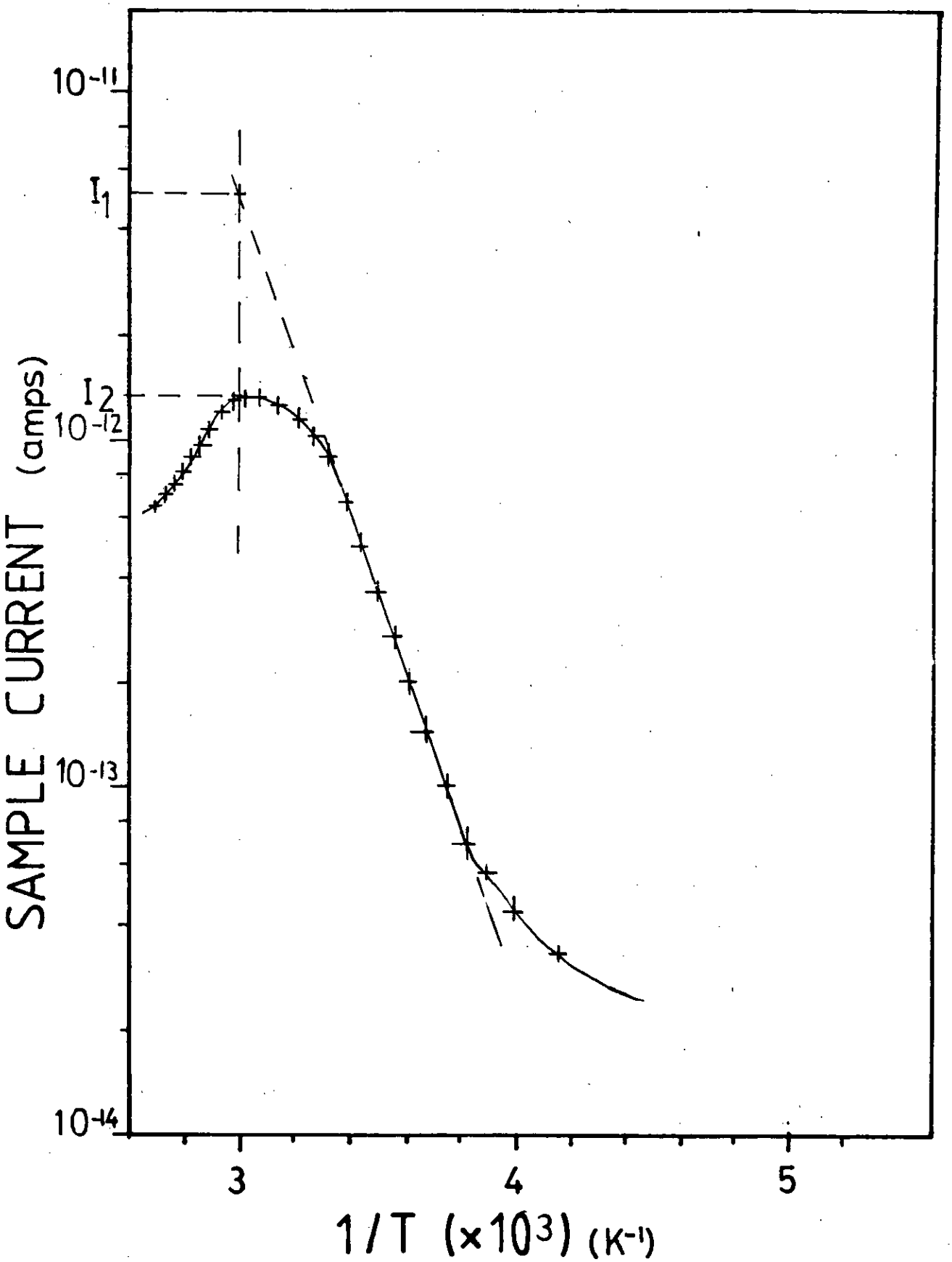

Temperature dependence of dark current through MIM cell.

5.9C

The most striking feature of Figures 5.8 and 5.9 are the maximum and minimum turning points. Simmons and Taylor[14,15] interpret similar observations for MIM films with blocking contacts as being due to a transition from a non-steady state conduction process at low temperatures which is bulk-limited to a electrode-limited steady-state process at high temperatures. The transition takes place as the dielectric relaxation time (DRT) changes from being very long to short. The temperature at which the maximum of current occurs is when the DRT is comparable with the experimental time say 100 s.

From the temperature, T_m, at which the maximum occurs it should be possible to gain information about the trap states in the energy gap of the insulator. The analysis of Simmons and Taylor is extended from the theory of thermally stimulated currents and depends crucially on the validity of three assumptions. These are that the current injected from the contacts into the bulk of the insulator is negligible, that the Fermi level is coincident with the trap level and that the trap level is discrete. Gupta and van Overstraeten[16] have extended the analysis to be valid when the Fermi level and trap level are close in energy but not necessarily coincident. They deduce that T_m depends on the heating rate, the applied field ($F_i(0)$), the occupied trap density ($f_t n_t$), and on the effective trap energy ($E_{CT} - 2\beta F_i^{\frac{1}{2}}$).

($E_{CT} - 2\beta F_i^{\frac{1}{2}}$) is given by the slope of the log I vs.1000/T plot in the straight line region at temperature less than T_m. The heating rate and the applied field are known from the experimental conditions and T_m can be measured. Thus is should be possible

to calculate a value of $f_t n_t$.

A striking feature of Figure 5.8 is the large magnitude of the current measured. All devices on a substrate exhibited similar values of current when the measurements were first taken irrespective of the previous history of the substrate. On repition, the currents were much smaller and a typical set of results are shown plotted in Figure 5.9. Temperature cycling without a bias voltage applied made very little difference to the magnitude of the currents observed for each device on a substrate. However, T_m seemed to move steadily to higher temperatures. The data shown in Figures 5.8 and 5.9 was substituted into the theory of Gupta and van Overstraeten and the results for the two sets of data are shown in the table below.

DATA	FIGURE 5.8	FIGURE 5.9
T_m	361 K	336 K
applied field	7.5×10^7 V m^{-1}	2.5×10^7 V m^{-1}
$E_{CT} - 2\beta F^{\frac{1}{2}}$	0.6 eV	0.46 eV
trap depth	0.77 eV	0.56 eV
$f_t n_t$	5×10^{29} m^{-3}	4×10^{23} m^{-3}

It should be noted that a value of $\phi - E_{CF}$, the barrier height between the electrode and insulator is required. Popova, Antov and Vitanov [17] quote a value of 3.64 eV for the barrier height between tungsten and SiO_2. Correcting for the difference in work function of gold and that of tungsten gives 4.0 eV for the barrier height between gold and SiO_2. It is very likely that the barrier height is

dependent on the method of preparation of the SiO_2. Values of between 1.5 eV and 1.0 eV for the electron affinity of SiO_2 are quoted by Chernyaev and Korzo.[18] The estimate of Popova et al suggests an electron affinity of 0.8 eV. Without any method of measuring directly the electrode-insulator barrier height, a considerable error is introduced into the calculation.

The calculated value of $f_t n_t$ of 5×10^{29} m^{-3} for the data shown in Figure 5.8 is absurd (there are about 10^{28} atoms m^{-3}) and obviously the theoretical model is not a good representation of the real situation.

Simmons and Taylor[19,20] describe a technique for determining if a single trapping level is active. The technique involves plotting current against temperature graph and measuring the half-width. If a single trap is active then the half-width, ΔT, is given by

$$\Delta T = 2KT_m^2/(E_{CT} - 2\beta\bar{F}_i^{\frac{1}{2}}) \qquad 5.3$$

where

$$F_i = F_i(0)\, e/(e - 1) \qquad 5.4$$

For the data shown in Figure 5.8, ΔT calculated from the above equation is 43^oK. From Figure 5.10 $\Delta T = 59^oK$.

Similarly for the data shown in Figure 5.9, ΔT by calculation is 47^oK but is 78^oK by direct measurement. It seems therefore that there is not a single discrete trap level operative but at least

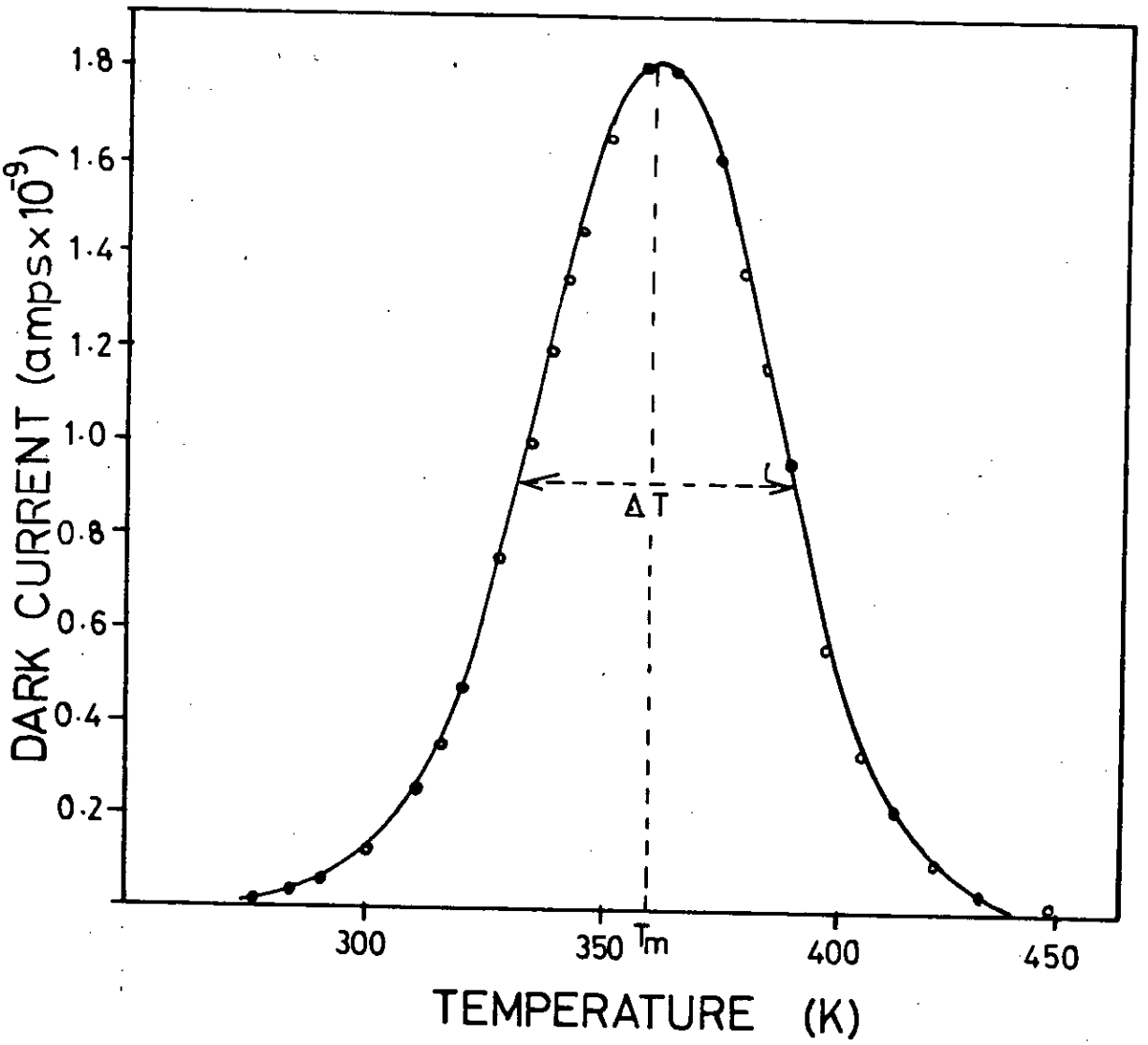

Temperature dependence of dark current through MIM cell - data of fig. 5.8

5.10

two levels or a distribution of traps. This makes the initial assumption about the trapping level being close to the Fermi level rather dubious and might explain the absurdity of the calculated trap density in the first case.

The calculation for the second set of data is more plasubile. However, it is assumed throughout the calculation that the potential dropped across the cathodic depletion region is small compared with the potential difference across the whole insulator. Thus the field in the interior of the insulator is to a good approximation that which would be given if the potential gradient throughout the insulator were uniform. The potential difference across the depletion region is given by

$$V_c(t_m) = F_i^{\frac{1}{2}}(0) \frac{hkT_m}{\beta} \times 2.303 \, (\log I_1 - \log I_2) \qquad 5.5$$

where h is the thickness of the insulator, $\log I_1$ and $\log I_2$ are shown on Figure 5.8 $V_c(t_m)$ = 2.3 V for this data which is not small compared to the total applied voltage of 10 V.

It seems that the theories of Gupta and van Overstraeten are inadequate in describing the particular experimental results shown here. The rather rigid constraint of the trapping level being single, discrete and very near the Fermi level could be the reason for failure of the calculations. The dramatic change in behaviour after heating with a bias from 200K to 500K is not accounted for.

Another experiment was conducted and the results are presented in Figure 5.11. Cooling took place with zero volts applied, heating with 10 V at a rate of 2K min^{-1}. After the temperature had reached 500K, the temperature ramp was reversed and the sample cooled again but with the bias remaining constant (10V). The heating stage produced a response similar to that of Figure 5.9 but during the subsequent cooling the current decreased with the same effective activation energy as in the high temperature region - no maximum in current is observed. The theories of Simmons et al and Gupta et al suggest that on heating, the field within the insulator will reach an equilibrium distribution. During this redistribution the current maximum is seen but on subsequent cooling there will be no redistribution of field and thus no current peak will be seen.

Another experiment was conducted in which a MIM sample was cooled with 0 volts applied, heated with 40V applied and then cooled with 40V applied. During the heating stage a response similar to Figure 5.8 was seen. The sample was then heated with 20V applied and the current was measured. The data is shown in Figure 5.12, where current is plotted against reciprocal temperature. A peak in current is seen at approx 250K but in opposite direction to the applied bias. At higher temperatures the current flow is in the normal direction as expected. The field distribution within the insulator as predicted from the theory of Simmons and Taylor[15] is shown in Figure 5.13.

The sample current is thought to be the sum of electrode limited and bulk limited currents. The bulk limited current dominates at low

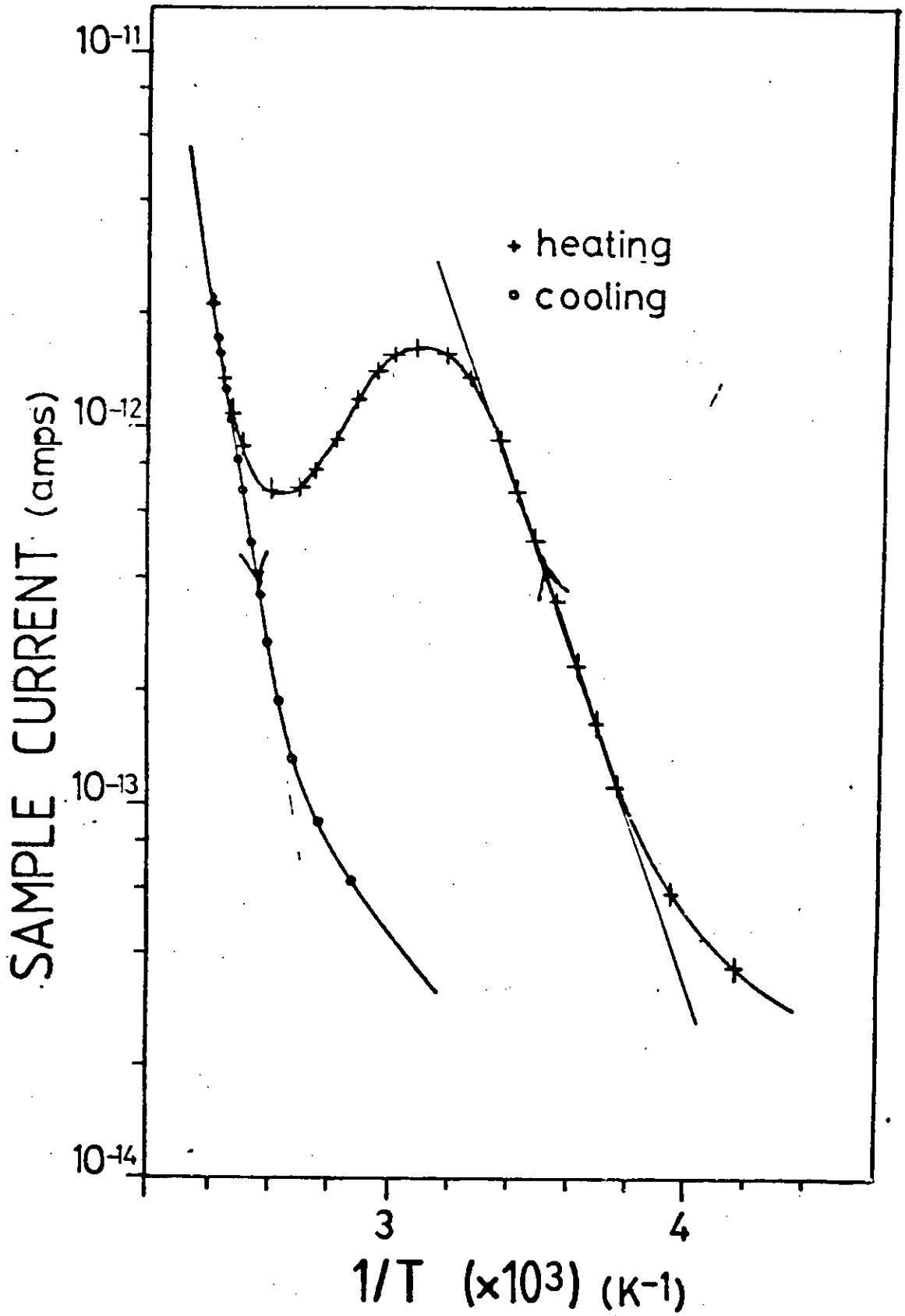

5.11

Temperature dependence of dark current through MIM cell during successive heating and cooling.

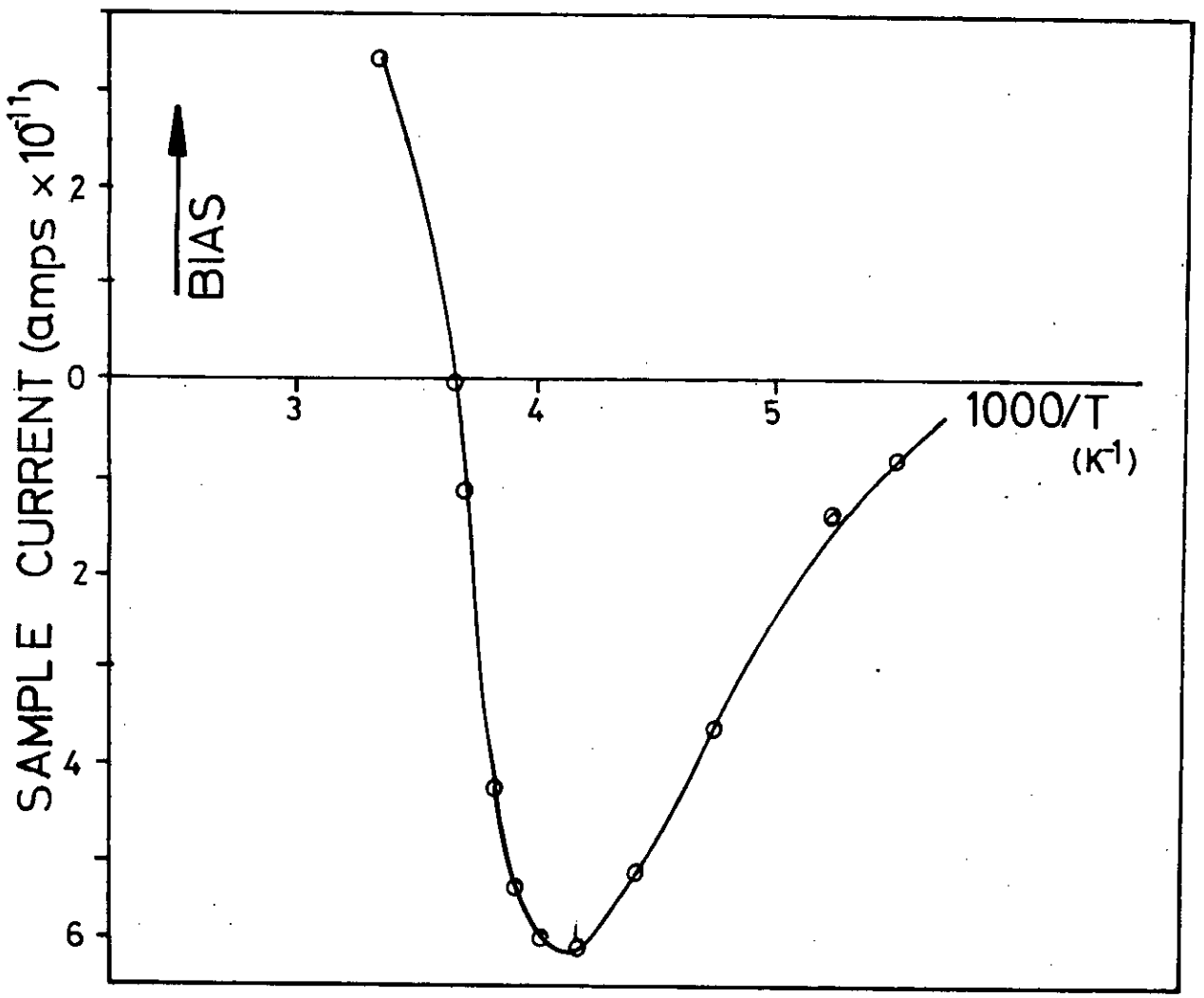

5.12

Temperature dependence of dark current through MIM cell.

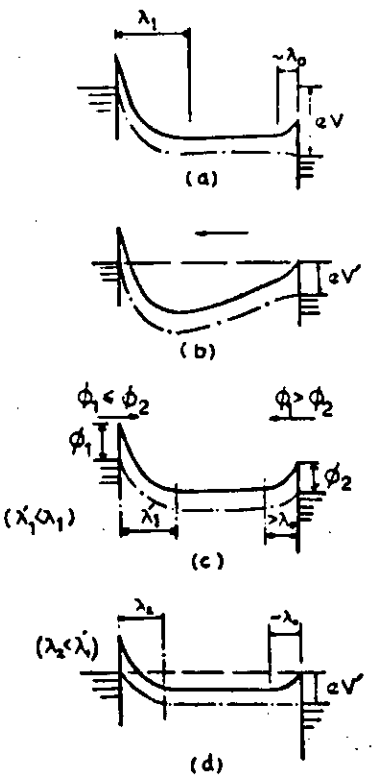

Figure 5.13: Insulator energy bands during:

a) heating with 40V applied and subsequent cooling
b) reduction of bias to 20V during heating
c) during heating
d) on reaching equilibrium

temperature and electrode limited current dominates at high temperature. Some dielectric relaxation experiments did not exhibit pronounced peaks. A typical result is shown in Figure 5.14(a) which is the data obtained when a MIM (Au-SiO_2-Mo) sample was cooled with 0V applied, heated with 40V applied (Au negative) at 1.5 K min^{-1}. An inflexion is seen when log (current) is plotted against reciprocal temperature. Also shown is the data for a similar experiment with the Mo electrode negative (Figure 5.14(b). A pronounced peak in current is shown at 340K. The electrode limited current is taken to be that at high temperatures. The high temperature plot for the Au negative response was extrapolated to low temperature and substracted from the measured plot. The resulting points are shown in Figure 5.14(c) which is similar to Figure 5.14(b). The Au-SiO_2 contact appears to allow more current to pass than the Mo/SiO_2 contact. This experiment shows that the electrode can influence the apparent response in the supposed bulk-limited region.

The dielectric relaxation experiments would suggest that the dominant trap depth lies between 0.4eV and 0.7eV below the conduction band of the SiO_2. There was a wide variation in results within this range but with a tendency towards the 0.4eV value. Water related electron traps have been reported in SiO_2 with an activation energy for detrapping of approx 0.35eV.[21] There is no doubt that a large amount of water is incorporated into CVD films during preparation and indeed enhanced trapping effects have been attributed to this water.[22]

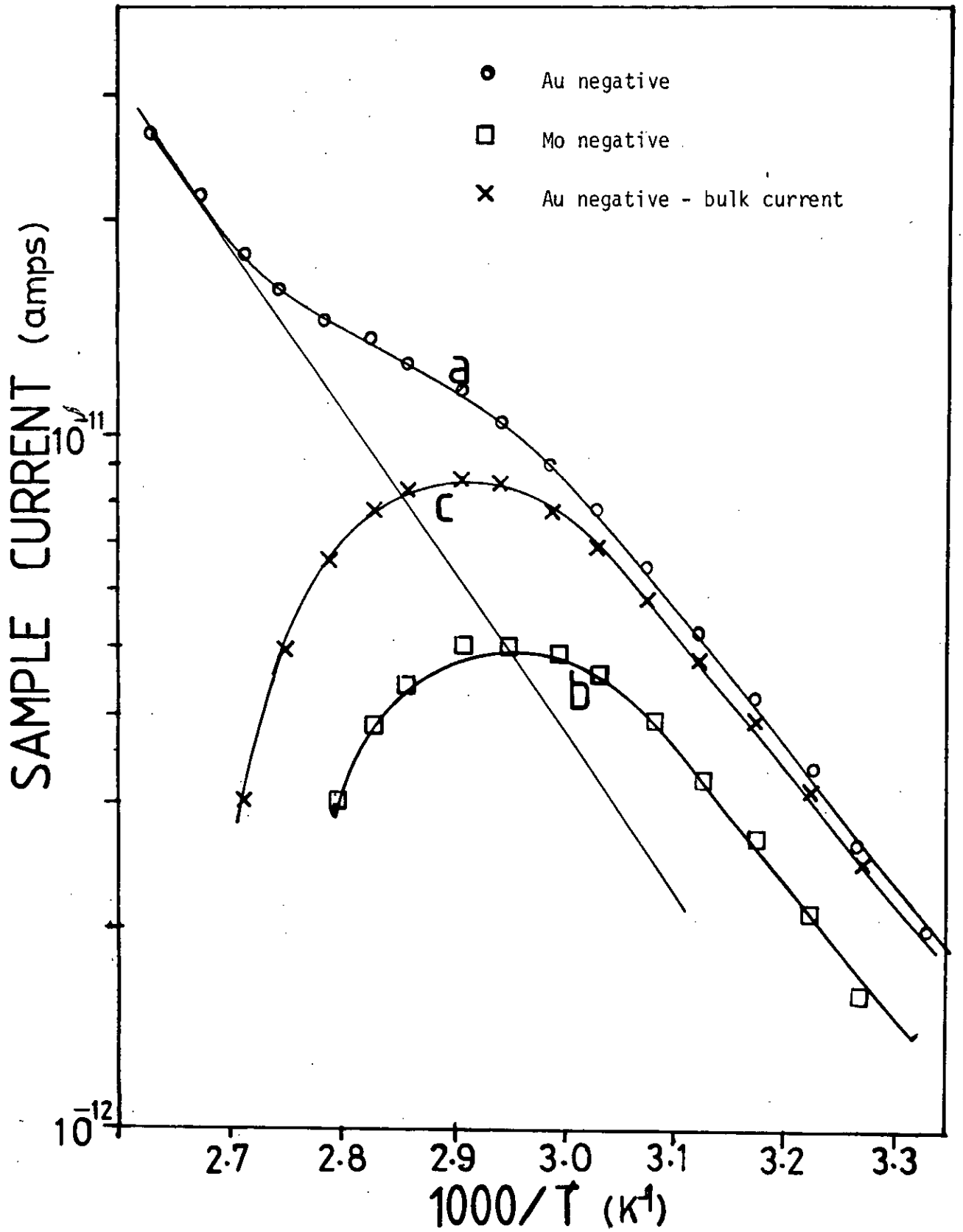

Temperature dependence of dark current through Au-SiO_2-Mo sandwich cell.

5.14

5.3 MDIM STRUCTURES

5.3.1 Time Dependence

The time dependence of the light-induced current through a MDIM sandwich structure, at room temperature, is shown in Figure 5.15. The dye H_2P_C dye-layer was approx 0.5μm thick; the insulator was silicon dioxide, produced by the silox process, and was typically 0.5 ~1.0 μm thick. Gold was used for both base and transparent top electrodes. The sample area was $2.5 \times 10^{-7} m^2$. The inset to Figure 5.15 shows the sample structure. A 5 volts bias was applied to the sample with the dye negative with respect to the insulator. After some time in the dark, during which the dark current dropped to 5×10^{-14}amp, the sample was illuminated, and the current showed a sharp transient increase which over some tens of seconds reduced to an apparently steady value of 1.2×10^{-13} amps. When a shutter was closed to remove illumination, the current quickly dropped, and, after a small overshoot, regained the previous dark value in a second or two. The response for opposite polarity i.e. dye positive is also shown. There was negligible photo-induced current flow. This polarity dependence i.e. appreciable current flow when the dye was negatively biased, negligible flow when the dye was positively biased seemed to be a general rule and was also observed for other dyes. e.g. cyanine dyes. In the results of Figure 5.15 which are typical, the magnitude of the photoinduced current is approximately 2.5 times that of the dark current. During these measurements, the electrometer shunt resistor was $10^{12}\Omega$ which makes the instrumental response

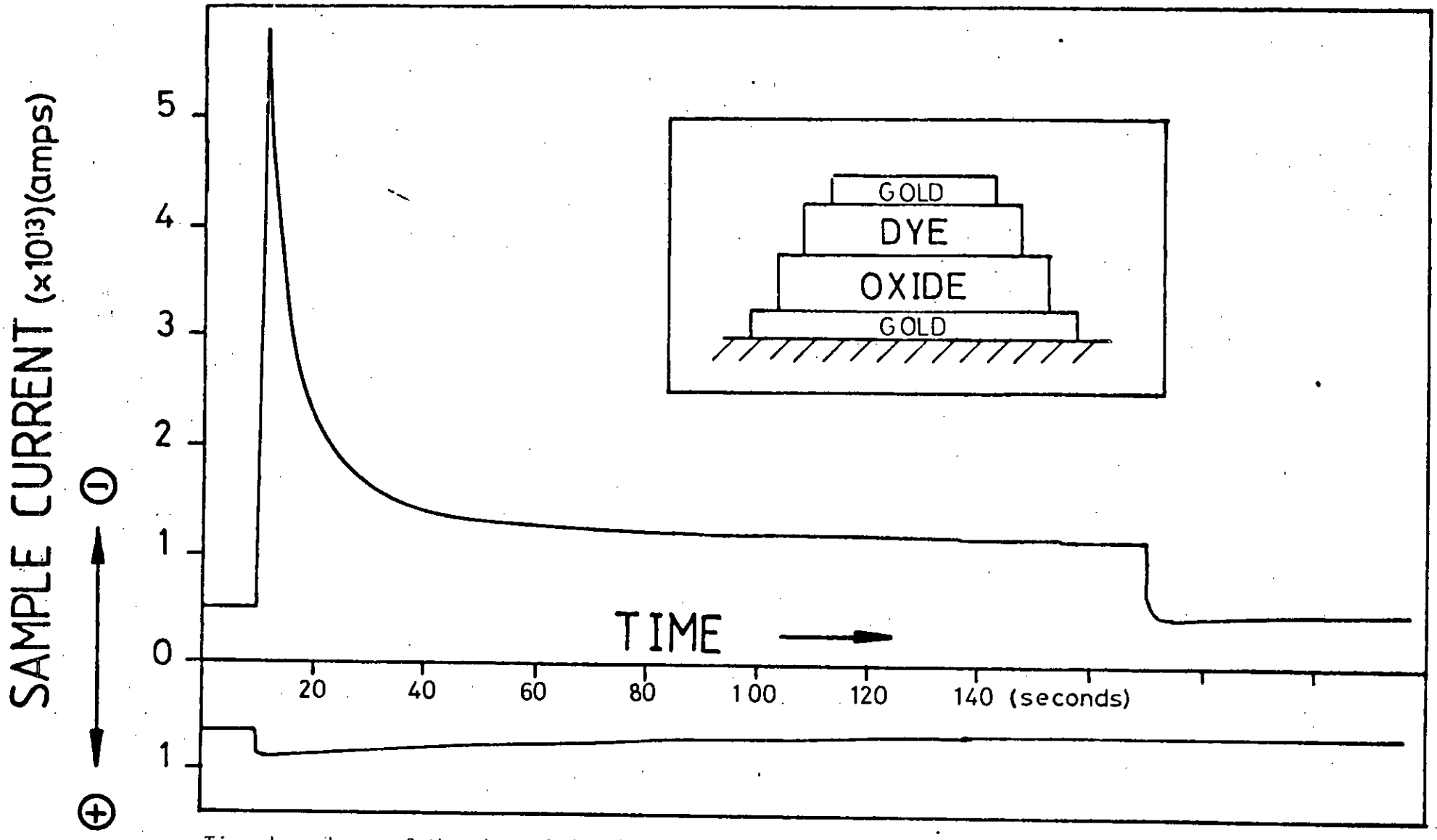

Time dependence of the photo-induced current in MDIM structure for both polarities of bias.

time <5 seconds.

The initial value of the photo-induced current was dependent on the time the sample was allowed to relax in the dark with bias applied. For example, Figure 5.16 shows the sample current for a repeated dark/light sequence. Initially the sample, with 40V applied, had been without illumination for several minutes. A dark current level of 1.8×10^{-12} amps was measured during which time the photo-induced current (in excess of the dark current) showed a transient of approximately 4×10^{-12} amps falling to 1.8×10^{-12} amps. The sample was returned to the dark condition for 10 seconds. The photo-induced current, under subsequent illumination of equal intensity showed a transient of 2.6×10^{-12} amps falling to 1.8×10^{-12} amps in 4 seconds. For these measurements a $10^{10}\,\Omega$ shunt resistor was used in the electrometer, giving a response time <0.5 seconds.

In Figure 5.17 the current flowing through a MDIM sample is plotted versus time for various values of bias voltage. The form of the transient decay is seen to be dependent on bias voltage.

5.3.2 Curve Fitting of Current vs. Time Data

The data presented in Figure 5.15 was digitised and stored in the memory of a Hewlett-Packard 9825 desk-top calculator. Equations of various forms could be plotted and compared with the experimental data. Figure 5.18 shows the best fit which can be obtained with a single exponential term. Figure 5.19 shows the

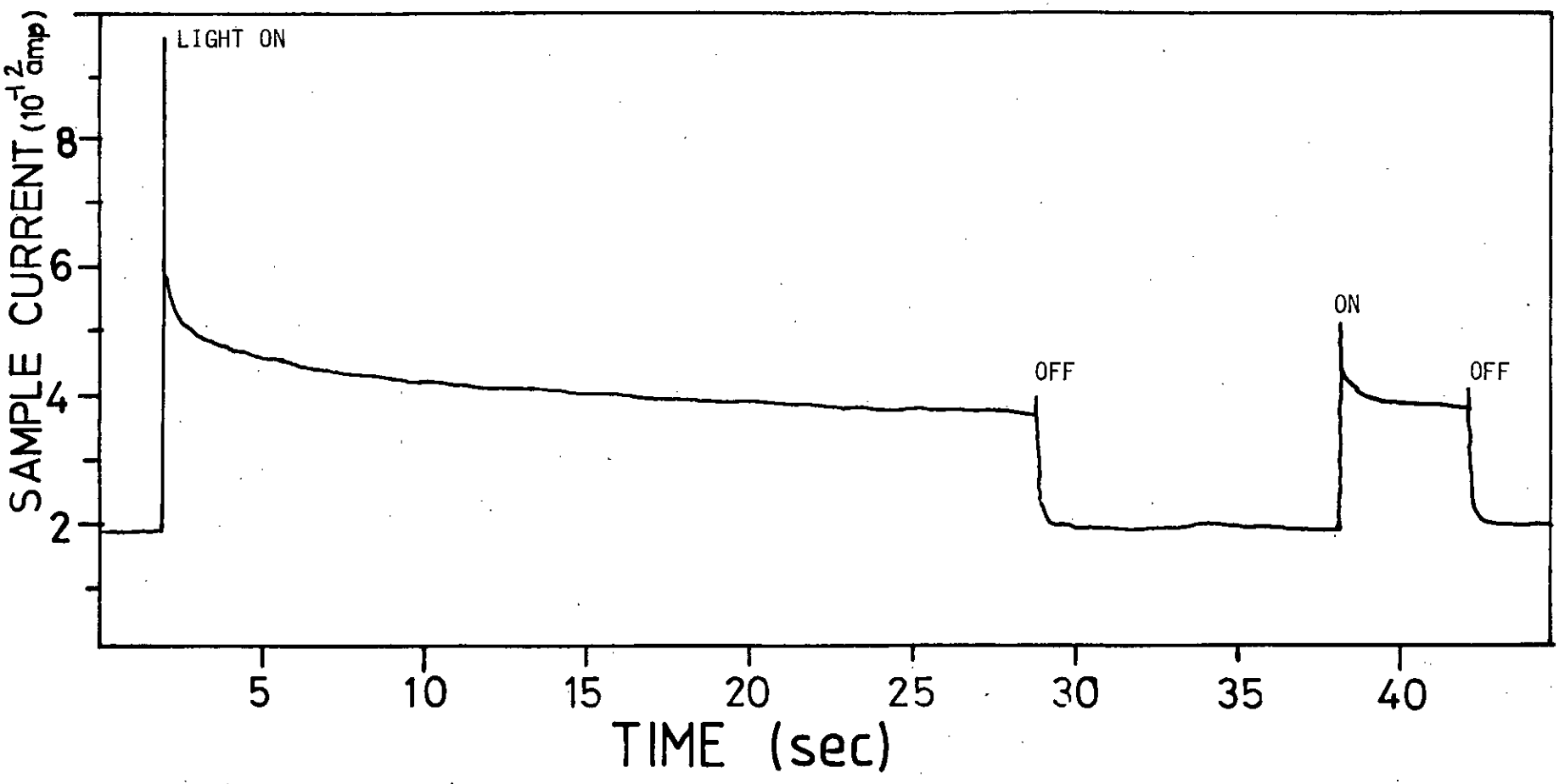

Time dependence of photo-induced current in MDIM cell under intermittant illumination.

5.16

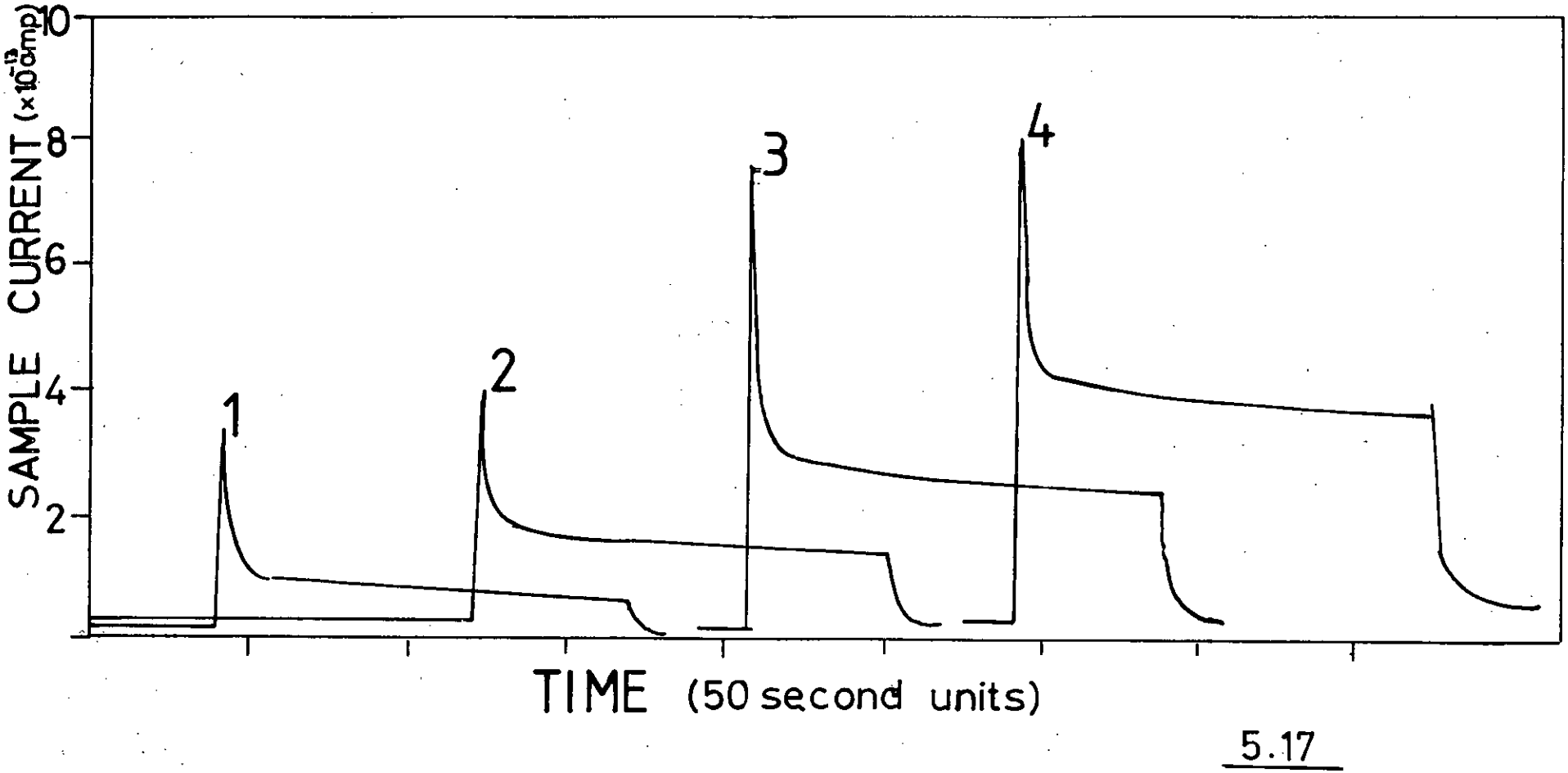

5.17

Time dependence of photo-induced current through MDIM sample for various bias voltages.

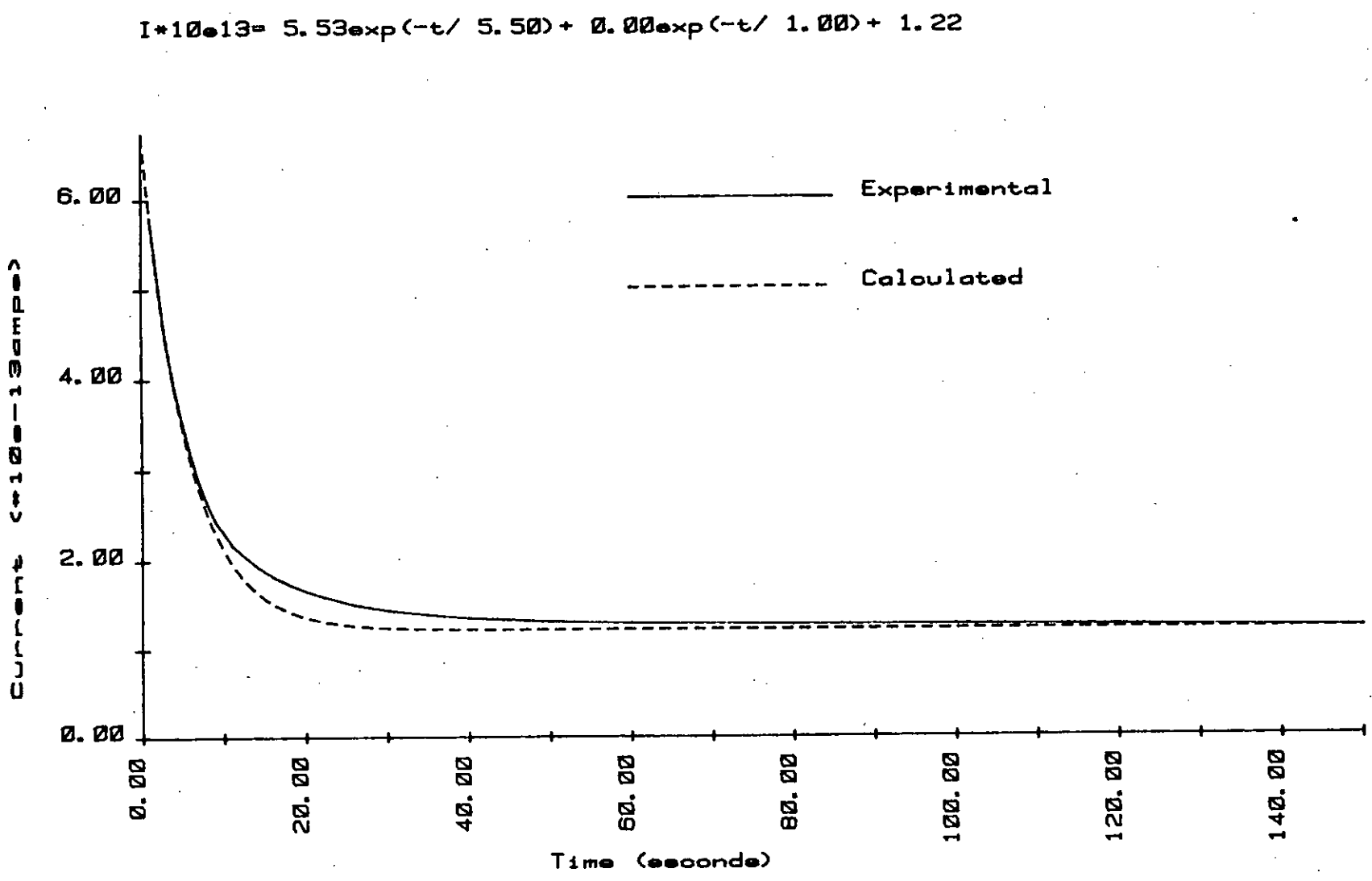
I*10e13= 5.53exp(-t/ 5.50)+ 0.00exp(-t/ 1.00)+ 1.22
Experimental
Calculated
Current (*10e-13amps)
6.00
4.00
2.00
0.00
0.00
20.00
40.00
60.00
80.00
100.00
120.00
140.00
Time (seconds)

5.18

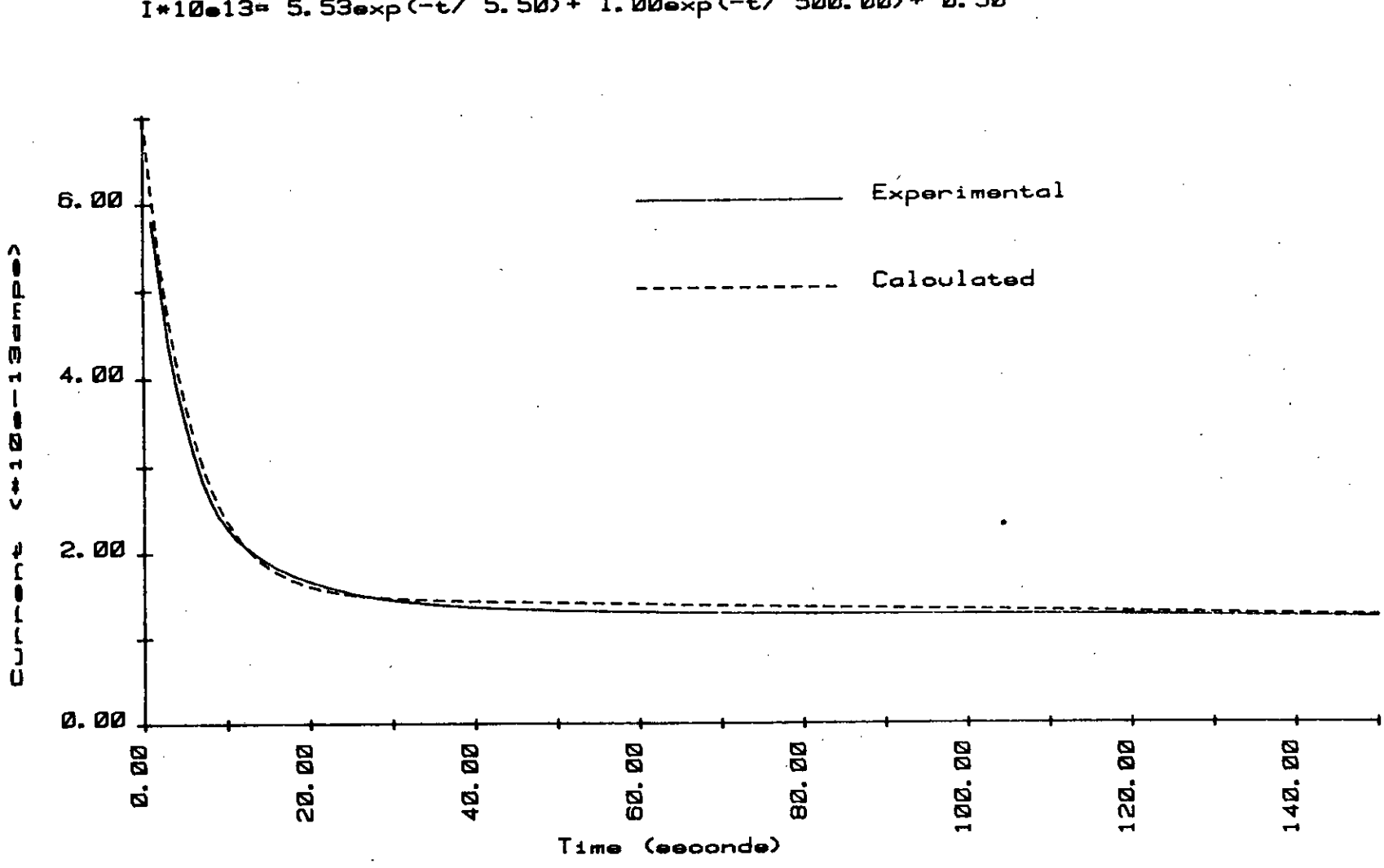
I*10e13= 5.53exp(-t/ 5.50)+ 1.00exp(-t/ 500.00)+ 0.50
Experimental
Caloulated
Current (*10e-13amps)
6.00
4.00
2.00
0.00
0.00
20.00
40.00
60.00
80.00
100.00
120.00
140.00
Time (seconds)

fit with two exponential terms and Figure 5.20 the very good fit obtained with a linear combination of three exponential terms. The equation plotted is

$$I \times 10^{13} = 4.55 \exp(-t/4.20) + 1.2 \exp(-t/15.0) + 0.8 \exp(-t/1800) + 0.5 \qquad 5.6$$

The constant term is the value of the dark current and the equation predicts that the photo-induced current will decay to the dark current with an extremely long time constant (1800 s).

Figure 5.21 shows a similar curve fitting of the data presented in Figure 5.16. The equation plotted is

$$I \times 10^{13} = 9 \exp(-t/0.15) + 1.50 \exp(-t/15.0) + 3.35 \qquad 5.7$$

Over the short time scale plotted, it is not possible to distinguish a term involving a very long time constant. The short time constant, in both cases presented, is close to the instrumental response time for $10^{12}\Omega$ shunt resistor in Figure 5.20 and $10^{10}\Omega$ in Figure 5.21.

5.3.3 Field Dependence

Figure 5.22 shows the dark and steady state photo-induced currents at low applied fields. Log (current) is plotted against (applied voltage)$^{\frac{1}{2}}$. A linear dependence between these parameters is predicted by the theories of Richardson-Schottky and Poole-Frenkel

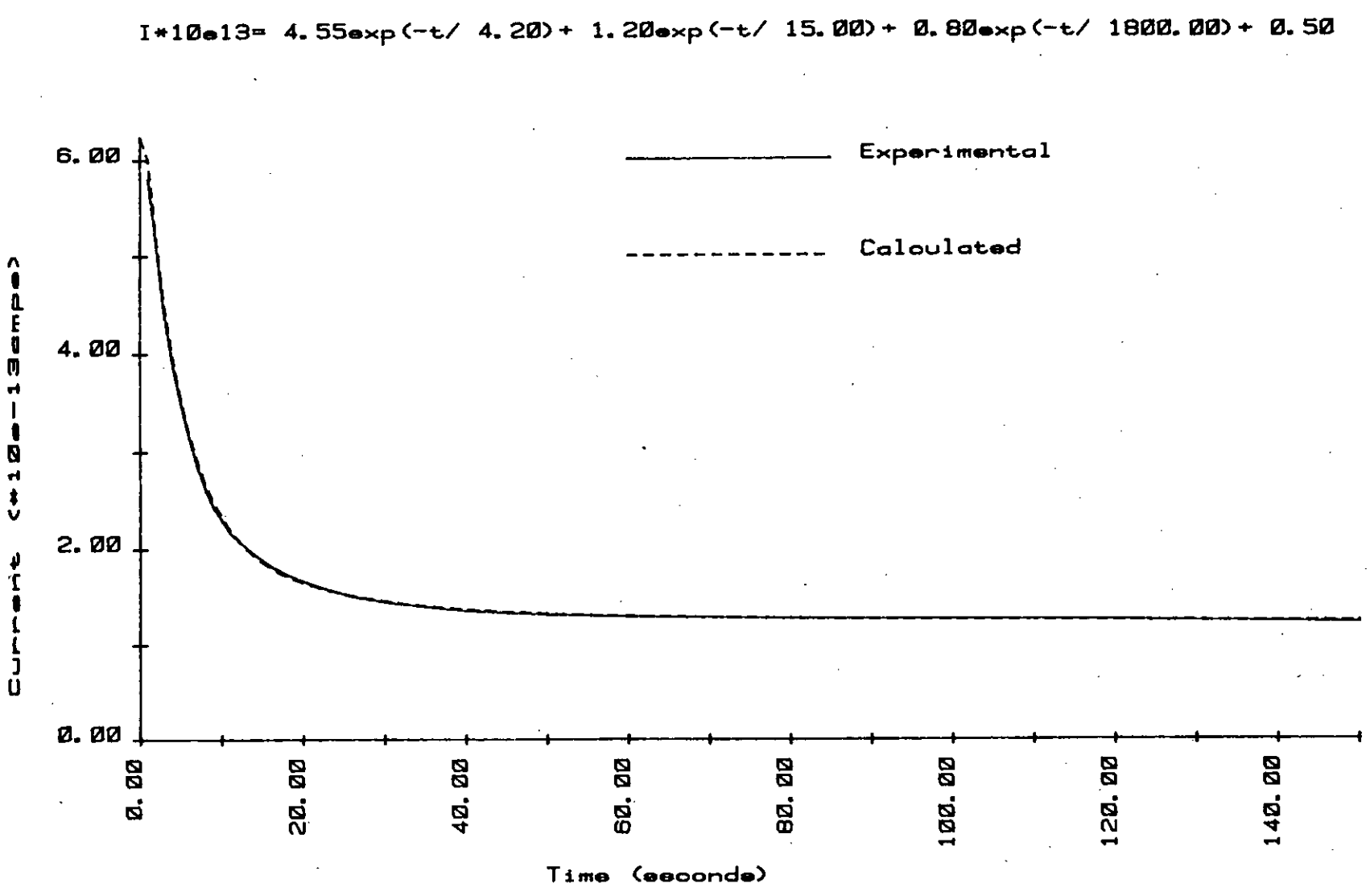
I*10e13= 4.55exp(-t/ 4.20)+ 1.20exp(-t/ 15.00)+ 0.80exp(-t/ 1800.00)+ 0.50
Experimental
Calculated
Current (*10e-13amps)
6.00
4.00
2.00
0.00
0.00
20.00
40.00
60.00
80.00
100.00
120.00
140.00
Time (seconds)

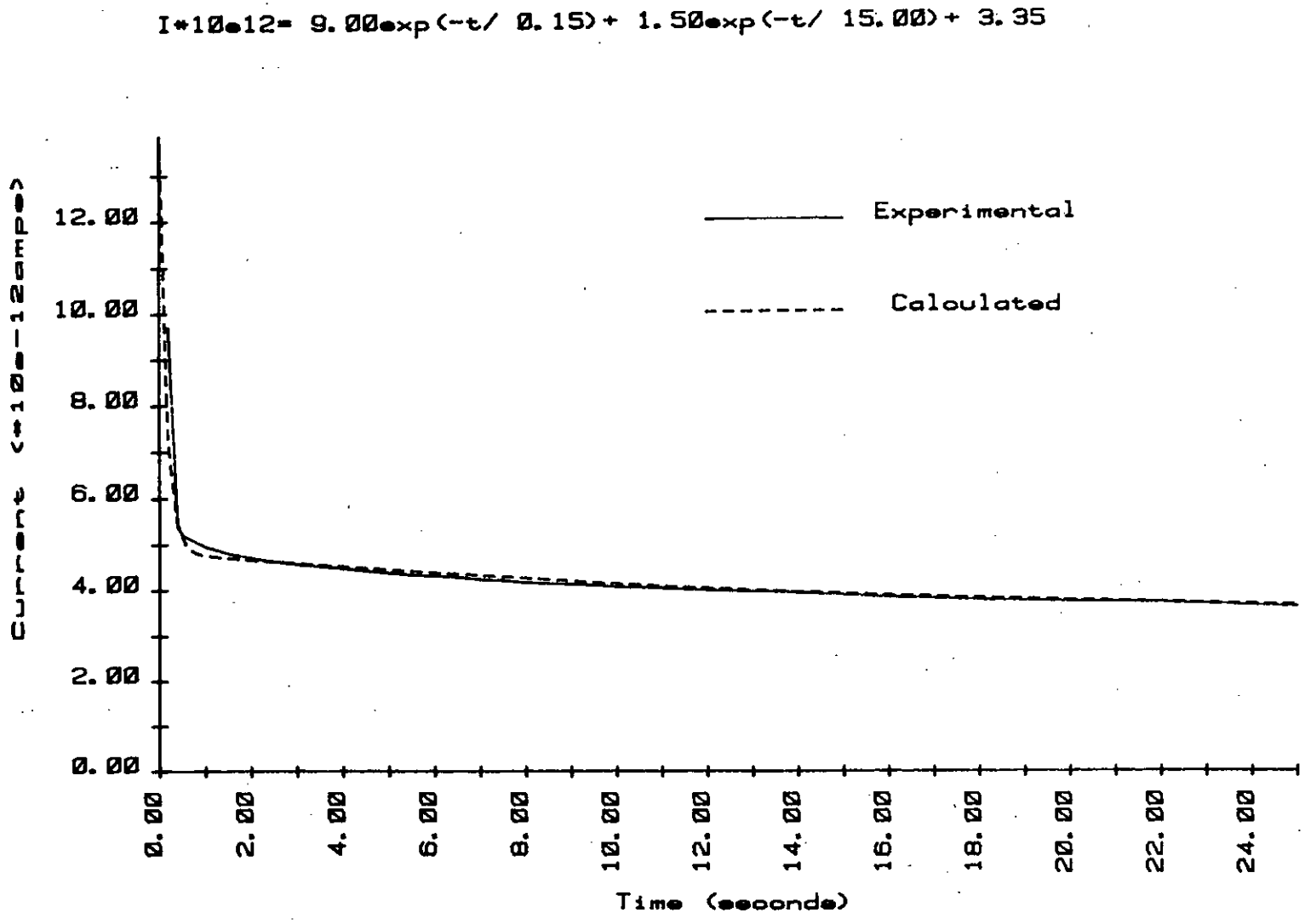
I*10e12= 9.00exp(-t/ 0.15)+ 1.50exp(-t/ 15.00)+ 3.35
Current (*10e-12amps)
12.00
10.00
8.00
6.00
4.00
2.00
0.00
Experimental
Caloulated
0.00
2.00
4.00
6.00
8.00
10.00
12.00
14.00
16.00
18.00
20.00
22.00
24.00
Time (seconds)

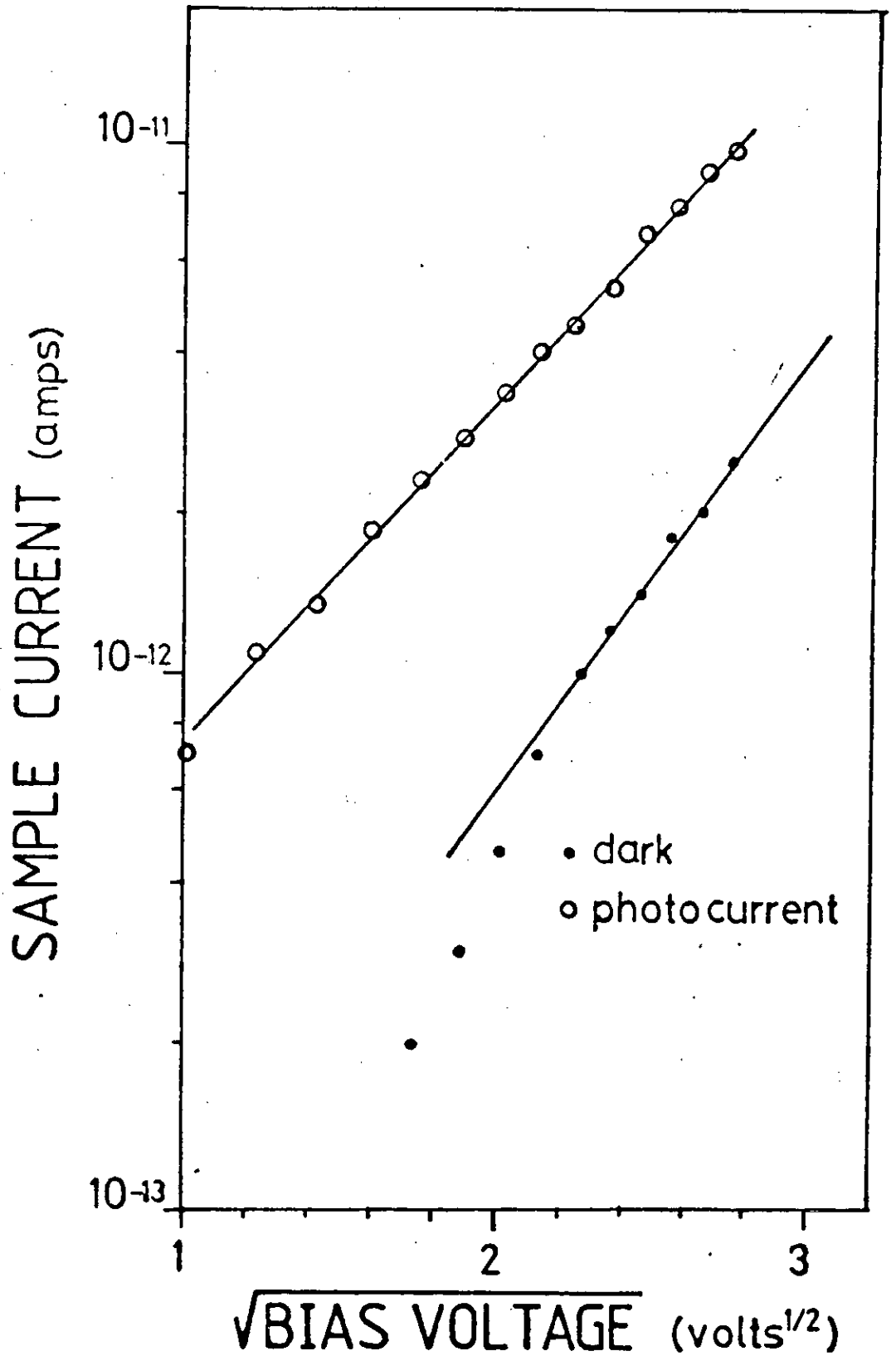

Field dependence of dark and photo-induced currents in MDIM sample.

5.22

types of conduction. The gradients of the plots (normalised for the area of the sample) are, $3 \times 10^{-3} m^{\frac{1}{2}} V^{-\frac{1}{2}}$ for the dark current and $3.6 \times 10^{-3} m^{\frac{1}{2}} V^{-\frac{1}{2}}$ for the photo-conduction. These results give values for the Poole-Frenkel coefficient, β, of 6.2×10^{-24} $JV^{-\frac{1}{2}} m^{\frac{1}{2}}$ and $7.4 \times 10^{-24} JV^{-\frac{1}{2}} m^{\frac{1}{2}}$ respectively.

The high field-dependence of the dark and the steady-state photo-induced current (i.e. in excess of the dark current) for a H_2P_C/SiO_2 sandwich cell at room temperature is shown in Figure 5.23. The currents plotted are the values of photo-induced current after the initial transient had decayed. The light was switched off between readings. Two main features of the photo-current are seen.

a) an inflexion between 15 and 25 volts, and,

b) a tendency for the current to saturate at higher voltages (>50V).

Measurements in the saturation region are difficult because at the resulting fields, $5 \times 10^{7} Vm^{-1}$, there is a tendency for the oxide film to breakdown.

5.3.4 Spectral Response

Shown in Figure 5.5(c) is the spectral dependence of the steady-state photo-induced current through an $Au/H_2P_C/SiO_2/Au$ sandwich cell. The experiment was conducted at room temperature and the same general features are observed as for the photo-conduction in H_2P_C (Figure 5.5(b)) i.e. a major peak at 730 nm and a smaller

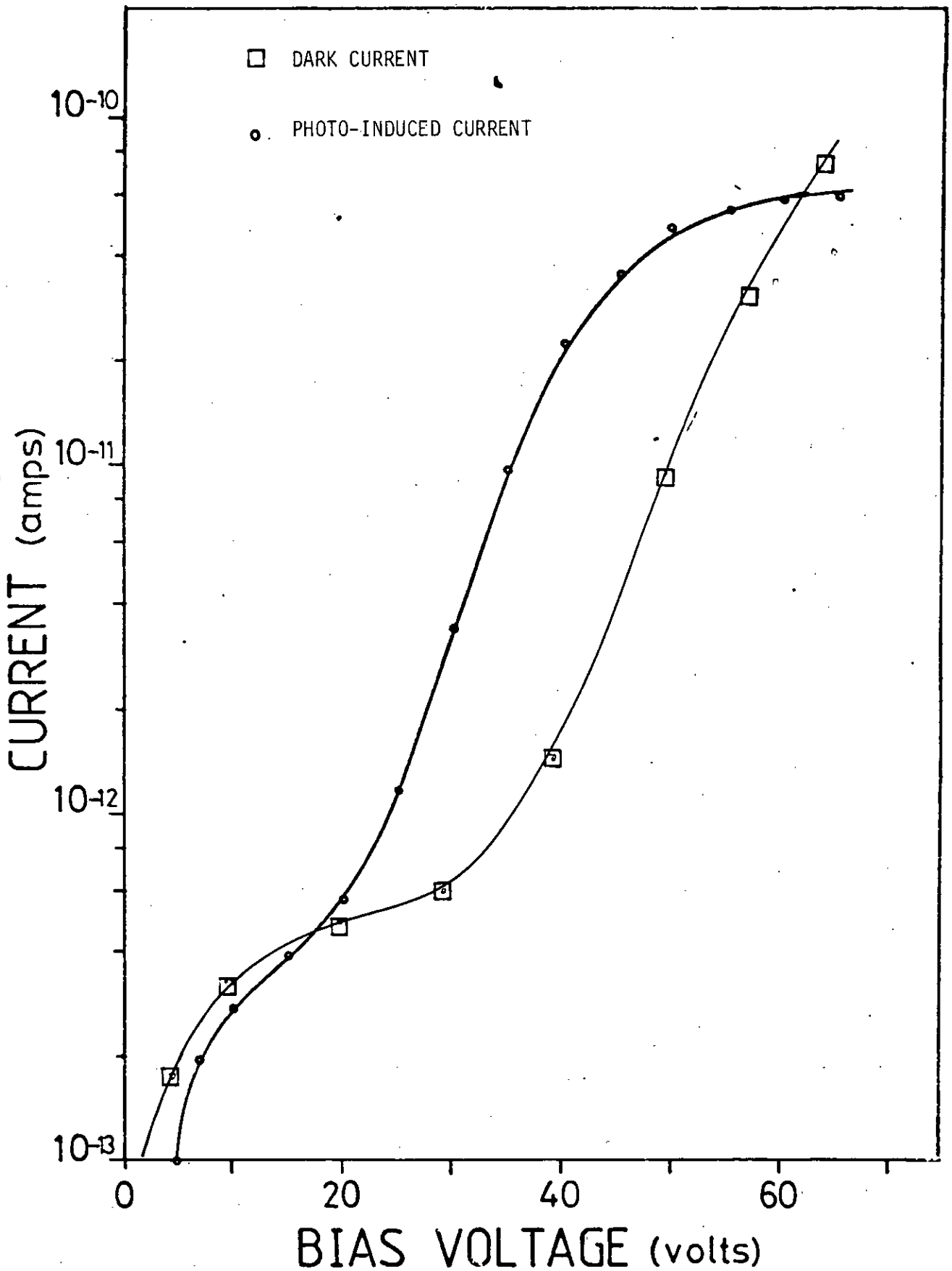

Field dependence of dark and photo-induced currents in MDIM sample.

5.23

peak at 570 nm but the relative sizes of the peaks is different in the two cases - the peaks are much closer in magnitude for the photo-induced current than for the photo-conduction in the dye itself.

5.3.5 Temperature Dependence

The temperature dependence of the dark and photo-induced currents through MDIM sandwich cells is shown for various samples in Figure 5.24 to 5.26. The cells were all of H_2P_C/SiO_2 and all nominally of identical dimension (~0.5 μm H_2P_C, ~0.5μm SiO_2). The currents are plotted logarithmically against reciprocal temperature The samples were all cooled with zero bias and heated with a bias of 40V. The heating rate was 2K min^{-1} and the dark and photo-currents recorded at various temperatures. The light was switched off between readings of photo-current. On illumination, the current was allowed to stabilise for some seconds (approx 10s) before taking a reading. A peak is observed in most cases, in both the dark and photo-induced currents, at temperature above 250K. At high temperatures, both currents increase monotonically with increasing temperature. The slopes (in eV) of the plots are summarised in the Table 5.1 overleaf for the low temperature and high temperature regions.

In both regions of temperature the slope of the dark current is higher than the photo-induced current and for both currents the slope is higher in the high temperature region.

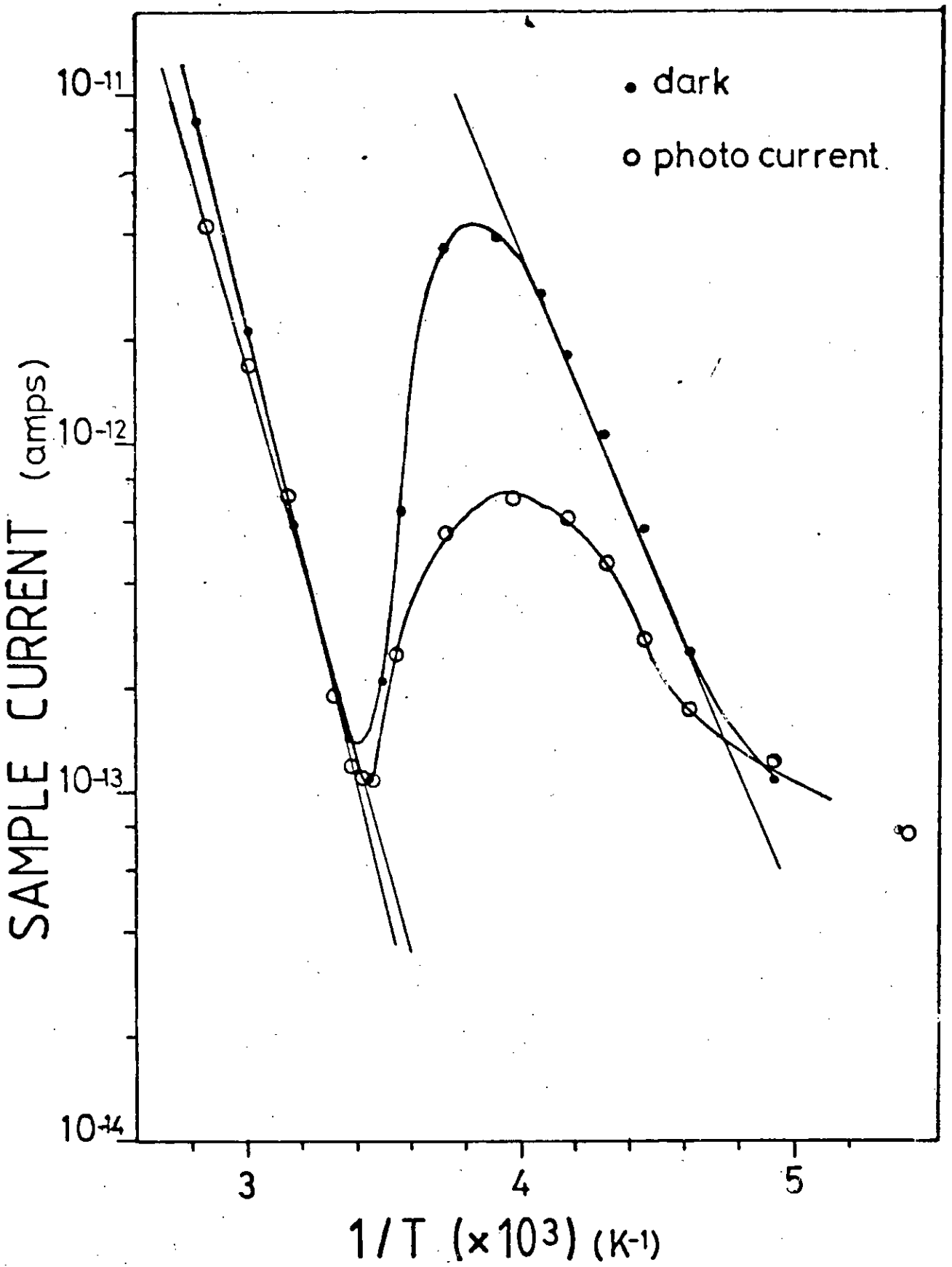

Temperature dependence of dark and photo-induced currents in a MDIM sample.

5.24

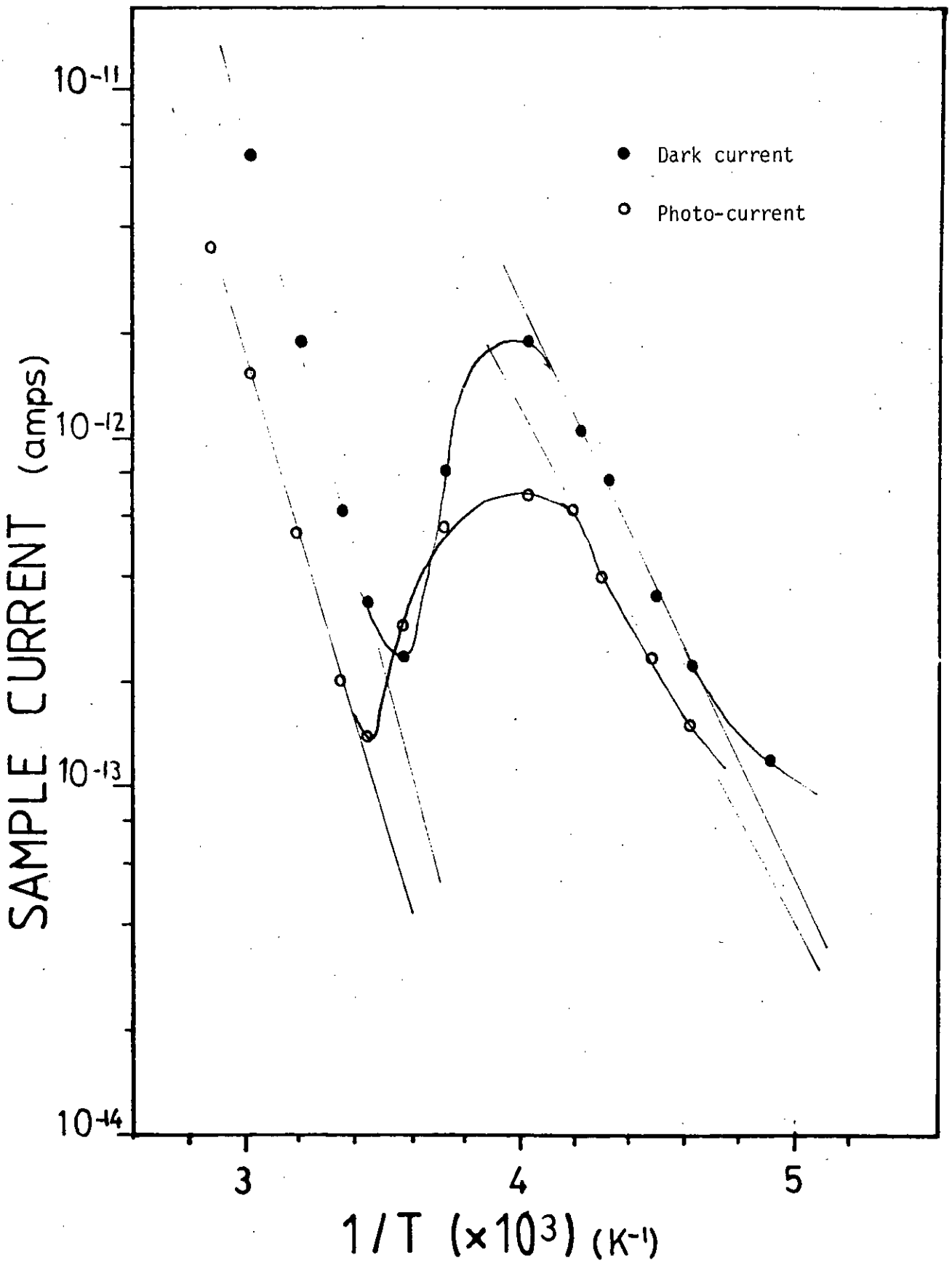

Temperature dependence of dark and phot-induced currents in a MDIM cell.

5.25

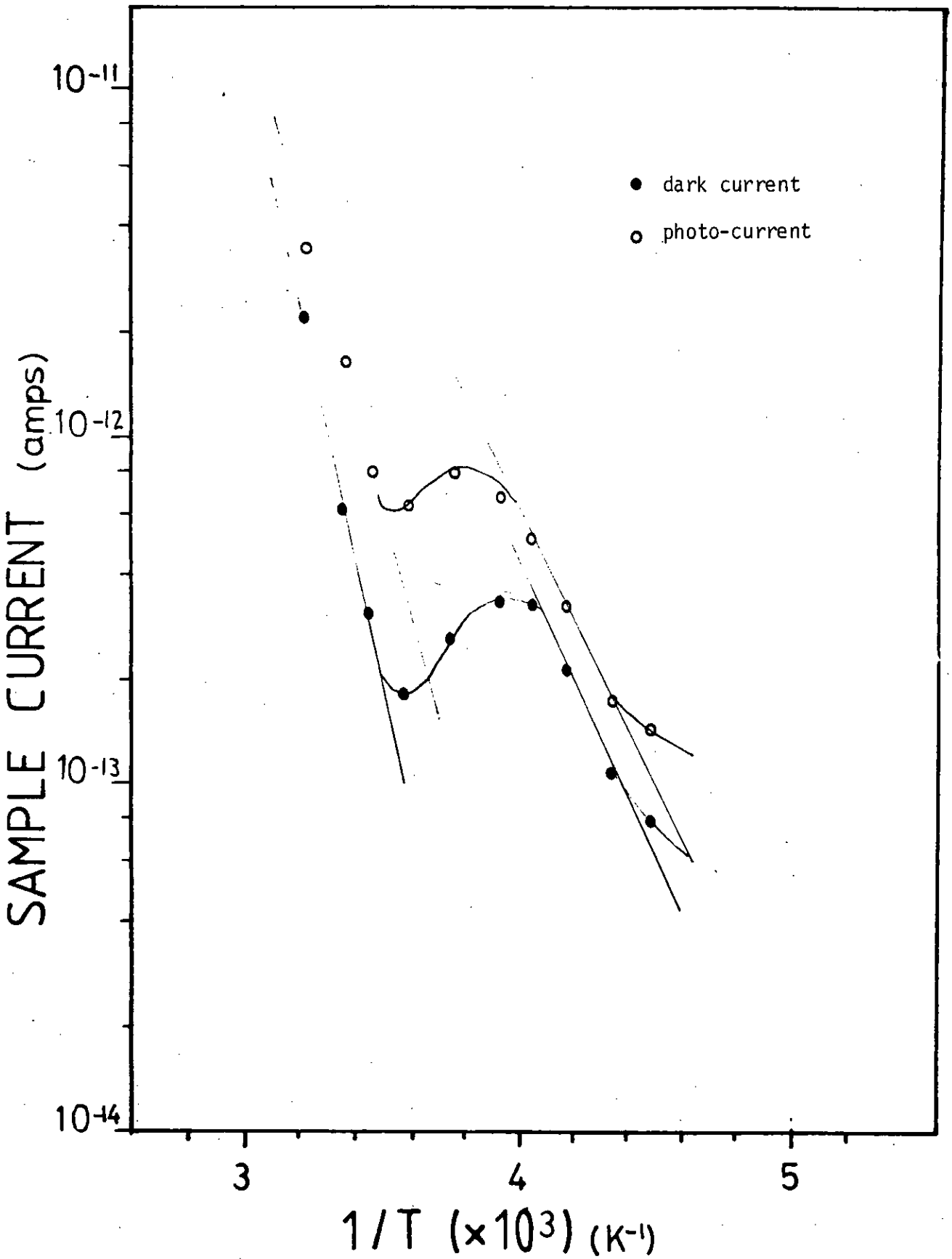

Temperature dependence of dark and photo-currents in a MDIM sample.

5.26

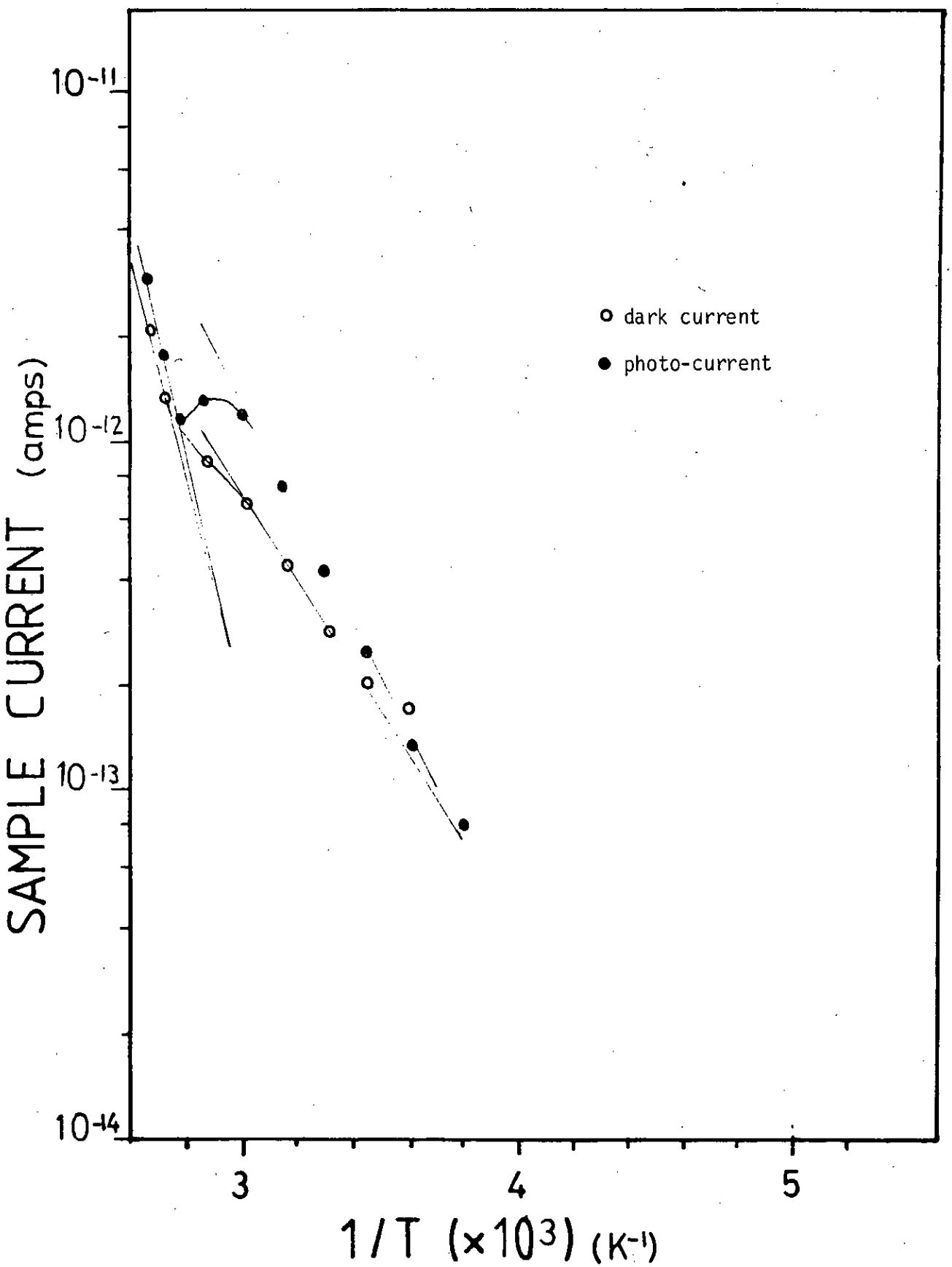

Temperature dependence of dark and photo-induced currents in a MDIM sample.

5.27

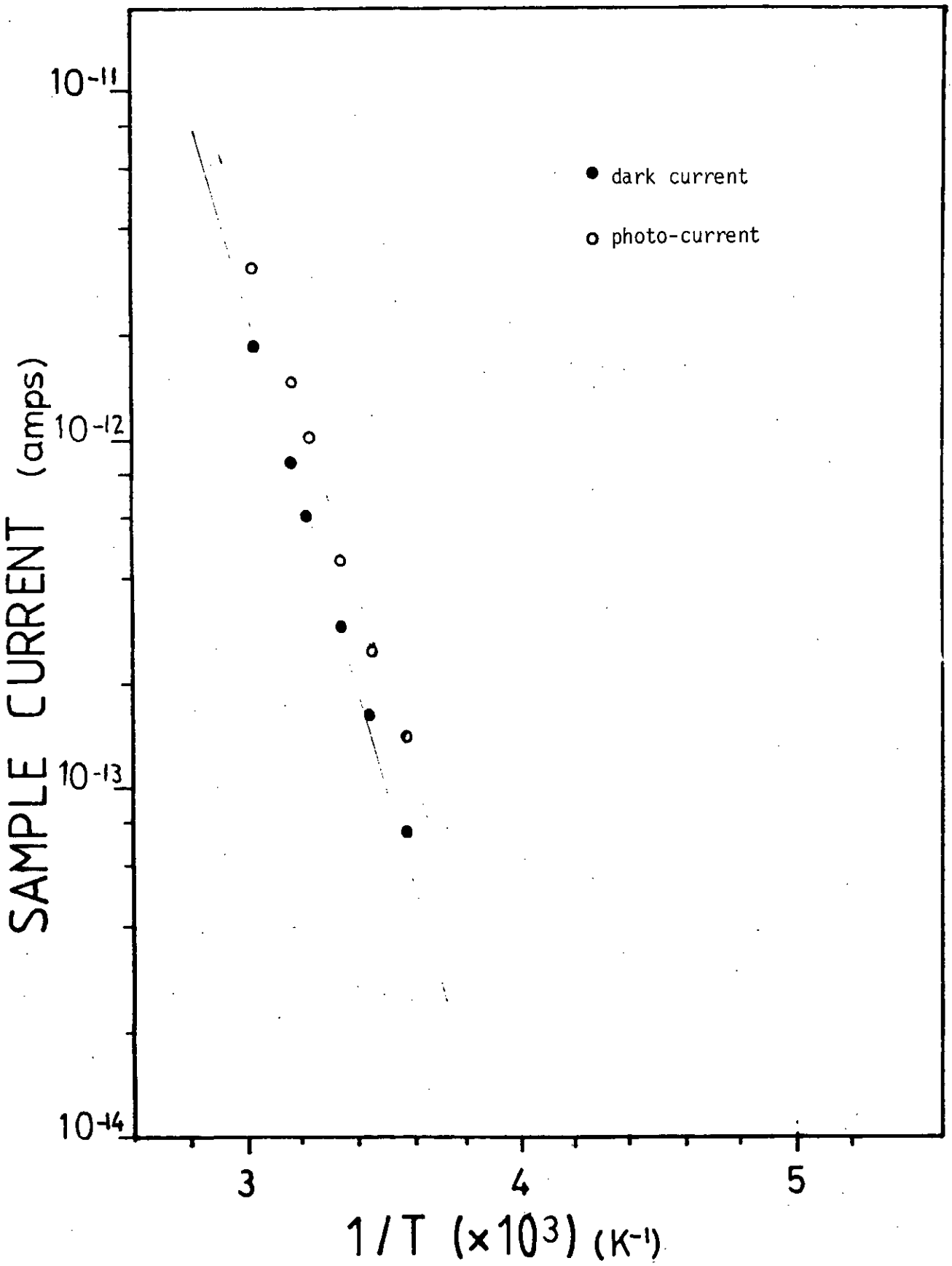

5.28

Temperature dependence of dark and photo-induced currents in a MDIM sample.

CURRENT	DARK		PHOTO-	
Temperature / Figure	Low	High	Low	High
5.24	0.37	0.63	0.29	0.54
5.25	0.32	0.63	0.28	0.53
5.26	0.33	0.68	0.30	0.59
5.27	0.29	0.68	0.24	0.60
5.28	-	0.53	-	0.49

Table 5.1:

5.3.6 Photo-Discharge Experiments

In this experiment a MDIM capacitor was first charged to a given potential (usually 10-30V) and then discharged through the electrometer in its "open input" mode. On illumination of the dye contact the rate of discharge was observed to increase substantially but, in contrast to the photo-induced current, there was no marked polarity dependence although the form of the transient decay is significantly different with positive or negative bias. Some typical results are shown in Figure 5.29. The light induced discharge rate varies with wavelength and, like the spectral response of the photo-current, roughly matches the spectral dependence of the dye itself. The spectral response of the photo-discharge rate is shown in Figure 5.5(d). Under intermittent illumination the rate of discharge responds essentially instantaneously, on the experi-

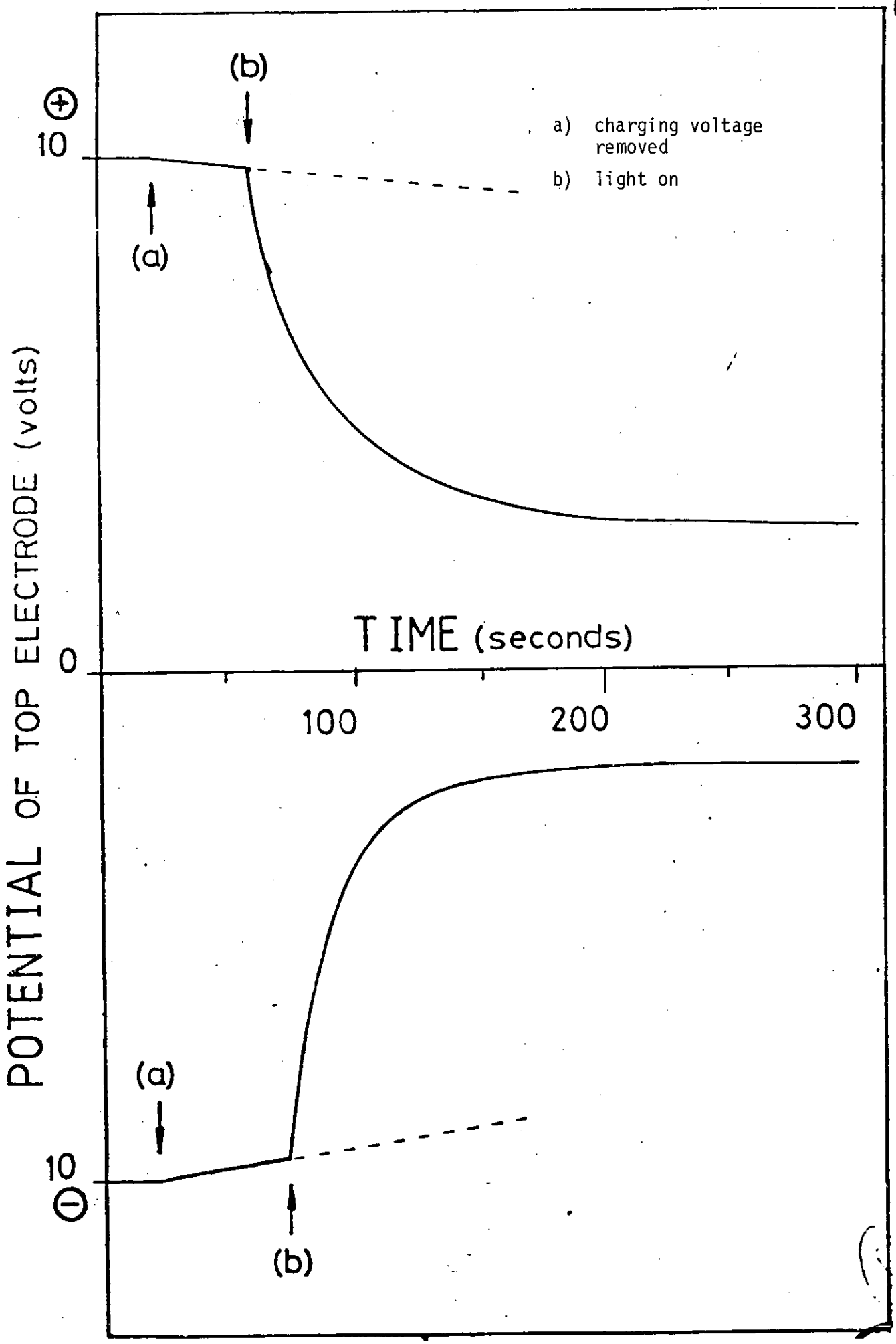

5.29

Time dependence of photo-discharge rate for both polarities.

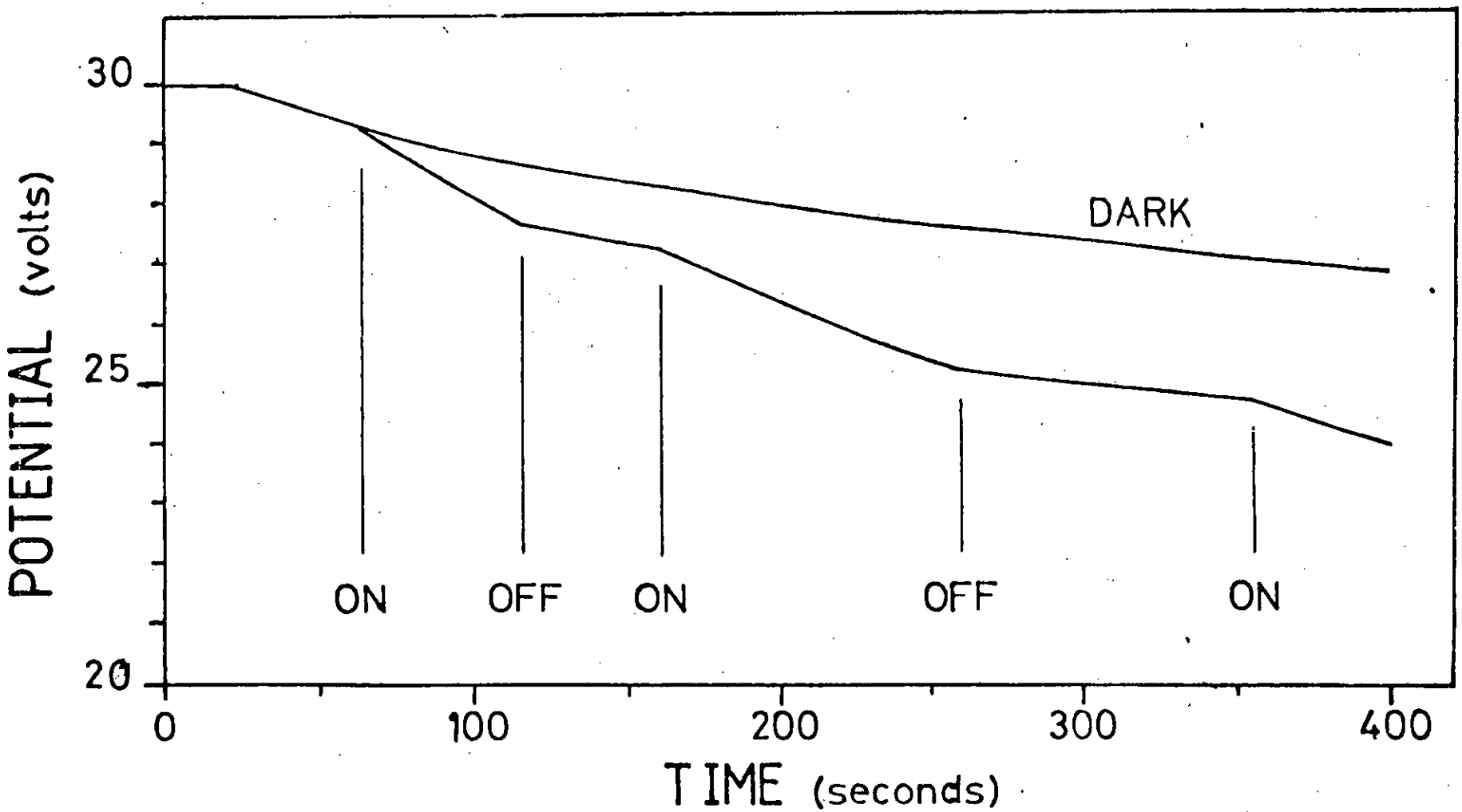

Photo-discharge rate under intermittent illumination.

mental timescale, to light being switched on and off as shown in Figure 5.30.

5.4 DISCUSSION OF EXPERIMENTAL RESULTS ON PHOTO-INDUCED CURRENT IN MDIM STRUCTURES

The experimental observations which will have to be satisfied by any proposed mechanism for the dye sensitisation of photoconductivity in SiO_2 are,

(i) A marked polarity dependence with current flow, i.e. a significant photo-current when the dye is biased negatively with respect to the SiO_2, but not with a positive bias.

(ii) A field dependence which at low applied bias satisfies a Poole-Frenkel or Richardson-Schottky-type of relationship.

(iii) A time dependence with a sharp initial transient on illumination, which decays with an extremely long time constant.

(iv) Virtually instantaneous reduction in current to the dark current level on switching off the illumination.

(v) A temperature dependence of photo-conduction which shows similar form to that of the dark current in the insulator but with consistently lower activation energies (see Table 5.1).

(vi) A spectral dependence similar to that of the photo-conduction in a dye film.

Of crucial importance is the relative positions of the energy levels in the dye and insulator. From values quoted in the literature it is possible to construct an energy level scheme, as shown in Figure 5.31 for dye and insulator. The case for dye and insulator separate i.e. without band bending, is shown. Values of the electron affinity for SiO_2 are given by Chernyav and Korzo [18] of between -1.0eV and -1.5eV. Depths of trap levels in SiO_2 are not known with great precision but a trap at 2.3eV below the conduction band, attributed to Na^+, has been widely reported. [23] A large number of low-lying trap levels between 0.3 and 0.7eV below the conduction band have also been reported [1] and the results presented earlier in this Chapter would tend to confirm their existence. Because of the variation in energy levels quoted for dyes, the general model of Schiebe is used, i.e. an excited level of the dye lies 3.4eV below the vacuum level and 2.0eV above the ground state. Thus, the excited level of the dye lies far below the conduction band of the insulator and could be very nearly coincident with the 2.3eV trap.

With this energy level scheme in mind, it is appropriate to consider the two basic theories of dye sensitisation.

5.4.1 Charge Injection

The charge injection theory, as described in Chapter 2,

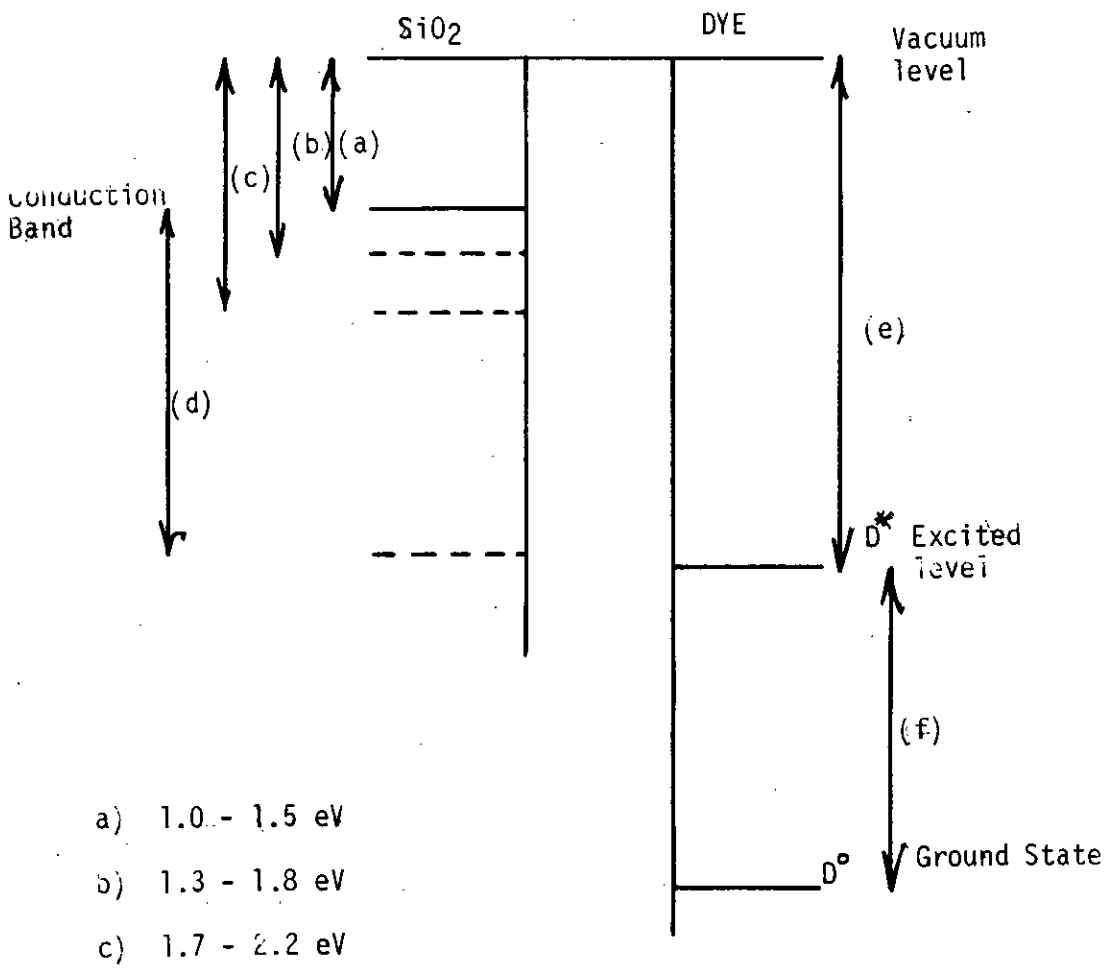

a) 1.0 - 1.5 eV

b) 1.3 - 1.8 eV

c) 1.7 - 2.2 eV

d) 2.3 eV

e) 3.4 eV

f) 2.0 eV

Figure 5.3: Dye and SiO_2 energy levels.

postulates that an electron raised, by absorption of a photon, to the excited level of the dye will be injected directly into the conduction band of the insulator. The criterion to be met by the energy levels of dye and substrate is that the excited level of the dye is an energy higher or equal to that of the conduction band edge of the substrate. For the SiO_2/dye system, this condition is obviously not met, there being a difference in energy of between 1.9eV and 2.4eV. This model of sensitisation cannot be applied without modification.

5.4.2 Resonant Energy Transfer

The energy level scheme, in which the exicted level of the dye is approximately coincident with a trap level in the insulator, is suitable for discussion in terms of the resonant energy transfer model. This model has been described in Chapter 2 and its behaviour can be deduced qualitatively as follows.

i Polarity Dependence

The alignment of the excited level of the dye with an electron trap in the SiO_2 would give rise to a strong polarity dependence. Under illumination, traps close to the dye/SiO_2 interface would empty and, if the dye were negatively biased, current would flow.

ii Field Dependence /

ii Field Dependence

The energy transfer would presumably have little or no field dependence. The applied field would however influence the effective depth of the trap and consequently the current could depend on applied field in a manner similar to the Poole-Frenkel effect i.e. log(current) proportional to (applied field)$^{\frac{1}{2}}$.

iii Time Dependence

It has been reported[24] that there is very little retrapping of carriers (<10%) released from the 2.3eV Na^+ trap in SiO_2. Thus any current flowing due to release of electrons from this trap, would be expected to decrease with time in an exponential manner. This is as observed for the photo-induced current in MDIM samples. On removing illumination, the current would cease extremely quickly, with a decay time of the order of the lifetime of the excited state of the dye. The photo-current level on subsequent illumination would depend on the degree of repopulation of the traps, possibly by electrons from shallower traps. This could be slow, which would account for the 'ageing' effect seen in experiment.

iv Temperature Dependence

The absorption of light by an H_2P_C film is independent of temperatures up to 400^{o}C, where a transition to the β polymorph takes place. The temperature dependence of the photo-induced current would thus be determined by the variation with temperature of either

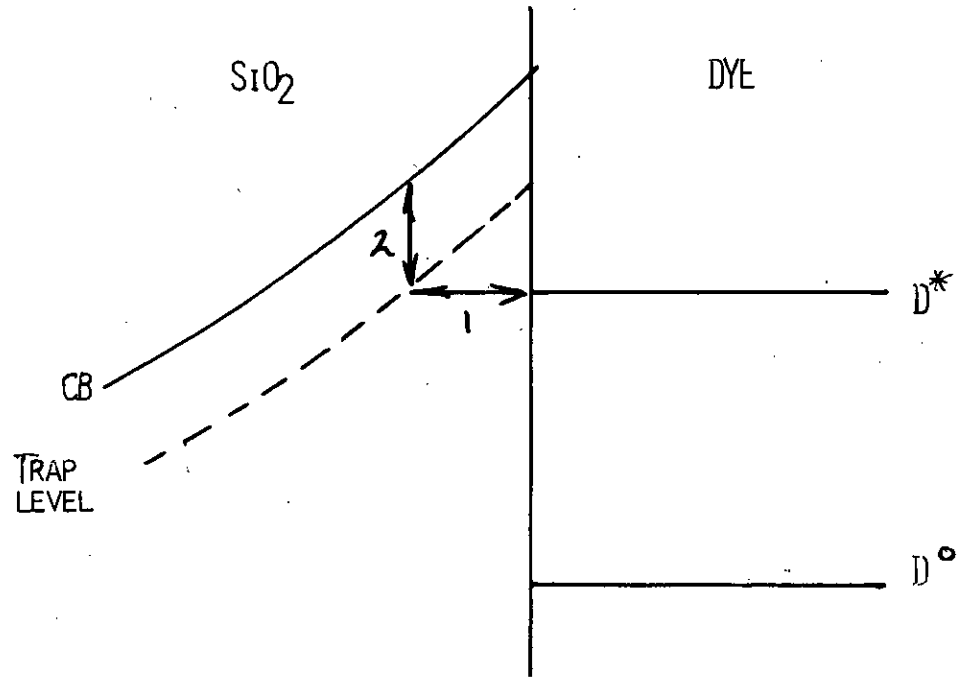

FIGURE 5.32: TRAP ASSISTED CHARGE INJECTION.

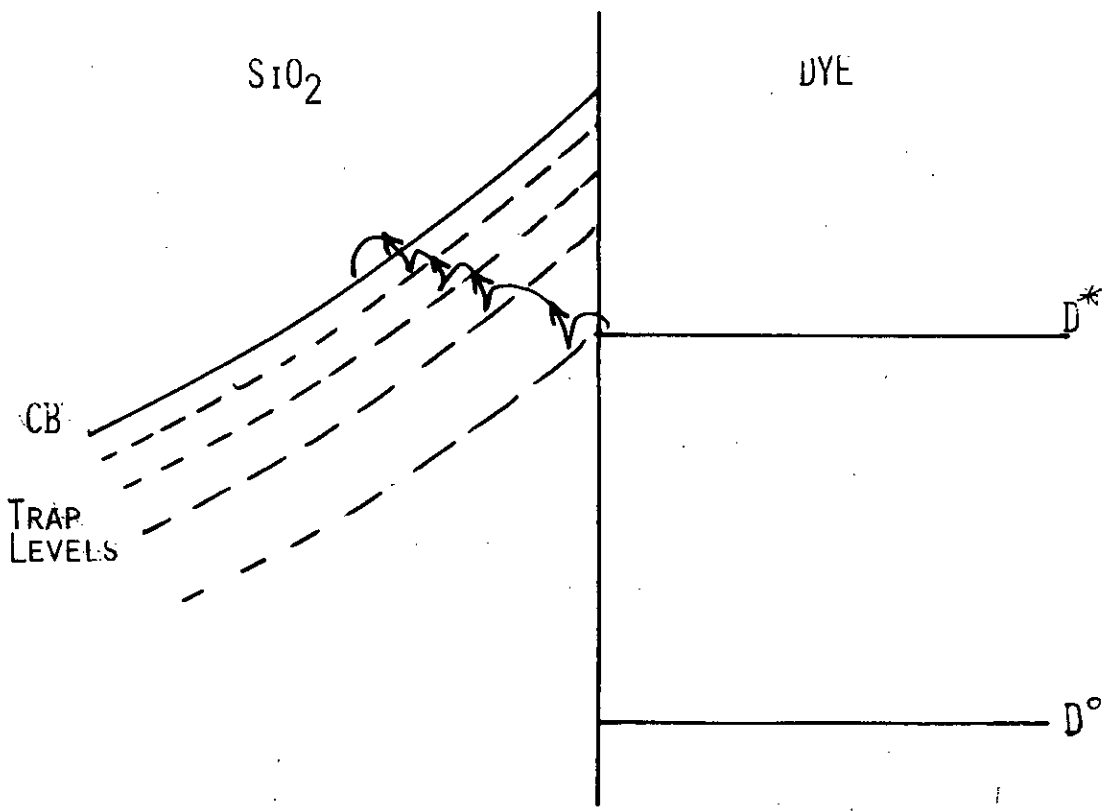

FIGURE 5.33: TRAP ASSISTED CHARGE INJECTION THROUGH MULTIPLE TRAP LEVELS.

the emission process or the subsequent transport through the SiO_2. If the latter, some correspondence might be expected with the temperature dependence of conductivity in an SiO_2 film i.e. in MIM samples.

v Spectral Dependence

The role of the dye is to absorb energy from the incident light; it is not required that charge carriers be generated in the dye layer. Consequently, the spectral dependence of the dye sensitised current might be expected to resemble the absorption spectrum of the dye rather than the spectral response of the dye photo-conductivity. However, the nature of the energy transfer is not known and it could be that the spectrum is modified.

5.4.3 Other Mechanisms

An alternative charge injection mechanism in which the charge carriers contributing to conduction, originate in the dye, is described in Figure 5.32.

The carrier is injected from the excited level of the dye to a trap level in the SiO_2 (process 1) with subsequent thermal emission to the conduction band (process 2). The diagram shows the band bending expected when the dye and SiO_2 are brought into contact. A similar trap-assisted charge injection has been discussed by Gupta and van Overstraeten for a metal/insulator contact.[25] The 2.3eV trap is suitably placed for receiving injected electrons but is far too deep for efficient thermal emission. The release time at room

temperature would be enormous and no measurable injected current would be expected to flow. At higher temperatures, some current would flow as the probability of release increases but the magnitude would be much smaller than observed in experiment. Gupta and van Overstraeten reported I-V characteristics with inflexions, similar to that presented in Figure 5.23. The inflexions take place corresponding to changes in the charge transfer mechanism from Schottky emission to trap-assisted injection and finally to direct tunneling into the conduction band. The analogy could be appropriate to the photo-current versus voltage curve of Figure 5.23.

It is possible that the trap emptying would take place via other higher energy traps as represented in Figure 5.33.

A spectrum of trap levels is thought to exist in SiO_2. The behaviour of this model can be summarised as follows,

i Marked polarity dependence due to the single carrier injection.

ii Field dependence is unlikely to follow the simple log (current) proportional to (applied field)$^{\frac{1}{2}}$ observed experimentally. For tunneling through a contact barrier with a discrete trap level, simple theory predicts[26] that

$$J = A\mathcal{E}^n \exp\{-B/\mathcal{E}\} \qquad 5.8$$

where $\mathcal{E}$ is the applied field, A and B are constants and n has value between 1 and 3.

iii Time response will depend on the occupancy of the various trap levels and on the barrier heights between. If there is no space charge due to electrons being trapped after reaching the conduction band, the current might be expected to be constant in time. On switching off the illumination, the current would decay to the dark level as the trap occupancy resumed the equilibrium (dark) value. It is possible that this could happen quickly with respect to the experimental time i.e. appear almost instanteous.

iv A similar conduction process could take place in MIM samples, the electrons being injected from the metal electrode rather than the dye. If so, the temperature dependences of the photo-induced current, dark current in MDIM samples and dark current in MIM samples might show similar features.

vi Spectral response would be close to that of the dye photoconductivity as the absorption of photons create charge carriers in the dye.

The possibility of electrons tunneling through the contact barrier to the conduction band must be considered. Fowlder-Nordheim tunneling has been reported for metal/SiO_2 contacts at high fields[10, 12] and in this case, the effect of light would be to raise electrons to the excited level of the dye where the contact barrier is narrower. Doherty and Ryan[27] have reported such currents in Al/SiO_2/Si structures and show that the current decreases with time, with an extremely long time

constant, due to trapping in the bulk of the insulator. Such trapping gives rise to a space charge which widens the barrier, reducing the probability of tunneling. The behaviour of the photo-induced current observed experimentally is consistent with such a model, except for the field dependence which is not characteristic of Fowler-Nordheim tunneling. It is possible however, that at high fields, charge injection could take place by this mechanism.

The final mechanism to be considered is thermal excitation of electrons over the potential barrier between dye and insulator, for which it is possible to predict the following behaviour.

(i) Polarity dependence

(ii) Field dependence as observed, if the Richardson-Schottky effect is dominant.

(iii) Time dependence as observed, if space charging takes place due to trapping of injected electrons.

(iv) The dye/insulator system is similar to the metal/insulator system except that the potential barrier heights are different. It is likely therefore that the same conduction mechanism controls the current through both types of sample and thus similaraties would be expected in the temperature dependence of currents in both. The activation energy would be smaller for the photo-induced current if the current is electrode limited and the barrier height is reduced by illumination.

(v) Spectral response would be as observed i.e. close to that of the photo-conductivity in the dye.

Whilst it is not possible to quantify the proposed mechanisms at the present time much of the observed behaviour can be explained quantitatively. It is likely that no single mechanism controls the photo-induced current under all conditions, but a combination of mechanisms, or transition from one mechanism to another is involved at certain conditions of field and/or temperature. For example, at low fields it is possible that excitation over a potential barrier occurs, while at higher fields there is a transition to Fowler-Nordheim tunneling.

5.5 PHOTO-DISCHARGE OF MDIM STRUCTURES - RESULTS AND DISCUSSION

The experiments conducted on the photo-discharge of MDIM structures were of a very preliminary nature and consequently it is difficult to draw more than qualitative conclusions.

The photo-discharge phenomenon in MDIM structures, unlike the photo-induced current, shows no marked polarity dependence. Typical results for this experiment are illustrated in Figure 5.29. The mechanism of photo-discharge might be expected to differ from that of the photo-induced current because, for complete discharge of the sample, both negative and positive charges must eventually be transported to the electrodes, while the current mode of operation could be due to unipolar transport.

The form of the discharge curve is different for the two polarities however. The data of Figure 5.29 was digitised to allow curve fitting and the results are presented in Figure 5.34 for positive bias. The calculated curve is defined by

$$V = 3.2 \exp(^{-t}/15) + 4 \exp(^{-t}/48) + 2.85 \qquad 5.9$$

For negative bias the results are presented in Figure 5.35 and are defined by

$$V = 5.7 \exp(^{-t}/15) + 1.8 \exp(^{-t}/38) + 1.9 \qquad 5.10$$

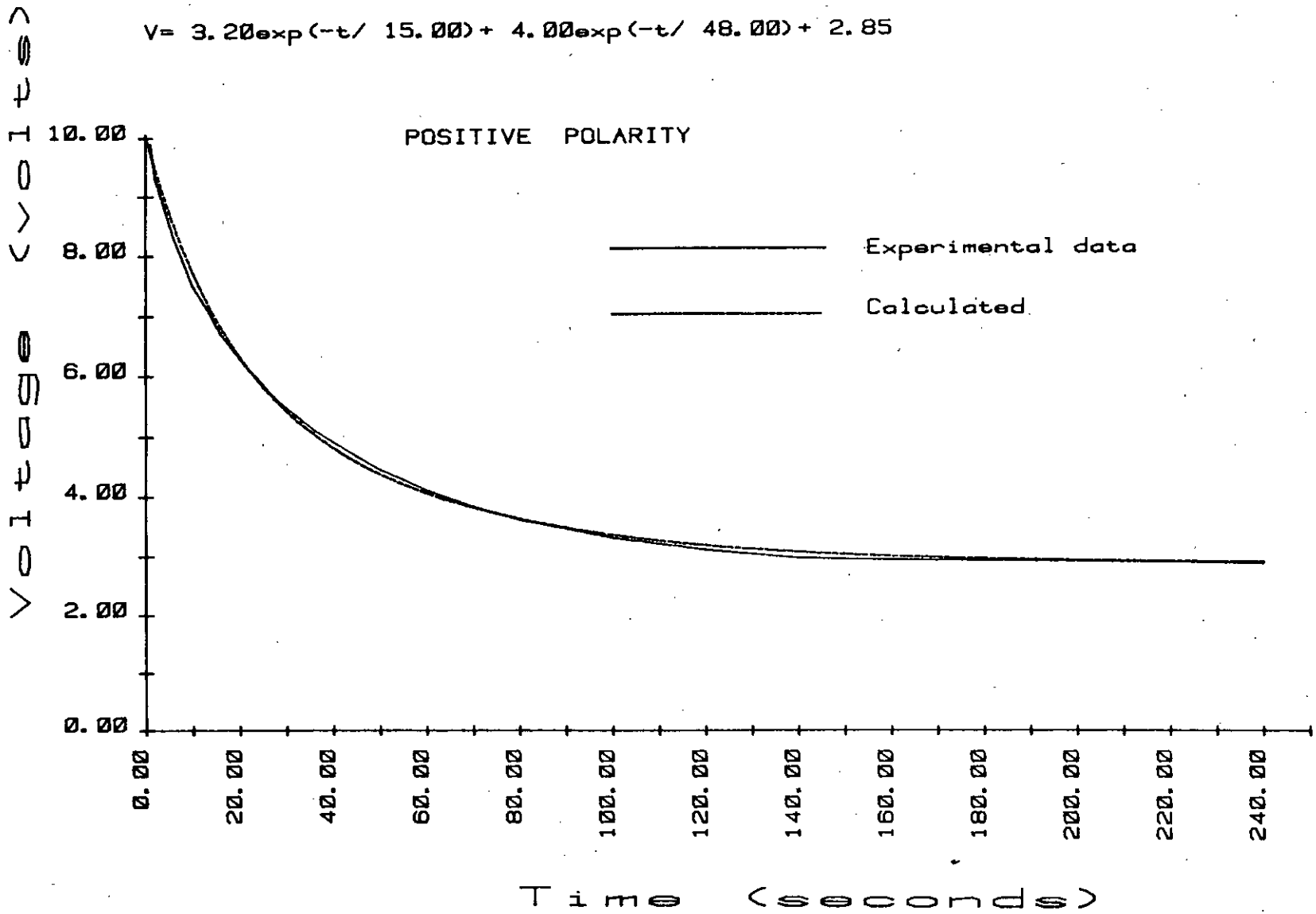
V= 3.20exp(-t/ 15.00)+ 4.00exp(-t/ 48.00)+ 2.85
POSITIVE POLARITY
Experimental data
Calculated
Voltage (volts)
10.00
8.00
6.00
4.00
2.00
0.00
0.00
20.00
40.00
60.00
80.00
100.00
120.00
140.00
160.00
180.00
200.00
220.00
240.00
Time (seconds)

5.34

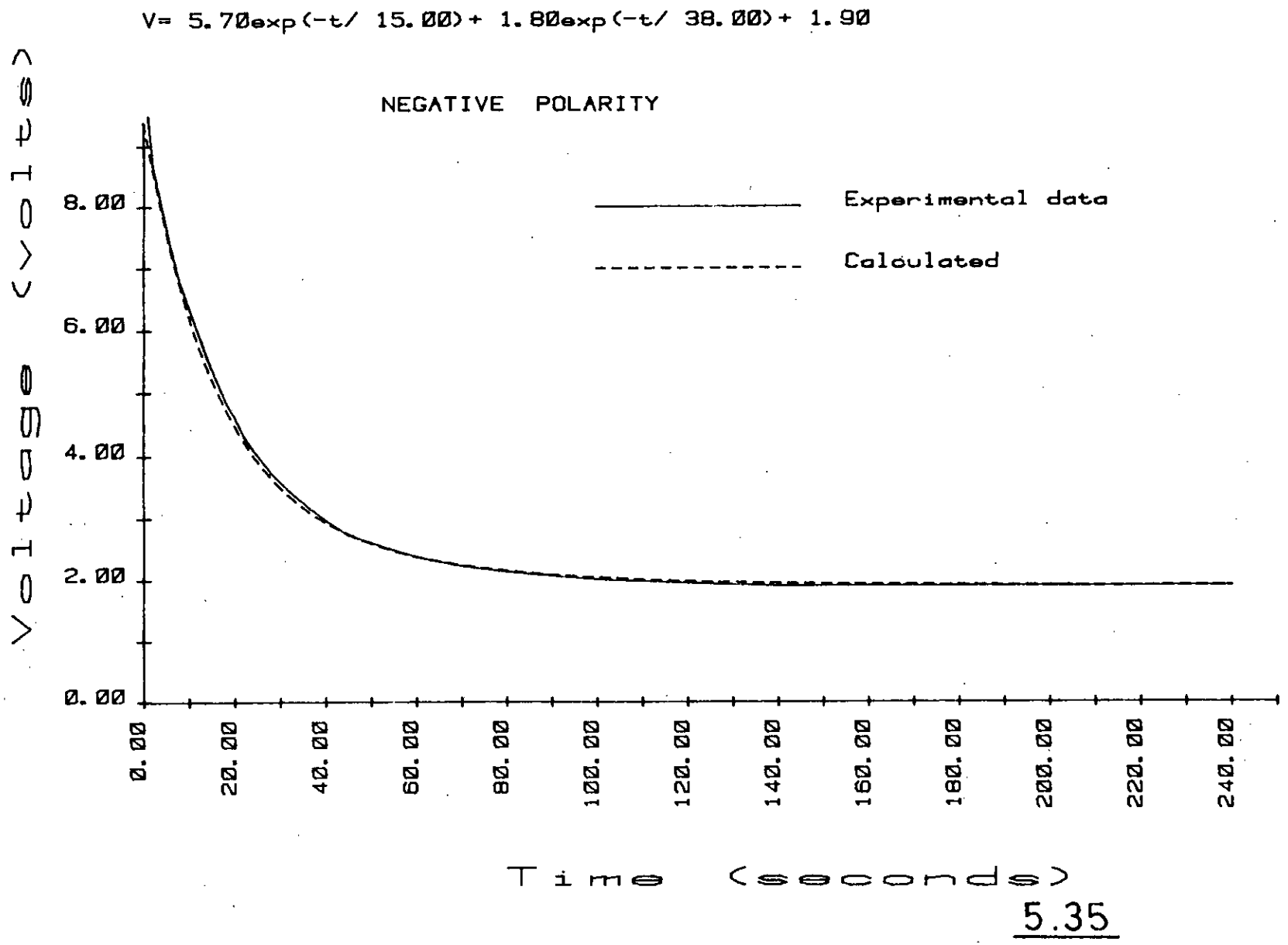
V= 5.70exp(-t/ 15.00)+ 1.80exp(-t/ 38.00)+ 1.90
NEGATIVE POLARITY
Experimental data
Calculated
Voltage (volts)
8.00
6.00
4.00
2.00
0.00
0.00
20.00
40.00
60.00
80.00
100.00
120.00
140.00
160.00
180.00
200.00
220.00
240.00
Time (seconds)

5.35

In equations 5.9 and 5.10 the time constants are given in seconds and the pre-exponential constants are in volts. The curve-fitting procedure is very sensitive to the magnitudes of the constants and it is estimated, for example, that the time constants quoted are accurate to within $\pm 4\%$.

Perhaps the most significant point to note is that the equations derived from the photo-induced current data (section 5.3.2) also include an exponential term with time constant of 15 seconds and it is reasonable to assume therefore that this term corresponds to a feature common to both phenomena.

From Figures 5.34 and 5.35 (and equations 5.9 and 5.10) it can be seen that the voltage apparently decays to a constant (non-zero) value, the polarity of which is the same as the polarity of the initial bias. This residual voltage must, of course, eventually decay to zero but the inference from the above results and curve fitting analysis, is that the time constant for this process is much greater than the time constants in equations 5.9 and 5.10.

A simple model can be developed to describe some features of these experiments. Consider the MDIM sample as two separate capacitors, connected in series, one with the dye as dielectric and the other with the insulator as dielectric i.e. there is no interaction between the dye and the insulator. If the sample is charged to a potential V, then V_D will appear across the dye and V_I across the insulator such that

$$\frac{V_D}{V_I} = \frac{C_I}{C_D} \qquad 5.11$$

where C_I and C_D are the capacitances of insulator and dye respectively.

It is further assumed that in the dark the rate of discharge is negligible, then under illumination, V_D will begin to decay but V_I will remain unchanged. After a time characteristic of the photo-conductivity of the dye, the voltage appearing on the dye will be essentially equal to that on the insulator alone. The form of this discharge would be a simple exponential decay to a constant value, and with a single time constant.

The experimental results can be discussed in terms of this model,

i) Experimental values of capacitance for MIM and MDM samples give:

$$\frac{C_I}{C_D} \sim 3$$

For example, C_I is typically 100 pF and C_D is usually 30 pF. Figures 5.34 and 5.35 give ratios of (V_D/V_I) equal to 2.5 and 3.9 respectively. Thus the observed voltage ratios agree approximately with the ratio of capacitances.

ii) The constant voltage approached for each polarity are different in magnitude, possibly due to the assymetry of the sample.

iii) The time constant of the dark voltage decay is approximately 1500 seconds. If the increase in discharge rate is due to a reduction in resistance of the dye i.e. $C\Delta R$, then the resistance of the dye would have to fall to ($^{1}/100$th) of its dark value when illuminated. The data of Figure 5.2 suggests that this is reasonable ($I_{photo} \simeq 100\ I_{dark}$).

This, this simple model, which regards the dye/insulator capacitor as independent and non-interacting components, does to a degree give qualitative agreement with the experimental observations but the model is clearly incomplete.

The important factor not accounted for is that described by the second time dependent term in equations 5.9 and 5.10 and it is reasonable to assume therefore that the feature is associated with some interaction between the dye and insulator i.e. with the dye-sensitised process (es).

It is not profitable to pursue the discussion at this stage, because of the preliminary nature of the photo-discharge experiments, but it is perhaps significant to note that the second (longer) time constant terms in equations 5.9 and 5.10 are polarity dependent in a way that may be related to the polarity dependence of the photo-sensitised conduction experiment.

CHAPTER FIVE : REFERENCES

1. Wihksne, K. & Newkirk, A.E., J. Chem. Phys. 34, 2184 (1961).

2. Heilmeier. B., Warfield, G.W., Harrison, S.E. & Assour, J. Phys. Rev. Letts. 8, 309 (1962).

3. Fielding, P.E. & Gutmann, F. J. Chem. Phys. 26, 411 (1957).

4. Vartanyan, A.T. & Karpovich, I.A. Zh. Fiz. Khim. 32, 178 (1958).

5. Faidysh, A.N. Chem. Abstr. 57 11952f (1962).

6. Kearns, D. Radiation Res. Suppl. 2 407 (1960).

7. Kaufhold, J. & Hauffe, K. Ber. Bungsenges 69, 168 (1965).

8. Harrison, S.E. J. Chem. Phys. 50 4739 (1969).

9. Gupta, H.M. J. Appl. Phys. 48 3448 (1977).

10. Lenzlinger, M. & Snow, E.H. J. Appl. Phys. 40, 278 (1969).

11. Forgacs, G., Lorinzcy, A. & Nemeth-Sallay, M. Phys. Stat. Sol. 20, K113 (1973).

12. Deal, B.E., Fleming, P.J. & Castro, P.L. J. Electrochem. Soc 115, 300 (1968).

13. Krause, H. & Grunler, R. Phys. Stat. Sol (a) 42, 149 (1977).

14. Simmons, J.G. & Taylor, G.W. Phys. Rev. B. 6, 4793-4804, (1972).

15. Simmons, J.G. & Taylor, G.W. Phys. Rev. B. 6 4804-4814. (1972).

16. Gupta, H.M. & van Overstraeten, R.J. J. Phys. C, 7 3560-3572 (1974).

17. Popova, L.I., Antov, B.Z. & Vitanov, P.K. Thin Solid Films, 38, 247-253 (1976).

18. Chernyaev, V.N. & Korzo, V.F. Thin Solid Films 34, 403-406 (1976).

19. Simmons, J.G. & Taylor, G.W. Phys. Rev. B, 5, 1619-1629. (1972).

20. Simmons, J.G. & Nadkarni, G.S. Phys. Rev. B, 6 p. 5825. (1972).

21. Nicollian, E.H., Goetzberger, A. & Berglund, C.N. Appl. Phys. Lett. 15, 174 (1969).

22. Gdula, R.A., J. Electrochem Soc. 123, 42 (1976).

23. Williams, R. Phys. Rev 140, A569, (1965).

24. Di Maria, D.J. "The Physics of SiO_2 and its Interfaces" ed St Pantelides Pergamon, New York, 1978, p 160.

25. Gupta, H.M. & van Overstraeten, R.J. J.A.P. 46 2675 (1975).

26. Perlin, Y.E. & Cheban, A.G. Soviet Physics Solid State, 4 11 (1963).

27. Doherty, J.G. & Ryan, W.D. ESSDERC '77, University of Sussex, Sept 1977.

6. IMPLICATIONS FOR MOS TECHNOLOGY

The patent by Owen & Mavor[1] suggested a novel light-modulated MOS transistor structure based on the dye-sensitisation phenomenon. It is the aim of this Chapter to consider the suitability of metal free phthalocyanine as a material in MOS processing. Also the electrical characteristics of proposed dye-sensitised MOS-transistors will be deduced.

6.1 CONVENTIONAL MOS PROCESSES AND POSSIBLE MODIFICATIONS

It seems likely that any dye-sensitised transistor would be strongly based on existing MOS processes. The deviation from a standard process would be in the later stages of processing, probably as an addition after the gate electrode had been defined. Gate electrodes are normally made of aluminium (metal gate) or polycrystalline silicon (silicon gate). The metal gate process is much simpler; after the metallisation has been defined (both gates and interconnections) a passivation layer of SiO_2 deposited by chemical vapour-phase decomposition is used to CVD cover the devices. A device structure, shown schematically in Figure 6.1a could easily be manufactured. The dye layer could be evaporated onto the devices before metallisation. The dye pattern (to cover channel regions) could be defined and a metallisation layer deposited. This metal would require to be transparent which would unfortunately

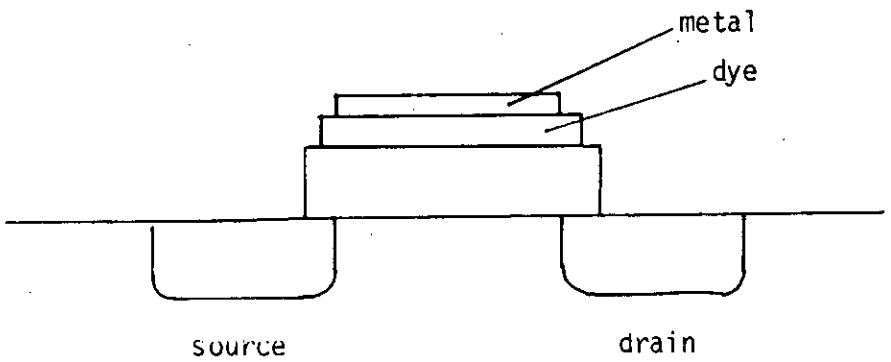

(a)

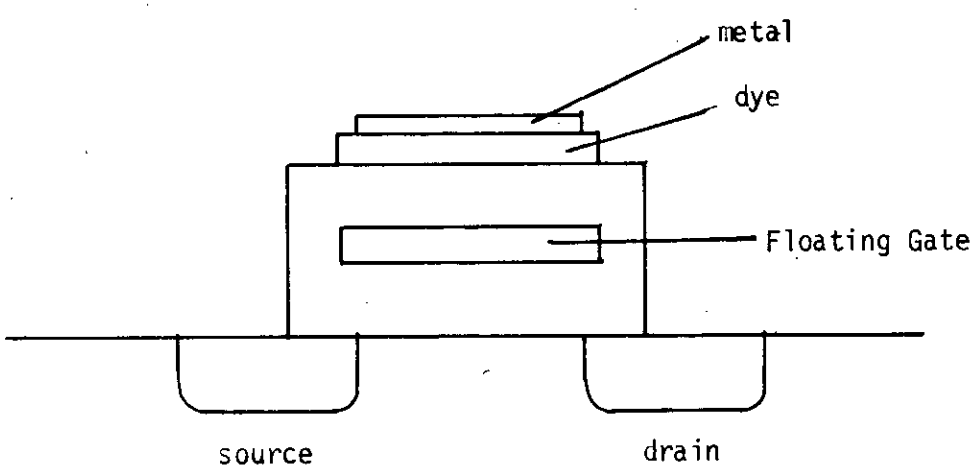

(b)

Figure 6.1: Proposed dye sensitised transistor structures.

not be suitable for interconnections (high sheet resistance) or bonding pads. Thus it would be more reliable to metallise twice - a thick layer (1μm) for bonding pads, metal gates, and interconnections and a thin semi-transparent layer over the dye-sensitised gates. This scheme is shown in Figure 6.2. The thick aluminium layer would make all connections to the substrate and thus it would be possible to sinter contacts (at 430°C in N_2/H_2 ambient) before deposition of the dye. This structure will be called MDOS, because of its section. Flynn et al[2] used a similar transistor in an investigation of dye-sensitised devices. He used p-channel technology (n-type substrate), with crude prototype transistor structures. A single (thin) metallisation layer was used.

An alternative structure is shown in Figure 6.1b which is basically an insulated gate (or floating gate) MOS transistor. Such structures (known as FAMOS) are used as memory devices. The gate is totally isolated in high quality oxide. It can be charged by avalanche injection from the channel and thus once charged, the device will remain on. In some memory devices, the gate is replaced by a silicon nitride/silicon dioxide sandwich (MNOS devices), the interface acting as a site for injected charge to accumulate. The FAMOS gate is usually of polycrystalline silicon, the surface of which can be thermally oxidised. The dielectric layer can be thickened by deposition of CVD silicon dioxide. The proposed structure has a dye/thin metal sandwich added over the floating gate area in the same manner as proposed for the MDOS device.

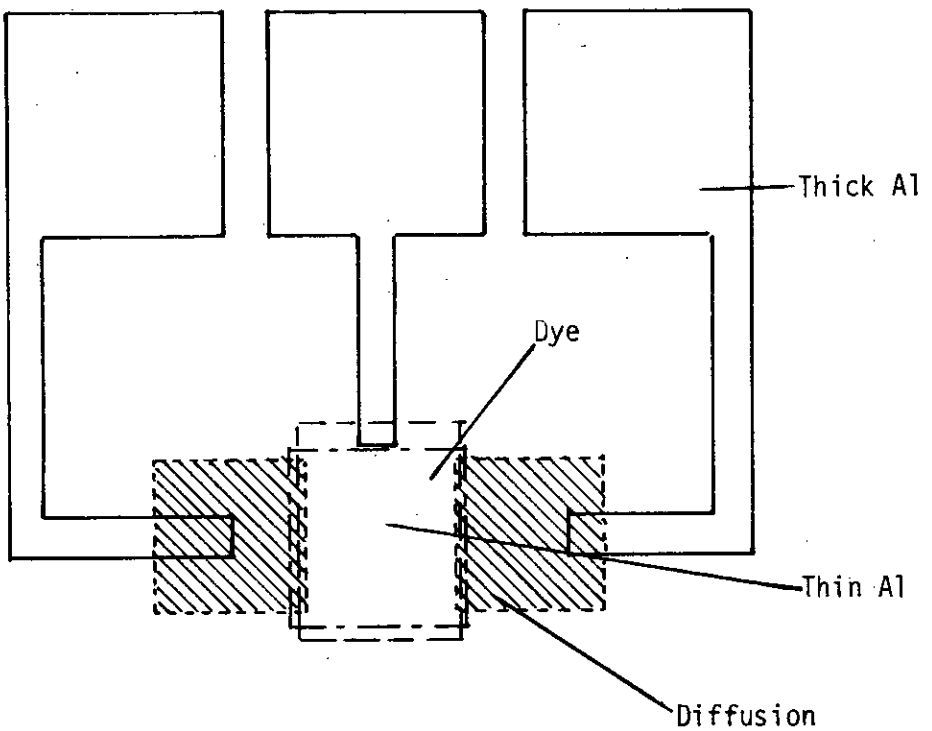

Figure 6.2: Proposed transistor structure

A suitable process schedule would be as follows.

i Process metal gate/FAMOS devices up to completion of metallisation definition. (1μm Al).

ii Sinter contacts, typically at 430°C in N_2/H_2 for 15 to 60 mins (dependent on substrate material).

iii Evaporate dye layer. Thickness up to 0.5μ.

iv Define dye regions by photolithographic means.

v Evaporate semi-transparent Al (1000Å).

vi Define semi-transparent electrodes over dye areas, contacting to previously defined metal pattern.

vii Possible passivation deposition and definition. (CVD SiO_2 or plasma deposited Si_3N_4).

The ease of evaporation of metal-free phthalocyanine has been demonstrated in the present work and the necessary equipment is compatible with conventional semiconductor processing.

6.2 DEFINITION OF DYE AREA

The technique of shadow masking used in the present work is not practical with small device geometries. Flynn[2] used shadow but his devices were of such a large size that alignment

of the mask to the wafer was not a problem. Conventional photolithography/etch processes are as follows. A film of the material to be etched is deposited over the entire wafer. No masking is used during deposition. The wafer is then coated with photoresist and the required pattern defined in the resist by printing from a mask and subsequent development. The underlying material is etched, chemically, through the photoresist mask. The photoresist is then stripped off. It can be seen that it is crucial to have a suitable etch for the film material that i), does not remove the photoresist and ii) does not, to any great extent, etch underlying layers of the circuit. Metal-free phthalocyanine is soluble only in concentrated acids, e.g. sulphuric and nitric acids. However, photoresist material is also soluble in such acids and so it would not be possible to use a photoresist etch mask for H_2P_c.

An alternative technique which would be successful is a lift-off process. Photoresist is spun onto the wafer and the negative of the required pattern is defined in the resist i.e. holes are developed into through the resist where dye areas are required. The resist layer is thick (1.5μm) in relation to the evaporated dye thickness (<0.5μm). Dye is evaporated onto the wafer through the windows in the resist. The resist is dissolved in an organic solvent and consequently the dye layer which was on top of the resist lifts off. Only the dye which passed through the resist mask will remain. The process is summarised in Figure 6.3. Good dimensional control is possible with this technique.

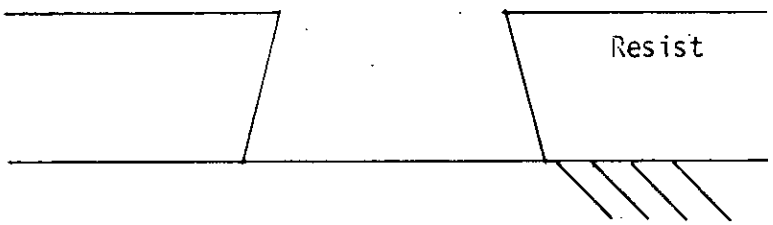

Define resist

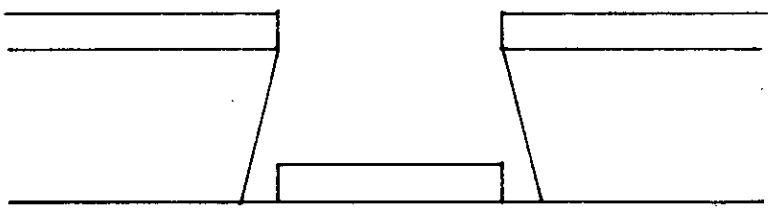

Deposit dye

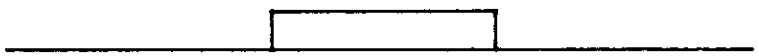

Remove resist

Figure 6.3: Lift-off technique

6.3 THE EFFECT OF SUBSEQUENT HEAT TREATMENT

Metal-free phthalocyanine is known to exist in several polymorphic forms and as deposited films consist of the α polymorph. but a transition to the β polymorph can take place on heating.[3] It is important to know at which temperature this takes place and the properties of the β polymorph.

Of the polymorphs, the β-form is the most stable and is the only form of which single crystals can be grown. It is a base-central monoclinic crystal. The α form is thought to have a tetragonal structure.

IR spectroscopy provides the most obvious evidence for a transition between α and β-forms. Figure 6.4 shows spectra for α-form and β-form. The bands at 724cm^{-1} and 728cm are characteristic of β-form only. A sample of dye was evaporated onto potassium bromide substrates, and the spectra of the α-form obtained. After heating at 300^{o}C for 1 hour however, the spectra of the β-form was obtained. After heating the H_2P_c film also had a different surface texture, appearing matt compared to the smooth appearance of the α-form. Films were prepared for electron microscope, SEM, analysis, and typical micrographs are shown in Figure 6.5. Crystal growth has obviously taken place on transition to the β-form.

Attempts to measure the electrical characteristics of the β-form were unsuccessful. Both surface gap cells and sandwich cells were produced, heated to convert to the β-form and their resistance

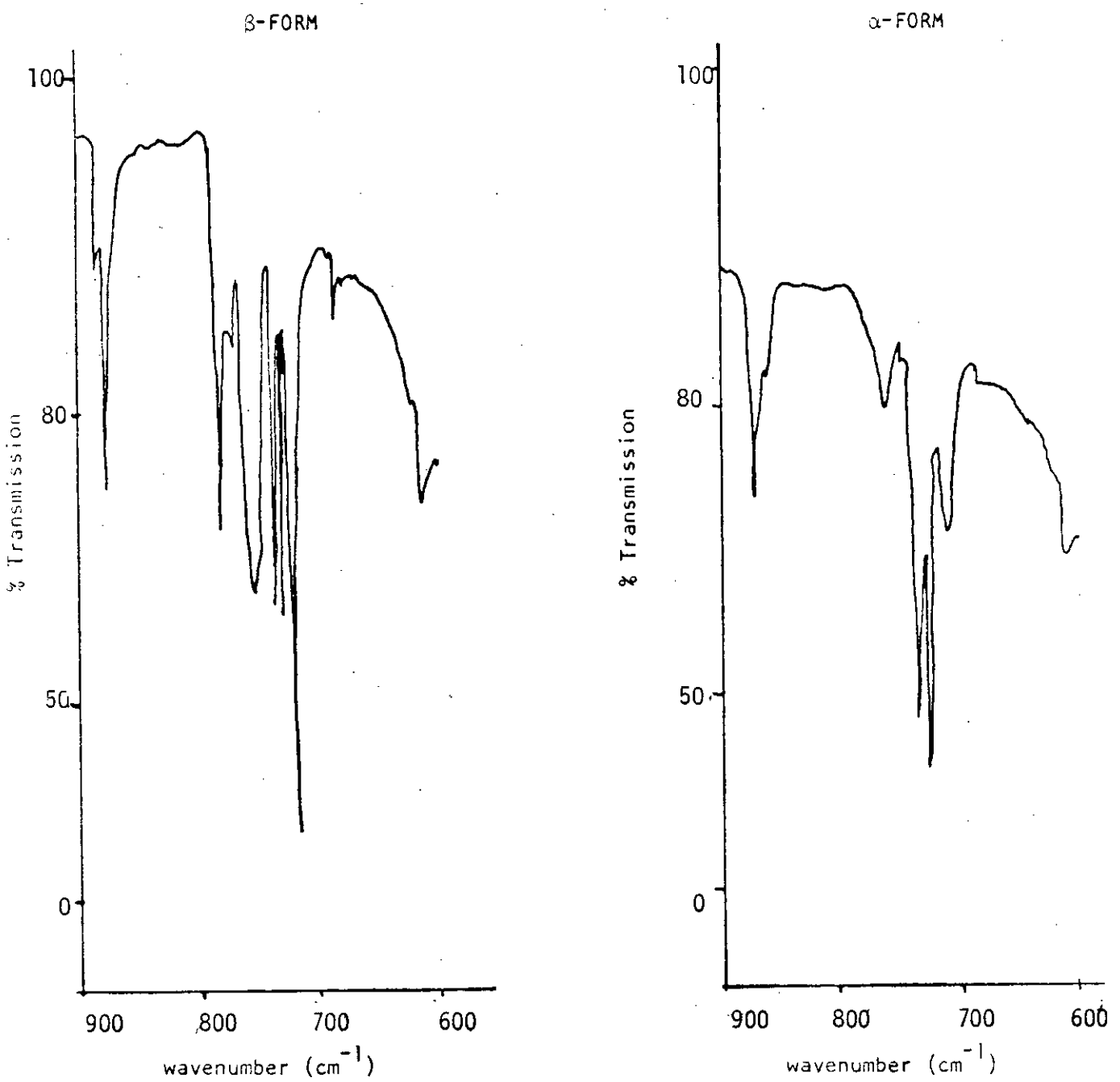

Figure 6.4: Infra-Red Transmission Spectra of Thin Films of Metal-Free Phthalocyanine. α-Form Converted to β-Form by Heating at 300°C for 1 Hour

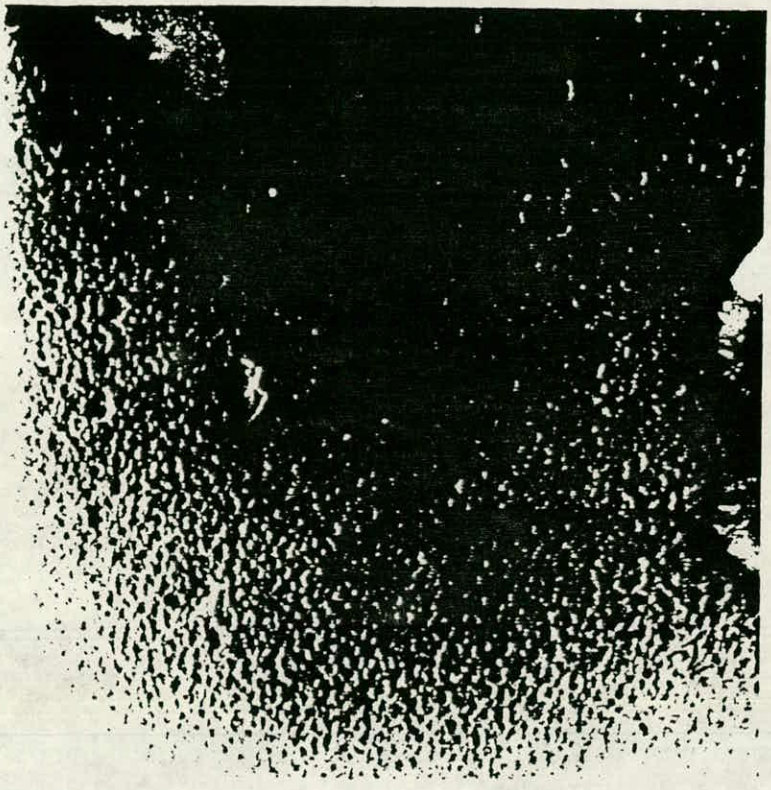

(a)

(b)

Figure 6.5: SEM Micrographs (x10,000)

a) as deposited
b) after heating to 300°C for five hours.

measured. The resistance was extremely high, probably indicating that the films were not continuous after conversion.

The implication for device manufacture is that after the dye is deposited, the temperature must be kept low (probably $<200^{o}C$). Thus sintering of contacts must take place before dye deposition i.e. the twin metallisation process suggested earlier in this Chapter could be used. Passivation layers could not be used on devices which have metal-free phthalocyanine on any part. This has unfortunate implications for proposed integrated circuits for optical signal processing incorporating some dye-sensitised transistors. Long term stability will not be good and for memory type devices, this limitation could be a crucial problem.

6.4 DEVICE CHARACTERISTICS

The MDOS device is a realisation of the photo-discharge experiment described in the last Chapter. The gate can be charged to turn the transistor on (or off if a depletion mode device). Under illumination, charge is injected through the gate oxide into the channel until the gate potential has dropped to a level below the threshold voltage. The transistor will then be off. The state of the transistor is thus optically alterable. Illumination of the dye will, with this device structure, result in illumination of the channel. If the lights has photon energy greater than the band gap of silicon i.e. wavelength $<1.1\mu m$, carriers will be generated in the channel. The transistor will appear to be switched

on. However, on removal of the illumination, gate control will again take place. Photo-carriers in the channel will not change the gate charge.

The carriers injected into the gate oxide during illumination will have a unsignificant effect in relation to the photo-carriers in the channel. The consequence is, that under visible illumination, such a transistor can not be used in an active mode, i.e. it is a "switch" whose state can be altered optically but can be interrogated only in the dark.

Of the mechanism for the operation of such a device is that of the photo-discharge experiment, devices of either p- or n-channel could be made to work.

The speed of operation can be simply calculated. With a gate oxide thickness of 0.1μm, the gate to channel capacitance will be approximately 5.3×10^{-4} Fm^{-2}. If the threshold voltage is 2V and the gate is initially charged to 4V (with respect of substrate) to ensure "turn on", the charge which has to be dissipated to turn off the device is 10.6×10^{-4} C/m^2. The dye-sensitised discharge effect described earlier (H_2P_C/SiO_2) is equivalent to a charge flow of $5 \times 10^{-6} C/Sm^2$. Thus it would be approximately 200 s to turn off such a device. This estimate is perhaps pessimistic as the data for the dye-sensitisation is based on thick oxide (0.5μm) systems and in device work, thinner oxides would be used.

However, with thinner gate oxide, the capacitance would increase, and thus the charge on to be neutralised would increase. If the discharge rate increased at a higher rate with decrease of oxide thickness than the capacitance, then an increase in speed would be expected.

Using high light intensities would also be expected to increase the discharge rate.

The proposed IGFET structure could be used in a similar way. The gate can be charged by avalanche injection from the channel and discharged by current injection from the dye electrode. This contrasts with the normal practice of using UV light to discharge the gate. Thus a novel way of erasing FAMOS memories can be anticipated. The time for erasure can be calculated in a similar way to the previous calculation and the result will be similar. Such times would be tolerated for this application. The polarity dependence of the dye-sensitised photocurrent would require n-channel processing to be used.

There is a possibility of using a floating gate structure in a dynamic manner. The gate, if opaque to light, would shield the channel from illumination and thus there would be no photo-carrier generation in the channel. It is conceivable that the source-drain current could be modulated by the photo-induced current to the gate. However, the biasing voltage required to cause the photo-current to flow would control the transistor, and the photo-modulation effect would be small.

CHAPTER SIX : REFERENCES

1. Owen, A.E. & Mavor, J. Improved Semiconductor Device. Brit. Pat. No 24081/72.

2. Flynn, B.W., Mavor, J. & Owen, A.E. Solid State and Electron Devices, 2, 94, (1978).

3. Harrison, G. J. Electrochem. Soc. 118, 138 (1971).

7. CONCLUSIONS AND RECOMMENDATIONS FOR FUTURE WORK

The work presented in this thesis was a preliminary study of the phenomenon of dye-sensitised photo-conduction in silicon dioxide.

The aims of the work were to quantify the phenomenon, speculate on possible mechanisms, and to assess the feasibility of using the dye-sensitisation effect to control the operation of an MOS transistor. Initially a study of the dye (metal-free phthalocyanine) and insulator (silicon dioxide deposited by chemical-vapour-phase and deposition, i.e. CVD) was carried out.

7.1 CONCLUSIONS

7.1.1 Dye Properties

Films of metal-free phthalocyanine can be prepared conveniently by vacuum evaporation, giving the α polymorphic form. Subsequent heating to greater than 300^{o}C results in the film being converted into the β form. As prepared films showed dark current and photo-current activation energies of 0.38 eV and 0.1 eV respectively. At room temperature, the dark resistivity is 7.5 x $10^{9}\Omega$m, dropping by a factor of approximately 100 under moderate intensity illumination. These experimental results are within the spread reported in the literature but it must be noted that a great variation is seen in the reported data. No obvious trends in this data can be determined in terms of sample type, preparation or experimental conditions. The conduction is probably extrinsic.

7.1.2 Insulator Properties

Au-SiO_2-Au structures, in which the SiO_2 is prepared from silane by the Silox process, shows a field dependence of conductivity which is consistent with Poole-Frenkel or Richardson-Schottky types of conduction. The temperature dependence of the DC conductivity is complex, maximum and minimum turning points are often observed. The interpretation is not straightforward, but it seems likely that trapping levels are dominant in the conduction process. The trap levels are probably centred in energy at 0.35 eV below the conduction band edge.

7.1.3 Metal-dye-insulator-metal sample properties - photo-induced currents

Under illumination, the current flowing through a MDIM sample increases rapidly and then relaxes, over some tens of seconds, to an apparently steady value, of 2 to 10 times the dark current (typically 10^{-12} amp). The photo-current does however seem to decay with an extremely long time constant (1800 seconds) and would presumably drop to the dark current. On removing the illumination, the current drops quickly to the previous dark level. Marked polarity dependence is seen with negligible current flowing when the dye is positively biased with respect to the insulator. At fields up to about 10^7 Vm^{-1} the field dependence is consistent with Poole-Frenkel or Richardson-Schottky conduction. At higher fields, the dependence is complex with a tendency for the current

to saturate. The spectral response is similar to that of the photo-conduction in the dye alone. The photo-current shows a temperature dependence similar in form to the dark current (and to the current in a MIM sample).

The activation energies in low and high temperature regions are, however, consistently lower for the photo-current than the dark current (at low temperature $\sim$0.3eV for the photo-current and $\sim$0.34eV for the dark current; at high temperatures, $\sim$0.55 eV for photo-current and $\sim$0.65 eV for the dark current).

Of the two basic theories of dye-sensitisation effects, the charge injection model cannot be applied without modification to the present work as the excited level of the dye lies below the conduction band of the insulator. The following tentative conclusions emerge from the experimental results on the dye sensitised photo-current in SiO_2.

i) The marked polarity dependence is probably attributed to the greater mobility of electrons in SiO_2.

ii) The time dependence can be described by the sum of three exponential times, the shortest time constant term can be attributed to instrumental response. The very long time constant (1800 s) can be due to either the formation of a space charge in the bulk of the insulator or the depletion in occupancy of a trap level.

iii) The spectral dependence is similar to the spectral dependence of the photo-conduction in the dye, suggesting that the carriers, contributing to conduction originate in the dye.

iv) The field dependence and temperature dependence are both similar to those of the dark currents in MIM and MDIM structures and this suggests that the dominating conduction process is due to the insulator. It is dependent, to some extent, on trapping levels in the insulator.

The energy transfer theory is qualitatively consistent with the observed behaviour but for the spectral response which might be expected to be similar to the absorption spectrum of the dye. The most likely mechanism would appear to be either one, or a combination of the following.

a) Electron generation in the dye and injection to a trap level in the insulator with eventual emission to the conduction band by tunneling between shallower trap levels.

b) Electron generation in the dye and emission over the interfacial potential barrier into the conduction band of the insulator.

7.1.4 Photo-discharge Phenomena/

A significantly higher discharge rate of a MDIM capacitor is observed when the device is illuminated. The form of discharge depends on the polarity of the charging voltage as does the magnitude of the residual voltage to which the sample voltage decays. The sample responds instantaneously to the illumination. The data for both polarities can each be described by similar equations with two exponential terms and both equations have a term with time constant of 15 seconds. A similar time constant is observed in the decay of the photo-induced current and could be due to some common feature. A simple model in which the dye and insulator are non-interacting gives qualitative agreement with some features of the observed behaviour but it is clearly incomplete. In particular, a model consisting of two independent capacitors in which the photo-effect is attributed entirely to the dye-capacitor, would have only a single time-constant. The second time constant presumably indicates therefore, that there is some photo-sensitised interaction between the dye and the insulators.

7.1.5 Implications to Device Performance

It is possible to devise two device structures which would utilise dye-sensitised effects, i) a FET with dye between gate electrode and gate dielectric and ii) a floating gate device in which the floating gate potential is controlled by a dye-sensitised current. The first class of device could utilise the photo-discharge phenomenon by which the gate potential could, under illumination, be made to decay to below the threshold voltage of the

transistor. Such a transistor would be turned 'on' by charging of the gate electrode and subsequently inerrogated to determine whether or not it had been illuminated after the initial charging. The second class of device could operate as an optically eraseable memory, working with light of visible wavelengths. A severelimitation for these devices (but mostly the first) is the slow speed which would be expected ($\sim$200 seconds to erase a memory). The speed would prevent their use in imaging applications.

7.2 RECOMMENDATIONS FOR FUTURE WORK

The magnitude of the dye-sensitised photo-current will have to be increased for realistic device applications. Several approaches could be investigated as follows.

i Use thin oxide layers. The use of very thin oxide layers (100Å) may increase the magnitude of the photo-induced current. Such thin oxides would not be produced reliably by CVD techniques and would have to be grown as thermal oxide on silicon.

ii) Use high light intensities. The light intensity used in the present work was low and more intense sources could be used e.g. laser.

iii) Other dyes could be used but the sample preparation would be possibly a problem.

A useful effect would be if the current would be sensitised to the infra-red and particularly to wavelengths longer than the intrinsic band gap of silicon. If this were the case, the illumination of the transistor would not create carriers in the channel and any effect would be due to the dye-sensitisation effect. A different choice of dye would be required.

APPENDIX ONE : PROPERTIES OF THE PHTHALOCYANINES[1]

The blue pigment, phthalocyanine, was first recognised in 1928. Metal-free phthalocyanine is a synthetic analogue of the naturally occuring porphyrins which are derived from the porphyrin ring system. The phthalocyanines are closely related in structure to chlorophyll, the pigment of green leaves, and kemin, the pigment which in association with protein is haemoglobin, the colouring matter of mammallian blood. Metal atoms can be substituted for the hydrogen in the centre of the metal-free phthalocyanine molecule (see Figure 2.1). The phthalocyanines are highly crystalline, vary in colour from reddish blue to bluish green, and are extremely stable. Copper phthalocyanine, for instance, sublimes without decomposition at 550 - 580^{o}C, dissolves in concentrated sulphuric acid and is recovered unchanged on dilution. All are insoluble in water.

The phthalocyanine molecule is a strain-free 16 membered ring and is formed when phthalonitrile is heated in a sealed glass vessel at 350 - 360^{o}C. Metal-free phthalocyanine yields metal phthalocyanines on heating with metals or suitable soluble salts in high boiling solvents.

REFERENCES

1. K. Venkataraman in "The Chemistry of Dyes, Vol II" Academic Press, 1952.

APPENDIX 2 .

Journal of Non-Crystalline Solids 40 (1980) 49–59
© North-Holland Publishing Company

DYE-SENSITIZED CHARGE INJECTION INTO AMORPHOUS SiO_2 FILMS

R. HOLWILL, A.E. OWEN and J. MAVOR

Department of Electrical Engineering, University of Edinburgh, Mayfield Road, Edinburgh, EH9 3JL Scotland

Results and analyses are reported on the dye-sensitized steady-state photo-conduction through metal–dye–SiO_2-metal (MDIM) structures, and on the photo-induced discharge of MDIM capacitors. In all the experiments the dye used was hydrogen phthalocyanine. The induced photo-current is substantial when the dye contact is negatively biased but is is negligible under positive bias, i.e. it appears that electron currents are fairly readily induced but not hole currents. Measurements as a function of temperature have included thermally-stimulated dielectric relaxation experiments and the results provide evidence for separate regimes of bulk- and electrode-dominated processes. The voltage dependence of the dark current and of the photo-current obeys an equation of the Poole–Frenkel type. The rate of discharge of MDIM capactors increases markedly on illumination but, unlike the photo-current, there is no significant dependence on polarity. The photo-induced discharge rate varies with wavelength and its spectral dependence matches the photo-conduction spectrum of the dye, as does the dye-sensitized photo-current.

1. Introduction

Preliminary results on the dye-sensitized photo-current through amorphous films of SiO_2 have already been described [1]. In the present paper more detailed results and analyses are reported on,

(i) the steady state photo-current through metal–dye–SiO_2–metal structures, and,

(ii) the photo-induced discharge of polarized metal–dye–SiO_2–metal capacitors.

A brief account of the experimental details is given in section 2. In section 3 we describe the measurements of photo-conduction, and in section 4 those concerned with the photo-induced discharge of dye-sensitized capacitors.

2. Experimental details

In all experiments a "sandwich-type" structure was used, either a metal–dye–insulator–metal (MDIM) structure as indicated in the inset of fig. 1, or a metal–insulator–metal (MIM) structure. For both structures substrates of Corning 7059

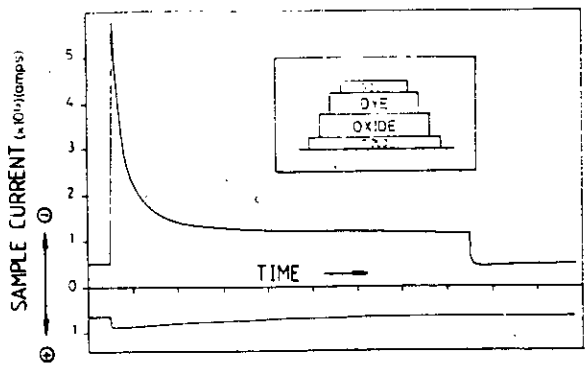

Fig. 1. The time dependence of the light-induced photo-current through a MDIM sample (the time axis is in divisions of 20 s). The inset shows the MDIM structure, diagrammatically, and the sign of the current axis corresponds to the potential of the upper electrode. The measurements were made at room temperature; the dye thickness was typically 0.5 μ, and the SiO_2 thickness 0.5–1.0 μ.

glass were used, onto which a gold film had first been deposited to form the lower metal electrode of the sandwich structure. Silicon dioxide was deposited by the thermally-induced vapour phase decomposition of silane gas at 450°C. A mixture of silane and oxygen was passed over heated substrates and oxide layers up to about 1 μ were grown. The dye used for all the MDIM structures was hydrogen (metal-free) phthalocyanine (H_2Pc); this is a particularly stable dye which can be thermally evaporated under vacuum without decomposition to give coherent films. A layer of dye of thickness up to about 0.5 μ was evaporated on top of the oxide and a test sample was completed by the evaporation of a transparent gold electrode onto the surface of the dye. All depositions used out-of-contact shadow masks to define the test area (0.25 mm^2). MIM structures were prepared in an identical manner but with the omission of the dye layer. More details of the test structures are given in ref. [1].

For all current measurements a Keithley 640 vibrating-reed electrometer was used in its "fast mode" while for photo-discharge experiments (see section 4) it was used as a voltmeter of very high input impedance ($>10^{16}$ Ω). A Fluke stabilized power supply provided biasing voltages when necessary. Experiments as a function of temperature were carried out in an Oxford Instruments continuous flow cryostat fed with liquid nitrogen. For measurements at room temperature the sample was mounted rigidly in an enclosure directly onto the input connector of the electrometer, thus reducing noise to a minimum.

Photo-conduction experiments involved applying a constant bias voltage to the test sample, allowing dielectric relaxation currents to decay away in the dark, and then illuminating the sample with a microscope lamp. The dark and photo-induced currents flowing through the structure were measured as a function of the polarity

and magnitude of the bias voltage, and of temperature. Some measurements of spectral response were also carried out with a Zeiss monochromator as the light source.

Thermally-stimulated dielectric relaxation experiments were conducted in the following manner. A test sample housed in the cryostat was cooled under vacuum with a constant bias applied (usually, but not necessarily, zero voltage). Cooling took place rapidly. When the sample was at the lowest temperature of the experiment the bias voltage was set to a new value which was kept constant during the remainder of the experiment. The temperature was then increased at a constant rate and the dark current through the sample was monitored continuously. For measurements of photo-injected current, the sample was illuminated only for a time sufficient for a reading to be taken – the sample was kept predominantly in the dark. A constant rate of heating was achieved by applying to the input of the temperature controller of the cryostat an error signal which was the difference between the voltage of the cryostat thermocouple and a very slow, low voltage DC ramp of constant rate. The controller was set to control the temperature in such a way as to make the thermocouple voltage equal the ramp voltage, i.e. zero input. Over the temperature range used the thermocouple emf was very nearly linear with temperature and hence the cryostat temperature increased at a constant rate.

In the photo-discharge experiment the light-induced discharge of polarized MDIM sandwich cells was monitored. Cells were polarized to a fixed potential, the supply disconnected and the voltage across the test sample measured as a function of time, using the electrometer in its "open input" mode. Under illumination the discharge rate was observed to be many times greater than the discharge rate in the dark.

3. Photo-conduction experiments

The dark and photo-injected currents through a MDIM cell are shown in fig. 1. The dark current was observed to be constant in time. On illuminating the sample there is an initial transient increase in current which decays to a constant level of, in this particular example, approximately 2.5 times that of the dark current. In other samples a ratio of photo-current to dark current of up to 10 has been observed. When the light is switched off the current quickly drops and, after a slight overshoot, regains the dark current value. Fig. 1 also demonstrates that the response is polarity-dependent. When the dye H_2Pc is negative with respect to the oxide the photo-injected current is significant; when it is positive the effect is negligible. It seems, therefore, that for this particular dye, electron injection occurs fairly readily but not hole injection. Fig. 2 illustrates the voltage dependence of the steady-state photo-current (i.e. the difference between the dark current and the total current under illumination after the transient decay) for a similar test sample at room temperature. The main qualitative features are: (i) an inflexion between 15 and 25 V

and (ii) a tendency for the steady-state photo-current to saturate at higher voltages (>50 V); in both respects fig. 2 is very similar to results reported for the dye-sensitization of the xerographic effect in selenium, also using phthalocyanine [2]. Measurements in the saturation region are difficult because of the high fields involved and the tendency for the oxide film to break down.

In fig. 3 the dark current and the steady-state photo-current are plotted (logarithmically) as a function of reciprocal temperature. The sample was first cooled in the cryostat to below 200 K with zero volts applied. It was then heated at 2 K min^{-1} with 40 eV applied and the dark and photo-currents recorded at various temperatures. As already noted the light was switched off in between readings of the photo-current. A peak is observed in the dark current and the photo-current in the region of 250–260 K; at higher temperatures both currents increase monotonically with decreasing $(1/T)$. In the latter region the slope of the log(current) versus $(1/T)$ graph is slightly higher for the dark current (e.g. in fig. 3 it corresponds to 0.64 eV for the dark current compared with 0.56 eV for the photo-current). For comparison, fig. 4 shows the results of similar measurements on a MIM sandwhich sample (dark current only in this case – as expected, there was no photo-effect). Cooling took place with zero volts applied, heating with 10 V at a rate of 2 K min^{-1}. After the temperature had reached 500 K the temperature ramp was reversed and the

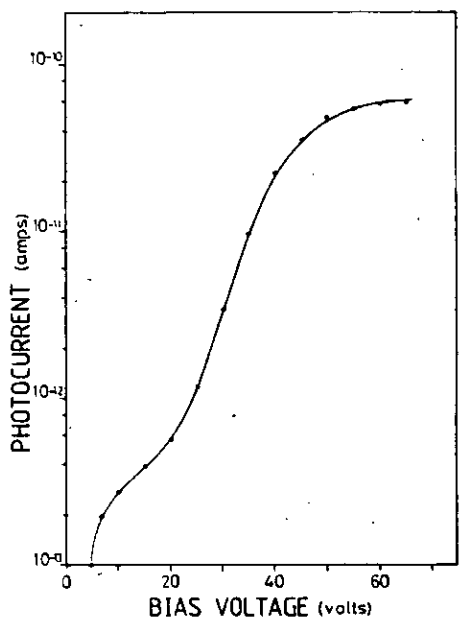

Fig. 2. The photo-current as a function of bias voltage for a typical sample. $T = 300$ K, oxide thickness 0.5 μ.

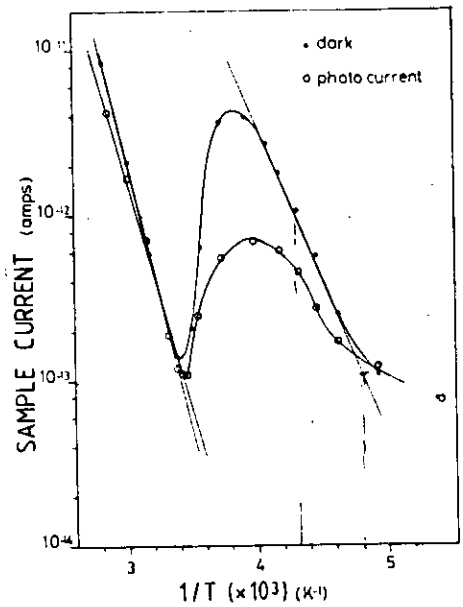

Fig. 3. The temperature dependence of the dark current and photo-current through a MDIM sample. The sample was cooled with zero volts applied and heated at a rate of 2 K per minute with a bias of 40 V.

sample cooled again but with the bias remaining constant (10 V). The heating stage produced a response similar in shape to that of fig. 3 but during the subsequent cooling (also shown in fig. 4) the current decreased with the same effective activation energy as in the high temperature region – no maximum in current is observed.

Results like those of figs. 3 and 4 have been interpreted in terms of the thermally-stimulated dielectric polarization of an insulator (dielectric) with deep-lying traps [3]. When a biasing voltage is applied at low temperature, the time for traps to depopulate, and for the potential barrier at the contact to establish itself, is long compared with experimental times. Thus, in this particular case, the bias conditions are changed at low temperatures but, because the probability of the traps emptying is very low, a non-equilibrium field distribution exists across the oxide. As the temperature is increased a point is reached at which the characteristic release time of carriers from traps becomes comparable with the experimental time. The field then adjusts itself to the steady-state distribution and the contact barrier is established. Because the density of trapped carriers decreases with increasing temperature, the rate of increase of current also decreases with increasing temperature, so that at some temperature the current actually decreases with further increase in temperature – i.e. there is a maximum in current versus temperature (or $1/T$).

It has been postulated [4–7] that a transition from bulk-limited to electrode-

limited conduction occurs during the heating cycle, the bulk processes dominating at low temperature below the current peak and electrode-limited conduction dominating at higher temperatures where the current rises monotonically. Reports in the literature have generally been limited to the case of a single discrete trapping level and some caution must be exercised in applying associated theories to the present situation where it seems unlikely that such a simple model would be adequate. However, the assumption that conduction in SiO_2 is normally by electrons alone, rather than being ambipolar or by holes alone, seems justified in view of the evidence that the mobility of electrons is so much higher than that of holes [8]. The cathode will then be the current-limiting contact, (i.e. the dye contact in MDIM structures). The activation energy of log(current) versus $(1/T)$ graphs at temperatures below the peak has been interpreted as the field-modulated depth of the electron trapping level below the conduction band; the activation energy in the high temperature region corresponds to the height of the contact barrier [4].

At temperatures below the current peak the dark current and photo-current results in fig. 3 have practically the same temperature dependence, corresponding to a trap depth of 0.65 eV after correction for the field-dependence. (Note that at very low temperatures the current levels are also becoming very low. Thus, the deviations from a straight line in the log(current) versus $(1/T)$ plots are most likely an artefact of measurement.) This suggests that the same bulk conduction processes are important in both cases. The difference in slope at high temperatures (0.56 eV for the photo-current, 0.65 eV for the dark current) probably indicates that the dye/oxide barrier is lowered under illumination.

The dark current and the steady-state photo-current through a MDIM sandwich cell at $T = 300$ K are plotted (logarithmically) as a function of the square root of the applied bias in fig. 5. A similar graph for measurements on a MIM cell is shown in fig. 6. This figure also includes points calculated from the equation proposed by Gupta [9] for the current density J flowing by the trap-controlled and bulk-limited Poole–Frenkel effect in insulators (or semiconductors), i.e.

$$J = q\mu N_C F_i \exp(-E_{cF}/kT) \exp(2\beta F_i^{1/2}/kT) \tag{1a}$$

or

$$J = AF \exp(BF^{1/2}). \tag{1b}$$

In eq. (1a) q is the electronic charge, μ the carrier mobility, N_C the effective density-of-states in the conduction band, E_{cF} the position of the Fermi-level with respect to the conduction band edge, k is Boltzmann's constant and F_i is the field in the insulator (oxide) which may be a function of time. The parameter β is given by $(q^3/4\pi\epsilon)^{1/2}$, where ϵ is the permittivity of the insulator. In eq. (1b) F is the applied field, while A and B are constants (for a given temperature) which can be deduced by comparison with eq. (1). The calculated points in fig. 6 were obtained from eq. (1b) with $A = 1.5 \times 10^{-13}$ (A V^{-1} m^{-2}) and $B = 3.3 \times 10^{-4}$ (V m^{-1})$^{-1/2}$.

Finally, fig. 7 illustrates the spectral response of the important wavelength-

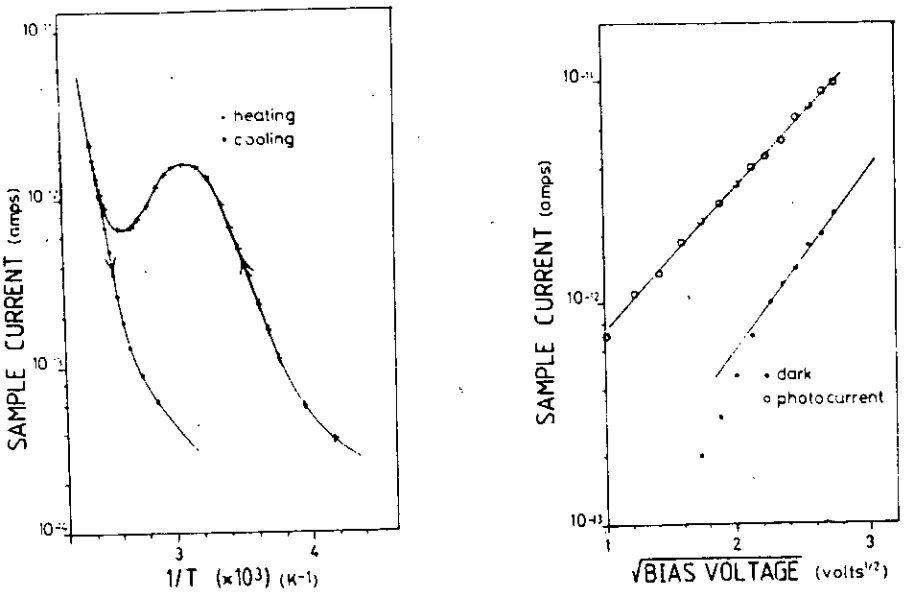

Fig. 4. Log current versus $(1/T)$ for a MIM sample (I is SiO_2). The sample was first cooled with zero applied volts and then heated at 2 K per minute with a bias of 10 V. Another cycle of measurements was then carried out during cooling, also with a bias of 10 V.

Fig. 5. The field-dependence of the dark current and steady-state photo-current through a MDIM sample. The measurements were made at room temperature and the oxide thickness was 0.7 μ.

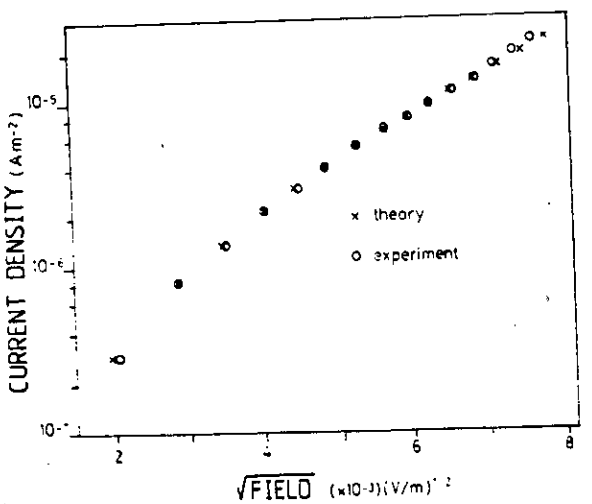

Fig. 6. Similar results to fig. 5 for a MIM sample (T = 320 K).

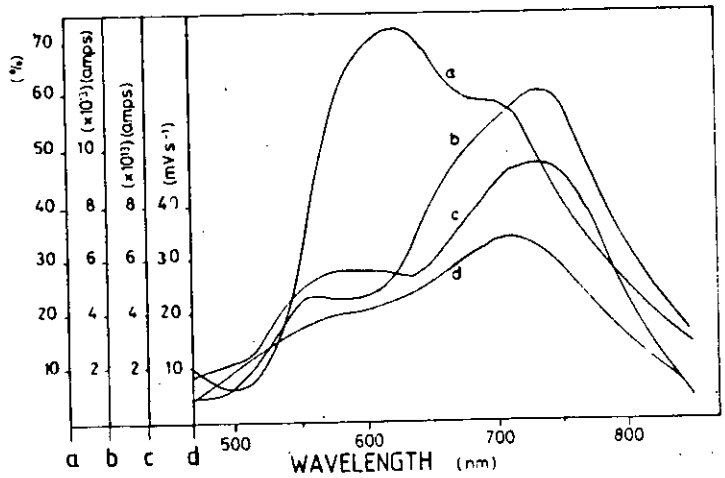

Fig. 7. Spectral dependence of (a) the relative absorption of a phthalocyanine film, (b) the photo-conduction of phthalocyanine, (c) the induced photo-current through a MDIM sample and (d) the rate of photo-discharge of a MDIM capacitor.

dependent phenomena. This figure includes the spectral dependence of the relative optical absorption of H_2Pc, of the normal photo-current in H_2Pc (measured using a co-planar "gap" cell of an evaporated film of the dye with gold electrodes), and of the induced steady-state photo-current through a MDIM sandwhich cell. The data has not been corrected for spectral variations in the monochromator. The spectrum of photo-conduction in the dye is similar in form to that reported in the literature [10]. The photo-current injected through the MDIM structure has a spectrum which is close to, but not exactly coincident with, that of photo-conduction in the dye itself. This suggests that the carriers responsible for the induced photo-current through the SiO_2 are generated in the dye by the same mechanism as that responsible for photo-conduction in the dye.

4. Photo-discharge experiments

In this experiment a MDIM capacitor was first charged to a given potential (usually 10–30 V) and then discharged through the electrometer in its "open input" mode. On illumination of the dye contact the rate of discharge was observed to increase substantially but, in contrast to the photo-current, there was no marked polarity dependence although the *form* of the transient decay is significantly different with positive or negative bias to the dye. Some typical results are shown in fig. 8. The light-induced discharge rate varies with wavelength and, like the spectral response of photo-current, roughly matches the spectral dependence of photo-con-

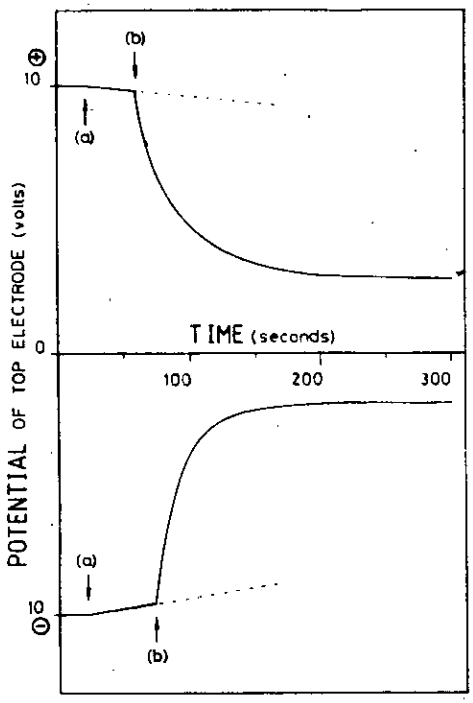

Fig. 8. The time-dependence of the discharge of a polarized MDIM capacitor. The sign of the potential on the vertical axis again refers to the upper (dye) electrode (see inset of fig. 1). On each curve the arrows (a) indicate the time at which the voltage source was switched off. The capacitor was then allowed to discharge for a short time in the dark until the point indicated by the arrows (b), when the dye was illuminated.

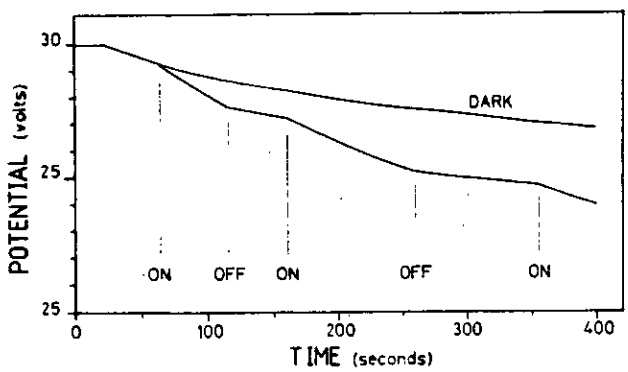

Fig. 9. Illustrating the variation in discharge rate of a MDIM capacitor with intermittent (light ON and OFF) illumination.

duction in the dye. This is also illustrated with the other spectra in fig. 7; note however that there are small differences between the spectra of the three light-induced electrical effects. Under intermittent illumination the rate of discharge responds essentially instantaneously, on the experimental time scale, to light being switched on and off as illustrated in fig. 9.

5. Discussion and conclusions

Observations on the light-sensitization of conduction through semiconductors and insulators via the illumination of a photo-conducting layer (organic or inorganic) is by no means new. The phenomenon is well-known in colour photography and is utilized in the electro-photographic technique known as the Electrofax process (for a comprehensive survey see ref. [11]). Two models have been invoked to explain the phenomenon:

(i) the resonant transfer of adsorbed light energy in the photo-conductor from the sensitizer to the substrate (semiconductor or insulator) causing the ionization of trapped carriers in the substrate.

(ii) the field-induced injection of carriers excited by light absorption in the photo-conductor into the substrate.

Thus, the difference between the two models hinges on whether the charge carriers causing the induced photo-current in the substrate originate in the substrate or in the photo-conductor. In general, the evidence from observations on a wide variety of materials seems to favour the second alternative, i.e. a charge-transfer mechanism from the photo-conductor to the substrate [12]. The key consideration of the direct charge-transfer mechanism is the relative alignment of the appropriate electronic energy levels in the photo-conductor and semiconductor or insulator, i.e. in the present case, between the dye (phthalocyanine) and SiO_2.

The results on dye-sensitized photo-conduction described in section 3, which show quite clearly that an electronic current is induced fairly readily but not a hole current, are certainly consistent with the conclusion that the electron mobility in SiO_2 is relatively high whereas the hole mobility is very low [8]. At first sight therefore, the electron injection implies the alignment of an excited electron state ("conduction band") in the dye with the conduction band of the SiO_2. From the evidence available this seems unlikely. In amorphous SiO_2 the conduction band edge is approximately 1 eV below the vacuum level [13] whereas the first excited singlet state (conduction level) of H_2Pc has been estimated to be about 3.3–3.6 eV below the vacuum level [2]. If a direct charge-transfer of electrons does occur it seems more likely therefore that it proceeds via an intermediate trapping state in the SiO_2 and subsequent thermal (and/or field-assisted) ionization into the conduction band. Gupta and van Overstraeten [6] have suggested an analogous mechanism for the field-injection of electrons from a metal electrode into SiO_2. They predict, incidentally, that the $I-V$ curves have "kinks" corresponding to changes in the dominant

transfer mechanism from Schottky emission to trap-assisted injection and finally to direct tunnelling into the conduction band. If the analogy is appropriate this could explain the "kink" in the photo-current versus voltage curve of fig. 2. It must be noted, however, that the data of figs. 3 and 4 indicate that the trapping level controlling the bulk conduction is at 0.65 eV and there is still therefore a substantial mis-alignment with the H_2Pc conduction level. There must, of course, be many other trapping levels in the forbidden energy gap of amorphous SiO_2 with which the excited state(s) of the dye *could* communicate but the present evidence is inconclusive about the mechanism of photo-sensitization of conduction in SiO_2. More experimental work is required and it will be particularly important to vary the thickness of the dye layer.

An explanation of the photo-discharge experiment is not possible without some understanding of the basic mechanism of photo-sensitized current. A particularly puzzling and distinctive feature of the photo-discharge results is the lack of any significant polarity dependence (fig. 8), in contrast to the photo-current results (fig. 1). It must be remembered, however, that in the photo-discharge experiment the structure used in present work is effectively a dual-dielectric capacitor in which the two dielectric layers (dye and SiO_2) are approximately the same thickness ($\sim 0.5\ \mu$). The complete discharge of the capacitor, looked at macroscopically, involves the transport of negative charges to the positively charged electrode *and* of positive charges to the negatively charged electrode. Thus, charge transport in the dye layer will also be a significant factor in the discharge process and it may be relevant to note that Heilmeier and Warfield [14] found evidence for deep traps (~ 0.8 eV) in H_2Pc, which would necessarily have thermal-release time constants of the order of 100 s or more at room temperature.

References

[1] B.W. Flynn, A.E. Owen and J. Mavor, J. Phys. C: Solid St. Phys. 10 (1977) 4051.
[2] P.J. Regensberger and N.L. Petruzella, J. Non-Crystalline Solids 6 (1977) 13.
[3] P. Müller, in: Amorphous Semiconductors 1976, Proc. Int. Conf., Balatonfured, Hungary, Sept. 1976, ed. Kosa Somogyi (Akademicai Kiade, Budapest, 1977) p. 199.
[4] J.G. Simmons and G.W. Taylor, Phys. Rev. B6 (1972) 4804.
[5] J.G. Simmons and G.S. Nadkarni, Phys. Rev. B6 (1972) 4815.
[6] H.M. Gupta and R.J. van Overstraeten, J. Appl. Phys. 46 (1975) 2675.
[7] H.M. Gupta, Appl. Phys. Letters 33 (1978) 778.
[8] R.C. Hughes, Phys. Rev. Letters 30 (1973) 1333.
[9] H.M. Gupta, J. Appl. Phys. 48 (1977) 3448.
[10] S.E. Harrison, J. Chem. Phys. 50 (1969) 4739.
[11] H. Meier, Spectral Sensitization (Focal Press, London and New York, 1968).
[12] H. Meier, Photochem. Photobiol. 16 (1972) 219.
[13] D.L. Griscom, J. Non-Crystalline Solids 24 (1977) 155.
[14] G.H. Heilmeier and G. Warfield, J. Chem. Phys. 38 (1963) 163.